



UNIVERSITÀ DEGLI STUDI DI PAVIA

Dipartimento di Biologia e Biotecnologie "L. Spallanzani"

Dottorato di Ricerca in Scienze Biomediche

XXX Ciclo

DIFFERENT PATTERNS OF Ca^{2+} SIGNALING DRIVE ACETYLCHOLINE AND GLUTAMATE INDUCED-NO RELEASE IN MOUSE AND HUMAN BRAIN MICROVASCULAR ENDOTHELIAL CELLS

Tutor: Chiar.mo Prof. Francesco MOCCIA

Coordinatore: Chiar.mo Prof. Egidio D'ANGELO

Tesi di Dottorato di Ricerca

Dott.ssa Estella ZUCCOLO

Summary

Abstract	1
INTRODUCTION	2
Cerebral blood flow regulation: cellular and biochemical pathways.....	2
The neurovascular unit.....	3
The blood-brain barrier	4
The neurovascular and neurometabolic coupling.....	6
The cellular and biochemical pathways of neurovascular coupling.....	7
The neurotransmitter Acetylcholine	10
The neurotransmitter Glutamate	11
Nitric Oxide.....	12
The calcium toolkit in vascular endothelial cells	14
Calcium signals in brain endothelial cells	19
MATERIALS AND METHODS.....	22
Cell culture.....	22
Solutions	23
Fluorescence microscope	23
[Ca ²⁺] _i measurements	23
RNA isolation and Real Time RT-PCR (qRT-PCR) of Ca ²⁺ -permeable channels	24
Immunoblotting.....	25
Statistics.....	25
RESULTS	26
Acetylcholine induces intracellular Ca ²⁺ oscillations in bEnd5 cells.....	26
Expression of the components of the Ca ²⁺ signaling toolkit in bEND5 cells.....	29
Acetylcholine-induced Ca ²⁺ oscillations derive from the periodic discharge of intraluminally stored Ca ²⁺ through InsP ₃ Rs	30
The acetylcholine-induced intracellular Ca ²⁺ oscillations requires extracellular Ca ²⁺ entry	32
SOCE is the major Ach-activated Ca ²⁺ entry pathway in bEND5 cells	33
Acetylcholine-induced intracellular Ca ²⁺ oscillations lead to NO synthesis in bEND5 cells	37
Acetylcholine induces intracellular Ca ²⁺ signals in human brain microvascular endothelial cells	39
Expression of the components of the Ca ²⁺ signaling toolkit in hCMEC/D3 cells.....	42
Acetylcholine-induced intracellular Ca ²⁺ response requires intracellular Ca ²⁺ release and extracellular Ca ²⁺ entry	43
Acetylcholine-induced intracellular Ca ²⁺ release is mediated by the PLCβ/InsP ₃ signalling pathway	45
SOCE participates to the Ca ²⁺ response to Ach in hCMEC/D3 cells.....	46

Acetylcholine-induced Ca ²⁺ signalling leads to NO synthesis in hCMEC/D3 cells	48
Glutamate induces intracellular Ca ²⁺ oscillations in bEnd5 cells.....	50
Glutamate-induced intracellular Ca ²⁺ oscillations require both intracellular Ca ²⁺ release and extracellular Ca ²⁺ entry.....	52
Glutamate-induced intracellular Ca ²⁺ oscillations are generated by Ca ²⁺ release from the ER	54
Glutamate-induced intracellular Ca ²⁺ oscillations are maintained by constitutive Ca ²⁺ entry.....	56
Glutamate-induced intracellular Ca ²⁺ oscillations lead to NO release in bEnd5 cells	57
Glutamate induces Ca ²⁺ -dependent NO synthesis in human brain microvascular endothelial cells	59
DISCUSSION	60
Acetylcholine stimulates intracellular Ca ²⁺ oscillations in bEND5 in a dose-dependent manner	61
The Ca ²⁺ toolkit of mouse brain endothelial cells.....	63
Acetylcholine-induced Ca ²⁺ response is driven by ER Ca ²⁺ release via InsP ₃ Rs and sustained by SOCE in mouse brain endothelial cells.....	64
Acetylcholine-induced intracellular Ca ²⁺ oscillations drive NO production in bEND5 cells	66
Acetylcholine driven intracellular Ca ²⁺ increase in hCMEC/D3 in a dose-dependent manner	66
The Ca ²⁺ toolkit of human brain endothelial cells	67
Acetylcholine-induced Ca ²⁺ response are driven by ER Ca ²⁺ release via InsP ₃ Rs and SOCE in human brain endothelial cells.....	67
Acetylcholine-induced intracellular Ca ²⁺ mobilization drive NO production in hCMEC/D3 cells.....	68
Glutamate stimulates intracellular Ca ²⁺ oscillations in bEND5 cells.....	69
Glutamate-induced Ca ²⁺ oscillations are driven by ER Ca ²⁺ release via InsP ₃ Rs and SOCE in bEND5 cells ...	70
Glutamate-induced intracellular Ca ²⁺ oscillations drive NO production in bEND5 cells	71
Glutamate induces intracellular Ca ²⁺ signals and NO release in hCMEC/D3 cells.....	73
CONCLUSIONS	74
References	75

Abstract

Acetylcholine (ACh) and glutamate (Glu) are two of the major excitatory neurotransmitters in the brain which increase cerebral blood flow by releasing nitric oxide (NO) from postsynaptic neurons and astrocytes and causing vasorelaxation in adjacent microvessels. An increase in intracellular Ca^{2+} concentration recruits a multitude of endothelial Ca^{2+} -dependent pathways, such as Ca^{2+} /Calmodulin endothelial NO synthase (eNOS). Surprisingly, the Ca^{2+} -dependent mechanisms whereby ACh induces NO synthesis in brain endothelial cells (ECs) is still unclear. On the other hand, Glu stimulates NMDA receptors to activate eNOS, but it is able to cause a metabotropic increase in intracellular Ca^{2+} concentration in brain microvascular ECs. The present investigation sought to fill these gaps by analysing murine (bEND5) and human (hCMEC/D3) brain microvascular ECs.

Herein, we first demonstrated that ACh induces NO release by triggering two different modes of Ca^{2+} signals in bEND5 and hCMEC/D3 cells. Of note, endoplasmic reticulum Ca^{2+} release via inositol-1,4,5-trisphosphate receptors and store-operated Ca^{2+} entry shapes the Ca^{2+} response to ACh in both cell types but their different Ca^{2+} toolkits result in two quite different waveforms, i.e. Ca^{2+} oscillations vs. biphasic Ca^{2+} elevation. Whatever its waveform, however, ACh-induced intracellular Ca^{2+} signals lead to robust NO release in both murine and human brain microvascular ECs. Likewise, we demonstrated for the first time that Glu activated metabotropic intracellular Ca^{2+} oscillation in bEND5 cells and a biphasic increase in intracellular Ca^{2+} concentration in hCMEC/D3 cells. We further showed that glutamate-dependent Ca^{2+} signals drive NO release in both types of cells. This NO signal is delayed as compared to the ACh-induced one and is likely to play a crucial role in the slower vasodilation that often follows brief neuronal activity or that sustains functional hyperemia during persistent synaptic transmission.

This information has a potential clinical relevance as the decrease in neuronal activity-induced cortical CBF is involved in a growing number of neurodegenerative disorders, such as Alzheimer's Disease. Understanding the underlying mechanisms could, therefore, be used in the future as target to rescue local blood perfusion in patients affected by neurodegenerative disorders.

INTRODUCTION

Cerebral blood flow regulation: cellular and biochemical pathways

The brain, which constitutes 2% of body mass but consumes 20% of the total energy produced at rest, has a limited capacity to store energy and therefore requires a continuous supply of oxygen and nutrients from the blood stream. Normal brain structure and function integrity thus rely on adequate matching between metabolic needs of neural cells and blood supply ([1], [2], [3], [4]). Normal brain functions depend on the fine regulation of the transport through the blood brain barrier (BBB), the interplay between the different cells that form the functional neurovascular unit (NVU) and the coupling between neurovascular and neurometabolic regulation ([5], [6]). The NVU controls BBB permeability and local cerebral blood flow (CBF), thereby maintaining the chemical composition of the neuronal 'milieu', which is required for proper functioning of neuronal circuits ([7]). Brain functions end within seconds after the interruption of CBF, while irreversible neuronal injury occurs within minutes ([7]). Therefore, local CBF must be very tightly regulated to prevent any unbalance between neuronal activity (NA), oxygen and nutrient delivery, and vessel reactivity. Based on functional and structural observations, it has been proposed that neurons may signal to adjacent blood vessels either directly or through the interposition of glutamate-sensitive glial cells ([8], [9]). This scenario has been further complicated by the recent evidence that CBF may in turn regulate NA, which gives rise to a bidirectional communication between firing neurons and neighbouring vessels ([10], [11]). Moreover, it is now evident that NA does not only control arterial and arteriolar tone, which depends on the contractile status of vascular smooth muscle cells (VSMCs) ([9]). A series of studies have convincingly shown that pericyte-mediated dilation or contraction may alter capillary diameter in response to neuronal activation or silencing ([12], [13], [14]). The control of CBF at capillary level might be indispensable to match the local tissue oxygen supply to local cerebral demand, as their shortest distance ($\approx 5 \mu\text{m}$) from neuronal soma significantly accelerates oxygen and carbon dioxide diffusion as compared to intraparenchymal arterioles ($\approx 15 \mu\text{m}$) ([15]). Surprisingly, it is still unclear whether endothelial signaling actively contributes to NVC ([16], [17], [18]) despite the fact that vascular endothelium has long been known to finely tune blood flow in peripheral [19] and coronary [20] vasculature.

The neurovascular unit

The concept of neurovascular unit (NVU) was defined by Harder ([21]) as a functional unit where neurons, interneurons and astrocytes are in close proximity and are functionally coupled to smooth muscle cells, pericytes, endothelial cells and extracellular matrix. Each component is intimately and reciprocally linked to each other, establishing an anatomical and functional whole, which results in a highly efficient system of CBF regulation ([22], [23]).

In detail, the pial arteries are intracranial vessels on the surface of the brain that give rise to smaller arteries, penetrating arterioles and parenchymal arterioles that go deep into the brain tissues, where they become almost completely surrounded by astrocytic end-feet ([24], [25]). At this level, the vascular basement membrane comes into direct contact with the neurons through the astrocyte-derived glia limitans membrane that forms the outer wall of the perivascular Virchow–Robin space. These arteries branch into smaller arteries and subsequently arterioles, which lose support from the glia limitans and give rise to pre-capillary arterioles and brain capillaries. In an intracerebral artery, the VSMC layer occupies most of the vessel wall. At the brain capillary level, vascular endothelial cells are covered by pericytes, from which they are separated by the basement membrane ([9]). At points of contact, pericytes communicate directly with endothelial cells through the gap junctions and adhesion molecules, such as cadherins and integrins ([26], [27], [28]). These structures not only provide direct contact between these two cell types but also controls vascular tone due to a unique intracellular and extracellular microdomain signaling environment ([12], [13], [14]). Of note, recent evidence has been brought forward to suggest that brain endothelium is a little bit more than an innocent by-stander during NVC ([16], [17], [29], [30]).

Once regarded as an inert barrier between circulation and neuronal tissue, endothelial cells constitute the largest signal transduction platform of the organism ([31]) and, therefore, it is not surprising that they are also essential for the proper functioning of the NVU ([9], [16]). Any alteration in the endothelial capability to detect and decode both physical and humoral stimuli may lead to an astonishing variety of severe diseases ([31]), including Alzheimer's disease ([4], [32]), stroke ([33]), hypertension ([32]) and spinal-cord injury ([34]). In particular, the dynamic interaction between capillary brain endothelial cells and neighbouring cells contributes to their unique characteristics, such as the manifestation of both endothelial and epithelial features ([24], [35], [36], [37]).

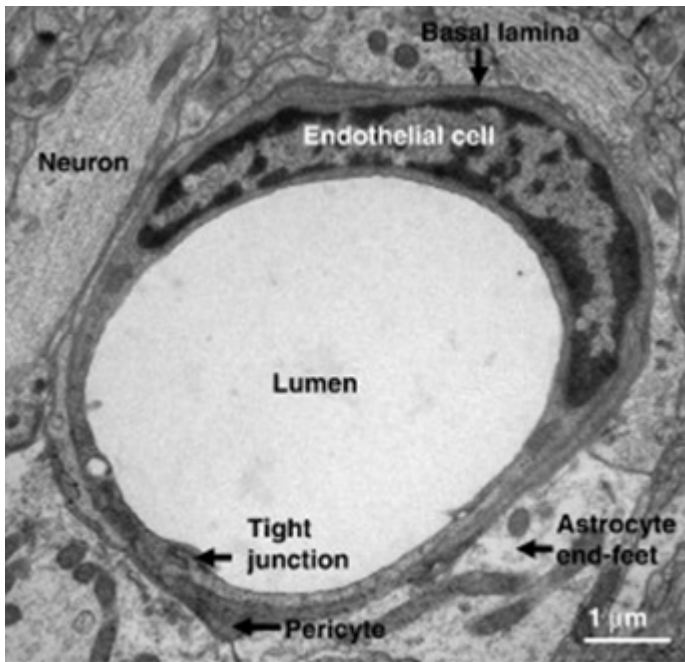


Figure 1. Electron microscopy (TEM) of rat brain section showing a neurovascular unit. This complex includes microvessel endothelial cells, based on basal lamina, pericytes embedded in basal lamina, astrocytes end-feet and in vicinity some neurons (from Weiss et al.,2008).

The blood-brain barrier

The blood–brain barrier (BBB) is a highly selective lipophilic barrier that separates the systemic blood circulation from the central nervous system. The BBB maintains the brain homeostasis and provides an optimal chemical environment for cerebral function. These properties are due to the unique characteristic of brain endothelial cells (bECs). Indeed, bECs significantly differ from non-brain ECs by the presence of intracellular tight junctions; a high number of mitochondria, associated with a strong metabolic activity; and the polarized expression of numerous membrane receptors and transporters which are responsible for the active transport of nutrients to the brain or the efflux of potentially toxic compounds from the cerebral to the vascular compartment ([38], [39], [40]). Tight junctions and adherens junctions interconnect bECs and form a highly specialized interendothelial junctional complex that limit paracellular diffusion form blood to brain and vice versa ([24], [41], [42], [43]). Many disease, such as Alzheimer’s disease, and acute conditions, such as ischemic stroke and hypertension, are able to modify the BBB permeability and dysregulate the proteins contents of the tight junctions ([32], [33], [44]). BBB permeability and CBF are controlled by the concerted action of non-neuronal cells and neurons. The maintenance of the constant chemical composition of the ISF is guaranteed by vascular cells and glia, while the BBB and the blood-spinal cord barrier (BSCB) work together with pericytes to prevent the entry in the CNS of

various potentially neurotoxic and vasculotoxic macromolecules, and to promote clearance of these substances from the CNS ([45]).

The low paracellular permeability of the BBB is conferred by the presence of tight junctions and adherens junctions that connected the endothelial cells that form the BBB. Normal brain endothelium lacks fenestrae and has limited vesicular transport; only oxygen, carbon dioxide and small lipophilic molecules are able to diffuse freely across the endothelial cells.

A high energy demand is required for activate ATP-dependent transport, such as the sodium pump ($\text{Na}^{2+}\text{K}^{+}$ ATPase) and the ATP-binding cassette (ABC) efflux transporters; for these reason endothelial cells are enriched of a high number of mitochondria. $\text{Na}^{2+}\text{K}^{+}$ ATPase control the sodium influx and potassium efflux across the abluminal side of the BBB. Changes in sodium and potassium levels in the ISF influence the generation of action potentials in neurons and thus directly affect neuronal and synaptic functions.

Disruption to tight and adherens junctions, an increase in paracellular fluid permeability, and/or enzymatic degradation of the capillary basement membrane cause physical breakdown of the BBB. The levels of many tight junction proteins, their adaptor molecules and adherens junction proteins decrease in Alzheimer's disease and other diseases that cause dementia, multiple sclerosis and various animal models of neurological disease. These decreases might be partly explained by the fact that vascular-associated matrix metalloproteinase (MMP) activity rises in many neurodegenerative disorders and after ischaemic CNS injury; tight junction proteins and basement membrane extracellular matrix proteins are substrates for these enzymes. Lowered expression of messenger RNAs that encode several key tight junction proteins, however, has also been reported in some neurodegenerative disorders.

The neurovascular and neurometabolic coupling

Brain activation is accompanied by a complex sequence of cellular, vascular and metabolic processes that help the brain to maintain an appropriate energy flow to the neural tissue under conditions of increased neuronal activity. Two coupling phenomena can be identified: neurovascular and neurometabolic coupling.

Neurovascular coupling or functional hyperemia refers to the relationship between local NA and changes in vessel diameter and thus in blood flow ([46], [47], [48], [49], [50], [51]). Functional hyperemia is the mechanism by which an increase in NA leads to a local elevation in CBF to adjust oxygen and glucose delivery to the requirements of the activated brain structures.

The mechanism by which an increase in NA activity leads to a corresponding elevation in energy metabolism has been known as neurometabolic coupling ([52], [53], [54], [55]). Glucose is under normal circumstances the main useful energy substrate for the brain energy metabolism ([56]). In the brain, about 90% of glucose is metabolized by oxidative metabolism, which requires oxygen and produces a large amount of ATP, the other 10% is metabolized by glycolysis, which is anaerobic and produces a small amount of ATP. A continuous supply of glucose and oxygen is required and is maintained by changes in CBF in response to variations in neuronal activity ([57], [58], [59], [60]). While it is clear that alterations in NA and metabolism are correlated with changes in CBF, the mechanisms whereby NA control the vascular supply of glucose and oxygen are still a matter of debate.

The cellular and biochemical pathways of neurovascular coupling

Autoregulation is the mechanism which maintains constant the total blood flow supply to the brain despite for the fluctuations in arterial pressure that occur during normal activities. Autoregulation of cerebral blood flow when pressure fluctuates is most likely due to the myogenic behavior of the cerebral vascular smooth muscle that constrict in response to elevated pressure and *viceversa* ([61], [62]). Locally, blood flow delivery to active brain areas may be finely regulated by neurovascular coupling (NVC) or functional hyperemia. Traditionally, it was thought that local CBF was directly controlled directly by the neuronal demand. In this view, regional blood flow is controlled by feedback mechanisms that are sensitive to variations in the concentrations of metabolic products. This hypothesis suggests that signals related to energy production, such as a rise in carbon dioxide (CO₂) or adenosine concentration or a drop in glucose or oxygen (O₂) concentration, may cause an increase in blood flow by triggering vascular smooth muscle cells vasodilation. This model was, however, discarded upon the discovery that regional CBF always overwhelms the local O₂ and glucose requirements; furthermore, the increase in CBF may persist even in the presence of excess O₂ and glucose ([4]). An alternative possibility is that a feedforward mechanism controls the vascular energy supply in response to NA; neurons either signal directly to blood vessels or activate astrocytes to release vasoactive agents onto the vessels. For both of these signaling routes, the coupling mechanisms involve neurotransmitter, particularly glutamate ([63], [64]).

The arteriolar component - Synaptic release of glutamate activates neuronal NMDA receptors, thereby resulting in Ca²⁺ entry and activation of neuronal nitric oxide synthase (nNOS). The following NO release is able to directly dilate brain arterioles both in brain slices and *in vivo* ([65]). Glial cells are well suited to mediate the vascular effect of glutamate release because of their close contacts with both neurons and blood vessels ([46], [66], [67]). Accordingly, glial cells respond with an increase in intracellular Ca²⁺ concentration ([Ca²⁺]_i) to synaptically released glutamate ([68], [69]), which lead to the Ca²⁺-dependent generation of a number of vasoactive messengers. These include the arachidonic acid metabolites, epoxyeicosatrienoic acids (EETs), which are vasodilating, 20-hydroxyeicosatetraenoic acid (20-HETE), which is vasoconstricting, and prostaglandins, which can be either vasodilating or constricting depending on the target receptor ([70], [71]). In more detail, for instance, glutamate binds to metabotropic glutamate receptor 1

(mGluR1) to stimulate phospholipase C (PLC) and induce an inositol-1,4,5-trisphosphate (InsP₃)-dependent intracellular Ca²⁺ waves which can propagate into the astrocyte endfeet. Glutamate-induced Ca²⁺ signals, in turn, recruit the Ca²⁺-dependent effector, phospholipase A2 (PLA2), which releases AA from plasma membrane phospholipids ([8]). Cyclooxygenase (COX) enzymes can then metabolize AA to vasoactive prostaglandins, such as prostaglandin E2 (PGE2), and epoxyeicosatrienoic 21 acids (EETs), which cause vasodilation. Moreover, as shown in rat cerebral arterial microsomes and *ex vivo* brain slices, astrocyte may convert PLA2-derived AA into the vasoconstricting, 20-hydroxyeicosatetraenoic acid (20-HETE), by membrane-bound cytochrome P450 4A, thereby causing local vasoconstriction ([72], [73]).

The capillary component - A novel finding in the field has been the discovery that, besides parenchymal arterioles, brain capillaries may also undergo significant changes in their diameter in response to local NA. Accordingly, Attwell's group reported the evidence that pericytes — which are contractile cells present at ~50- μ m intervals along capillaries — can markedly alter capillary diameter upon stimulation of glutamatergic synapses. Pericytes express contractile proteins, and their location on capillaries led to the suggestion that they could constrict the microvasculature ([74]). This idea was reinforced with observations that substances that alter arteriole diameter, including arachidonic acid (AA) derivatives and neurotransmitters, can contract and relax pericytes cultured on rubber membranes ([75]). More recently, it has been shown that pericytes constrict in response to noradrenaline and dilate in response to glutamate in brain slices ([76], [13]), thereby demonstrating that endogenous transmitter release can regulate capillary diameter ([76]). Regulation of CBF at the capillary level has yet to be demonstrated *in vivo* in physiological conditions ([74]), although it does occur after ischaemia ([77]). Signals for contraction and perhaps for dilation can propagate from one pericyte to another ([76], [78]). This signal spread may occur through gap junctions between the interdigitating processes of the pericytes themselves, or through gap junctions with ECs. Because active neurons are, on average, closer to pericytes than to arterioles (8–23 μ m away versus 70–160 μ m), this raises the theoretical possibility that vascular responses to changes in neuronal activity may be initiated by pericytes and then propagated to upstream arterioles ([79]).

The endothelial enigma - In addition to these direct and direct interactions between active neurons and brain microvessels, recent studies have discovered that significant vasoactive signals may be directly generated by the endothelium itself, adding a new complex level of interaction in the NVU. ECs release vasodilating (e.g., NO, endothelium-derived hyperpolarizing factor, or EDHF,

prostanoids) and vasoconstricting (e.g., endothelin, TXA₂, prostaglandin) substances ([18]) in response to either chemical or mechanical stimulation ([31]). It has been shown that Ach stimulates vasodilation in adult mouse middle cerebral arteries by activating Transient Receptor Potential Vanilloid 4 (TRPV4) channels, which leads to Ca²⁺ entry and endothelium-dependent EDHF-mediated dilation ([80]), whereas glutamate may stimulate NMDA receptors to locally increase cerebral blood flow in an endothelial and NO-dependent manner ([30]). Moreover, endothelial reactive oxygen species (ROS) act as vasodilators at low concentrations, but at high concentrations they can cause vasoconstriction ([81], [82]). However, the role played by brain microvascular ECs in NVC has been rather neglected ([16]). It is, indeed, still unclear whether and how brain microvascular ECs directly sense neuronal activity by responding to synaptically-released neurotransmitters with the production of vasoactive agents. As mentioned earlier, the best characterized interaction is that described between Ach and brain endothelium. For instance, basal forebrain neurons increase cortical blood flow by releasing Ach, which binds to endothelial muscarinic receptors (mAChRs), thereby leading to NO production and microvessel vasodilation ([83], [84], [85]). In other vascular beds ([86], [87]), Ach stimulates NO production by initiating an oscillatory increase in [Ca²⁺]_i, which is patterned by the interaction between InsP₃ receptors (InsP₃Rs) and the so-called store-operated Ca²⁺ entry (SOCE). However, the waveform of Ach-induced Ca²⁺ signaling in brain microvascular endothelial cells and its relationship with NO release are still unclear. Likewise, recent studies revealed that glutamate may stimulate NMDARs in the presence of the co-agonist d-serine to engage in the eNOS (, [29]), but it remains to be elucidated whether mGluRs are expressed and promote NO release in brain microvascular endothelial cells.

The neurotransmitter Acetylcholine

Acetylcholine (ACh) is one of the major excitatory neurotransmitters in both the central and peripheral nervous system of CBF in man and in many other species (for a review see [88]). ACh was the first neurotransmitter discovered. The concentrations of ACh in the extracellular fluid range from 0.1 to 6 nM ([89]), while in the brain range from 0.01 to 0.5 nM [90]. ACh is also known to be a powerful dilator of most blood vessels, including cerebral arteries and microvessels ([91], [92]). Stimulation of basal forebrain neurons causes regional increases in CBF which are particularly pronounced in the neocortex and hippocampus ([93], [94]). As anticipate above, basal forebrain cholinergic fibers project to intraparenchymal microvessels, thereby establishing a neurovascular interaction that does not require the interposition of local interneurons and directly controls cortical microcirculation ([93], [94]). Accordingly, ACh released by post-synaptic terminals binds to endothelial muscarinic receptors (mAChRs), thereby leading to NO production and microvessel vasodilation ([83], [94], [85]).

The ACh biosynthesis involves acetyl coenzyme A (ACo-A), choline and ACh biosynthetic enzyme choline acetyltransferase. Primarily, during ACh biosynthesis, choline is taken up from the extracellular space by a high affinity Na^+ -dependent uptake system present in cholinergic neurons ([95]). Similar to common neurotransmitters, ACh is biosynthesized in the cytosol of nerve terminals and is then stored into synaptic vesicles prior to release by exocytosis ([96]). In response to an action potential, it is released by exocytosis into the synaptic space, from which it diffuses to the postsynaptic site for interaction with appropriate receptors, which results in specific effects according to the receptor type (nicotinic or muscarinic). These receptors are functionally different, the muscarinic type (muscarinic ACh receptor - mAChR) being G-protein coupled receptors (GPCRs) that mediate a slow metabotropic response via second messenger cascades, while the nicotinic type (nicotinic ACh receptor – nAChR) are ligand-gated ion channels that mediate a fast synaptic transmission of the neurotransmitter ([97]).

Muscarinic receptors are involved in a large number of physiological functions, including modulation of heart rate and force, vasorelaxation, and neurotransmitter release. There are five mAChR subtypes which have been distinguished based on pharmacological activity (M1-M5 AchRs) and are all found in the central nervous system (CNS). However, M1-M4 AchRs are also present outside the CNS. M1, M3 and M5 receptors cause the activation of phospholipase C, generating two secondary messengers (IP_3 and DAG) eventually leading to an increase of intracellular calcium concentration, while M2 and M4 inhibit adenylate cyclase, thereby decreasing the production of

the second messenger cAMP ([97]). M5-AchR is the most abundant endothelial isoform in brain microvessel and mediate Ach-induced vasodilation by activating NO release in a Ca^{2+} -dependent manner ([83]). Yet, the signaling mechanisms that couple Ach to the Ca^{2+} -dependent activation of the eNOS remain elusive.

The neurotransmitter Glutamate

The excitatory neurotransmitter glutamate (Glu) is a vasodilator in cerebral circulation *in vivo* ([98], [99], [100], [101], [102], [103]). The glutamatergic synapses *are found throughout the brain and spinal cord in neurons and glia*. Glu increases CBF by activating postsynaptic neurons and pery-synaptic glial cells; as mentioned earlier, Glu can also activate the pericytes that wrap around brain capillary endothelial cells ([13], [14]). Glu concentration in the plasma range between 50-100 $\mu\text{mol/L}$ in human and in other species ([104]), while in the brain it falls to 0.5-2 $\mu\text{mol/L}$ due to BBB activity ([105]). However, during synaptic transmission, Glu concentration within the synaptic cleft may rapidly reach 160-190 $\mu\text{mol/L}$ ([106]), Glu concentration inside the synaptic vesicles being around 60 mM ([107]); Glu can be synthesized by transamination of 2-oxoglutarate, an intermediate of the Krebs cycle ([108]) or by the mitochondrial enzyme glutaminase from the precursor glutamine. Glu act by binding to and activating an array of Glu receptors (GluRs). GluRs in the central nervous system are divided into the ionotropic GluRs, which are ligand-gated ion channel receptors, and metabotropic GluRs, which are associated with G proteins ([109]). Ionotropic GluRs are in turn classified into three groups based on their pharmacology and structural properties. N-methyl-D-aspartate (NMDA)-type receptors are heteromeric complexes comprised of NR1 subunit combined with one or more NR2 subunits ([110]). In the brain, NMDA receptors were detected in cerebral cortex and most other structures. Non-NMDA ionotropic GluRs include AMPA (GluR1–GluR4) and kainate receptors (GluR5–GluR7) that have similar pharmacologic properties. Multiple metabotropic GluRs (mGluR1–mGluR5) that are coupled to diverse second messenger systems, including phosphoinositides, phospholipase D, and cyclic AMP (cAMP), are also widely distributed in the brain ([111]). Glu-mediated signaling leads to an increase in $[\text{Ca}^{2+}]_i$ in the target cells which is mediated either by the Ca^{2+} -permeable NMDA receptors or by the Gq-coupled mGluR1 and mGluR5, which activates the Ca^{2+} /Calmodulin-dependent neuronal nitric oxide synthase (NOS) to release NO ([100], [101], [103], [112], [113]). Glu-induced NO release, in turn, causes vasodilation in both cerebellar ([13, 114]) and hippocampal microvasculature ([115]), while it plays a permissive role in AA metabolites-induced

vasodilation in the cortex by suppressing 20-HETE synthesis ([8]). Furthermore, the relative importance of the different Glu-released messengers (i.e. release of NO from neurons and release of arachidonic acid derivatives from astrocytes) varies between brain regions. Actually, it is unclear whether brain endothelial cells also sense Glu through an elevation in $[Ca^{2+}]_i$ and NO production. As mentioned above, recent publications have showed that NMDA receptor coactivation by glutamate and D-serine increases lumen diameter in pressurized mouse middle cerebral arterioles in an endothelial and eNOS-dependent mechanism ([30]).

Nitric Oxide

Nitric oxide (NO) is the signaling molecule originally identified as endothelium-derived relaxing factor mediating relaxation of blood vessels ([91]). It is a small, highly diffusible, and reactive molecule with a short lifetime that is generated by NO synthase (NOS) through enzymatic conversion of L-arginine to L-citrulline ([116]). Three NOS genes with distinct tissue localization and properties are known: neuronal (nNOS), inducible (iNOS) and endothelial (eNOS). Activation of eNOS and nNOS is classically Ca^{2+} /calmodulin dependent, with nNOS being closely coupled to Ca^{2+} -permeable NMDA receptors at the postsynaptic neurons ([117]), and eNOS tethered to Orai1 in vascular endothelial cells ([118], [119]). NO decreases vascular tone by stimulating cGMP synthesis, thereby leading to the subsequent activation of cGMP-dependent protein kinase (PKG). VSMC contraction is driven by an increase in $[Ca^{2+}]_i$, which recruits the Ca^{2+} /calmodulin-dependent myosin light chain kinase (MLCK). MLCK, in turn, phosphorylates the two light chains of myosin, thus allowing the sliding of these filaments along those of actin and inducing VSMC contraction. The contractile state can also be favored by the action of the RhoA protein, capable of phosphorylate the lateral myosin chain (MLC) and the lateral chain phosphatase of myosin (MLCP) by inactivating it. NO acts by increasing the activity of a protein, termed soluble guanylated cyclase (sGC), which catalyzes the transformation reaction of GTP (Guanosine-5'-triphosphate) into cGMP (guanosine cyclic monophosphate), an intracellular second messenger inside the cells that is capable of activating PKG. PKG phosphorylates its target proteins, thereby inhibiting voltage-gated the Ca^{2+} entry and activating Ca^{2+} -dependents K^+ channels, which cooperate to hyperpolarize the plasma membrane and terminate the contraction. Moreover, PKG may also block Ca^{2+} release from sarcoplasmic reticulum (SR) and the RhoA protein-mediated contraction. In addition to inhibiting VSMC contraction, NO may activate the PGE2 receptor to suppress 20-HETE synthesis and cause arteriolar dilation ([12]). Therefore, if the main cause of the blood flow increase is AA

generation by astrocytes, then having NO present to inhibit 20-HETE formation will ensure that only the vasodilatory prostaglandin and EET derivatives of AA will affect arteriole diameter. More in general, it has been proposed that NO induces vasodilation in both cerebellar [13, 114] and hippocampal microvasculature [115], while it plays a permissive role in arachidonic acid (AA) metabolites-induced vasodilation in the cortex by suppressing the synthesis of the vasoconstricting 20-hydroxy-eicosatetraenoic acid (20-HETE) [8]. It should be pointed out that, according to the general agreement, the main NOS isoform responsible for modulating CBF is nNOS. However, as mentioned earlier, eNOS drives arteriolar dilation during cholinergic transmission and has been recently linked also to glutamatergic signalling. In addition, many experiments indicate that eNOS activation can influence synaptic plasticity in the cortex and striatum ([120], [121]). Current literature also strongly supports the major role of eNOS in modulation of synaptic function in the hippocampus which is the first and most severely affected brain region in the pathogenesis of Alzheimer's disease ([122]). Indeed, studies conducted in mice that are doubly mutant in eNOS and nNOS demonstrated that long-term potentiation is dependent on phasic release of NO caused by nNOS activation, as well as tonic release of NO caused by eNOS activity ([123]). This conclusion was confirmed by the results generated by pharmacological and genetic inactivation of eNOS ([124]). Moreover, prior studies indicate that endothelium-derived NO can travel up to 100 mm distance from endothelial cells ([125], [126]). The distance between brain capillaries and neuronal cells is around 40 μm well within the range of NO diffusion. Consistent with these observations, studies in experimental animals (reviewed by [127], [128]) support the concept that intact NO/cGMP signaling is an essential mechanism required for memory formation. Altogether, these results underline a key role of endothelial NO produced by brain endothelial cell in synaptic plasticity and memory formation; therefore, it is becoming apparent that the role of endothelial NO in the control of central nervous system function is very complex.

The calcium toolkit in vascular endothelial cells

It has long been known that an increase in $[Ca^{2+}]_i$ plays a key role in the intricate network of signal transduction pathways exploited by vascular ECs to regulate most of the cellular processes ([129], [130]). Due to its strategic location at the interface between vascular wall and blood stream, the endothelium is exposed to a myriad of transmitters (release by automatic and sensory nerves or platelets), circulating hormones, autacoids, cytokines, growth factors and drugs, as well as to mechanical stimuli, such as pulsatile stretch, shear stress and changes in the local osmotic pressure ([131], [132]). An extensive array of proteins, membrane receptors, transporters and ion channels, which are located both on the plasmalemma and within the intracellular Ca^{2+} reservoirs (namely, endoplasmic reticulum, lysosomes and Golgi), may be utilized by ECs to selectively detect and properly react to the incoming stimulus ([31], [133]). The spatio-temporal profile of the ensuing Ca^{2+} signal further contributes to enable ECs to select the most suitable response to extracellular inputs, i.e. production of vasoactive mediators (NO, PGI₂, H₂S, EDHF and EDCF), biosynthesis of von Willebrand factor and tissue plasminogen activator, control of intercellular permeability, ICAM-1 expression and NF- κ B activation, cell proliferation, angiogenesis and wound repair ([129], [134], [135], [136], [137], [138], [139], [140], [141]).

In the absence of extracellular stimulation, the $[Ca^{2+}]_i$ is very low (100 nM) due to the combined activity of two high affinity/low capacity Ca^{2+} transporters, that extrude Ca^{2+} out the cytosol ([142]). More specifically, the plasma membrane Ca^{2+} -ATPase (PMCA) and the sarco-endoplasmic reticulum Ca^{2+} -ATPase (SERCA) remove cytosolic Ca^{2+} by direct ATP hydrolysis, while the Na⁺/ Ca^{2+} exchanger (NCX) clears intracellular Ca^{2+} by exploiting the Na⁺ gradient across PM ([142], [143]). The increase in $[Ca^{2+}]_i$ is caused by the opening of Ca^{2+} -permeable channels located both in the PM and in the endoplasmic reticulum (ER), the main intracellular Ca^{2+} reservoir, the channels are activated by extracellular chemical and physical stimuli and permit the passive passage of the ions that are permeable to. The Ca^{2+} concentration in the extracellular medium and in the ER lumen is very high (in the range of mM and μ M, respectively) when compared to cytoplasm concentration. The entry of Ca^{2+} from outside and its release from ER lumen represent the main ways to increase $[Ca^{2+}]_i$ in all cell types. Endothelial cells are considered electrically non-excitable as they do not have voltage-dependent Ca^{2+} channels which are typical in neurons and muscle, skeleton and cardiac fibres. The most common Ca^{2+} entry pathway from the extracellular space of those cells is the so-called store-operated calcium entry (SOCE), which is activated following depletion of the ER Ca^{2+} pool ([144], [145], [146], [128]).

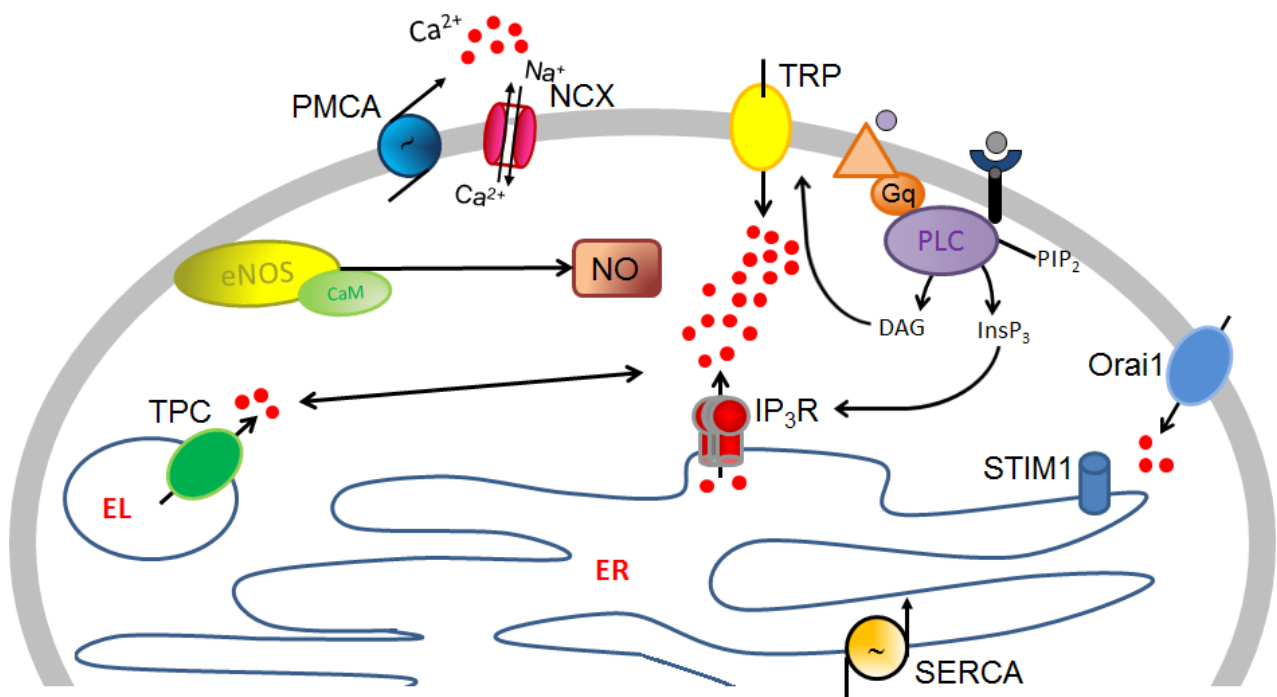


Figure 2. Overview of the basic elements of the Ca^{2+} signaling toolkit in endothelial cells.

An increase in $[\text{Ca}^{2+}]_i$ is the physiological response to a variety of extracellular chemical and physical stimuli that bind to their specific receptors. The following activation of PLC cleaves PIP_2 in InsP_3 and DAG. InsP_3 , in turn, releases Ca^{2+} from the ER binding InsP_3Rs , while DAG may induce Ca^{2+} entry by gating some of TRP channels. The InsP_3 -dependent Ca^{2+} release from ER causes the translocation and clustering of Stim1 with Orai1, an alternative Ca^{2+} -permeable route on the PM that obliged to the process of CICR. Another way to increase the $[\text{Ca}^{2+}]_i$ is due to the depletion of EL reservoir, though the NAADP-dependent opening of TPC. Ca^{2+} signals return to pre-stimulated levels through the concerted action of the mitochondrial uniporter, SERCA and PMCA pumps, as well as through NCX. The signalling function of Ca^{2+} is carried out by a number of Ca^{2+} -sensitive decoders (eNOS, calmodulin, NO) and downstream targets.

ER, endoplasmic reticulum; EL endo-lysosomal system; Gq, Gprotein coupled receptor; PLC, phospholipase C; PIP_2 , phosphatidylinositol-4,5-bisphosphate; InsP_3 , inositol-1,4,5-trisphosphate; DAG, diacylglycerol; InsP_3R , InsP_3 receptors; TPC, two pore channels, NCX, Na^+ - Ca^{2+} exchanger; PMCA, plasma membrane Ca^{2+} ATPase; SERCA, Sarco-Endoplasmic Reticulum Ca^{2+} -ATPase; NO, nitric oxide; CaM calmodulin; eNOS endothelial NO synthase.

An increase in $[\text{Ca}^{2+}]_i$ up to $1 \mu\text{M}$ is the key signal to activate vascular ECs following recruitment of either tyrosine-kinase linked receptors (TRKs) or G-protein coupled receptors (GPCRs) by growth factors and vasoactive agents, respectively ([137], [139], [132], [138], [140]). More specifically, the β isoform of PLC ($\text{PLC}\beta$) is engaged by GPCRs, while TKRs recruit $\text{PLC}\gamma$ ($\text{PLC}\gamma$) ([142], [31]). $\text{PLC}\beta$ and $\text{PLC}\gamma$ are part of a larger family of PLC isoforms that additionally includes $\text{PLC}\delta$, $\text{PLC}\epsilon$, and $\text{PLC}\zeta$. $\text{PLC}\epsilon$ is proposed to be activated by small GTPases like Rho and Ras whereas $\text{PLC}\delta$ is activated by $[\text{Ca}^{2+}]_i$ in the range of 0.1–10 mM ([147], [148]). PLC, in turn, cleaves phosphatidylinositol-4,5-bisphosphate (PIP_2) into InsP_3 and diacylglycerol (DAG). DAG remains bound to the PM, where it

recruit both protein kinase C (PKC) and some Ca^{2+} -permeable, nonselective cation channels belonging to the canonical transient receptor potential (TRPC) family of ion channels ([142], [149]). The InsP_3Rs represent the most important channels for the release of Ca^{2+} from the ER. It is well known that at least three isoforms of InsP_3Rs exist both in animal and human cells ([150]). ECs, in particular, express the subtypes 1 and 3 ($\text{InsP}_3\text{R1}$ and $\text{InsP}_3\text{R3}$). From the structural point of view, InsP_3Rs are tetramers made up by four subunits, each constituted by approximately 2700 aminoacidic residues and containing a binding site for InsP_3 . The InsP_3 -mediated Ca^{2+} release is a cooperative process, since it requires the intervention of all subunits for the channel to open ([151]). A characteristic of InsP_3Rs is that they are differentially regulated by InsP_3 , Ca^{2+} and ATP. The Ca^{2+} dependence of InsP_3Rs is biphasic. Nanomolar doses of Ca^{2+} activate the channel, while concentrations in the range of hundreds of μM inhibit InsP_3R activity. InsP_3Rs are associated to various proteins involved in decoding Ca^{2+} signals; for instance, calmoduline (CaM) plays an important role in InsP_3 channels regulation. Similarly, the cytosolic site of the receptor-channels presents consensus sequences for numerous protein kinases, including protein kinase C (PKC), protein kinase A (PKA), and calmodulin-dependent protein kinase II (CaMKII) ([152]). Finally, endothelial InsP_3Rs are mainly distributed in the perinuclear region: the recruitment of a InsP_3Rs cluster generates a localized Ca^{2+} signal (termed “ Ca^{2+} puff”) which is then transformed in a global Ca^{2+} wave by the opening of the adjacent receptors following diffusion of InsP_3 and Ca^{2+} itself. This mechanism has been given the name in Ca^{2+} -induced Ca^{2+} release (CICR).

Intracellular Ca^{2+} pools may be also recruited by ryanodine receptors (RyRs), which are stimulated by Ca^{2+} itself and modulated by the cyclic ADP-ribose (cADPr). RyRs have been found in different tissues, in particular in striated muscles. Three isoforms have been identified: RyR1, RyR2 and RyR3 which are typical of the skeletal muscles, cardiac tissue and striated muscle respectively. The three isoforms are assembled as homo-tetrameric channels consisting of four 560 kD polypeptides [153]. At the subunit level, each RyR subunit presents with a very large cytosolic NH_2 domain followed by a central regulatory domain that recognized and binds to several regulatory proteins such as CaM, calstabin, sorcin and presents binding sites for cytosolic ions and modulators, including Ca^{2+} , Mg^{2+} and adenine nucleotides [154]. RyRs may also be modulated PKA- and CaMKII-mediated phosphorylation, may undergo oxidative/nitrosative modifications and undergo pH modulation ([155], [31]). Ca^{2+} release from RyRs in ECs, as well as in both excitable and non-excitable cells ([155]), is triggered by CICR ([156]), that occurs 1-10 μM Ca^{2+} nearby the receptor and is prevented when Ca^{2+} is 1-10 mM ([155]). RyRs may be pharmacologically activated by the

methylxanthine derivate, caffeine, which sensitizes the receptor to resting Ca^{2+} levels, and by ryanodine, which binds to and locks the receptor in an open state ([157]).

Along with the Ca^{2+} release through InsP_3Rs and/or RyRs , luminal ER Ca^{2+} can be spontaneously released through other mechanisms that have not yet been identified. Indeed, under resting conditions, a continuous leakage of Ca^{2+} from RE occurs. This leakage is generally resequenced back into ER lumen by SERCA pumps. As a consequence, the blockade of SERCA activity, which can be accomplished by specific inhibitors such as thapsigargin and cyclopiazonic acid (CPA), results in the slow accumulation of Ca^{2+} in the cytosol. The mechanism which is responsible for Ca^{2+} leakage from ER is still subject of study, although a number of proteins have been involved, including translocons, pannosins, TRPM8 channels, Orai3 channels, InsP_3Rs and RyRs , the latter two channels being constitutively gated by the basal levels of InsP_3 and Ca^{2+} .

The latest addition to the family of intracellular Ca^{2+} channels is constituted by two pore channels (TPCs), which sit on the membrane of the endo-lysosomal (EL) system ([158], [159]). TPCs have been regulated by the nicotinic acid adenine dinucleotide phosphate (NAADP) ([160], [161], [162]). NAADP is generated from nicotinamide adenine dinucleotide phosphate (NADP) by CD38 in a base-exchange reaction occurring at acidic pH, targets acidic organelles and mobilizes Ca^{2+} from the EL Ca^{2+} storage compartment. Ca^{2+} is sequestered into EL by a putative $\text{Ca}^{2+}/\text{H}^+$ exchanger, which is driven by a vacuolar- H^+ ATPase ([158]). TPC1 is expressed on both endosomes and lysosomes, while TPC2 is exclusively present on lysosomes ([163]). Due to the limited amount of Ca^{2+} in the endolysosomal compartment, which consists in small vesicles (0.2-1 μm in diameter) trafficking throughout the cytosol, NAADP-induced Ca^{2+} signals *per se* appear as scattered, discrete events ([160], [163]). The relatively small quantity of Ca^{2+} discharged by EL may, however, be amplified into a global Ca^{2+} wave by recruitment of InsP_3Rs and RyRs via CICR ([164], [161]).

Emptying of ER Ca^{2+} stores through the process of CICR leads to the opening of the so-called "store-operated" channels (SOCs), which are located on the PM and mediate Ca^{2+} responsible for store refilling via SERCA ([142], [165]). The best characterized SOC is the Ca^{2+} release-activated Ca^{2+} (CRAC) channel, which was first identified in lymphocytes, mast cells and other immune cells ([166]), but has since identified in many other cell types, including ECs ([167], [168]) and mouse neuronal progenitor cells ([169]). CRAC channels are activated by InsP_3 -dependent store depletion due to the physical coupling between the ER Ca^{2+} -sensor, Stromal Interaction Molecule-1 (Stim1) and the channel protein, Orai1, on the PM ([170], [171], [145], [146], [172]). Stim1 is a single-pass transmembrane protein endowed with a Ca^{2+} -binding EF domain on the amino (N)-terminal ER

luminal portion ([173]). When ER Ca^{2+} concentration falls below a threshold level due to InsP_3 -dependent Ca^{2+} release, Ca^{2+} dissociates from EF1, Stim1 proteins rapidly redistribute to peripheral ER sites in close proximity to PM, where they multimerized ([173], [174]). Orai1, in turn, is a 33 kDa PM protein with a tetraspanning PM topology and cytosolic NH_2 - and COOH - tails ([173], [174]). Orai1 serves as the pore-forming subunit of CRAC channels: it exists as a dimer in un-stimulated cells, but forms tetramers after the InsP_3 -dependent store emptying ([173], [174]). Stim1 and Orai1-mediated Ca^{2+} entry is gated a current displaying biophysical features similar to those of the Ca^{2+} release activated Ca^{2+} (CRAC) current recorded in hematopoietic cells, i.e. strong inward rectification, reversal potential (E_{rev}) $>+60$ mV, permeability to Ca^{2+} , but not to Na^+ and K^+ under physiological conditions, and a single-channel conductance in the order of fS ([144], [175]). This current is characterized by its high selectivity for Ca^{2+} ions, an inwardly rectifying current-voltage relationship, and an extremely small single channel conductance in the sub-picoSiemens range ([176], [177]). Other CRAC-related proteins are Stim2, Orai2, and Orai3, which may be involved in store-dependent Ca^{2+} influx in heterologous expression systems, although their contribution to SOCs in naïve cells is yet to be fully appreciated. Nevertheless, Orai2 mediates the I_{CRAC} in mouse neurons ([178]), whereas Orai3 is one of the main candidates to mediate SOCE in cancer cells ([179]).

An alternative pathway for endothelial SOCE has been reported in a number of vascular beds, as Stim1 may recruit additional Ca^{2+} -permeable pathways, which include some members of the Canonical Transient Receptor Potential (TRPC) sub-family of cationic channels, such as TRPC1 and TRPC4 ([180]). The formation of a supermolecular complex involving Stim1, Orai1, TRPC1 and TRPC4 has indeed been reported ([181]). Moreover, Ca^{2+} entry may occur through DAG-sensitive channels, such as TRPC3 and TRPC6 ([182], [183]). Of note, DAG itself may be converted by DAG lipase into AA, which may be further metabolized to EETs to activate Ca^{2+} influx through TRPV4 channels ([184]). Alternately, extracellular autacoids may recruit phospholipase A2 to cleave off AA from membrane-bound fatty acids ([185]). An additional mode for agonists-induced Ca^{2+} entry in vascular ECs is provided by ionotropic receptors, such as nicotinic receptors (nAChRs), ATP-sensitive P2X receptors, and cyclic nucleotide gated channels ([186]). Finally, mechanical stimuli (e.g. pulsatile stretch, laminar shear stress, and changes in the local osmotic pressure) may promote Ca^{2+} entry through a number of mechano-sensitive channels, including polycystin TRP 2 (TRPP2) ([187]), TRPV4([184], Piezo1 [188]) and heteromeric TRPC1-TRPP2 ([189]).

Calcium signals in brain endothelial cells

Calcium ions play an important role in the control of BBB permeability. Every time that the extracellular Ca^{2+} concentration is decrease under the normal condition around 1.5 mM at the blood side and 1 mM at the brain interstitial side ([190]) and/or when the intracellular free Ca^{2+} concentration rise up the normally 50–100 nM ([191], [192]), normal BBB function may be modified or disturbed. Decreased extracellular Ca^{2+} levels result in a disruption of cell–cell and cell–matrix adhesive interactions ([193]), but also give rise to intracellular Ca^{2+} signaling pathways ([194]). Less is known about the vasoactive outcome of endothelial Ca^{2+} signals inside the cerebral circle. The $[\text{Ca}^{2+}]_i$ changes in brain endothelial cells can occurs in many different way, that are highly organized in time, localization and duration: usually the increase of $[\text{Ca}^{2+}]_i$ may appear as a localized elementary blips or puffs that result from the activation of single or clustered InsP_3Rs , that will eventually merge to form a global intracellular Ca^{2+} wave. These waves are not restricted to the cytoplasm of one cell but may pass through the cells and spread as an intercellular Ca^{2+} wave that is defined as a propagating $[\text{Ca}^{2+}]_i$ increase that originates in a single cell and sequentially engages neighboring cells ([195]). Often, in brain endothelial cells, chemical stimulation results in a series of high frequency Ca^{2+} oscillations, which are supported by Ca^{2+} mobilization from the intracellular store and Ca^{2+} entry from the extracellular space. The variations in Ca^{2+} spike duration, frequency and amplitude, combined with different mechanism that sustain Ca^{2+} oscillations, induced the activation of different Ca^{2+} -dependent pathways that achieve distinct response. Additionally, a continued oscillation pattern is important to avoid the possible toxic effect of a prolonged increase of the $[\text{Ca}^{2+}]_i$ and in the meantime may exert temporal control over cellular functions ([196]).

It has long been appreciated that Ca^{2+} oscillations result from a coordinated release of intracellular stores and increased Ca^{2+} influx across the plasma membrane ([197], [198]). The intracellular release of Ca^{2+} most commonly results from InsP_3 -dependent Ca^{2+} release, whereas Ca^{2+} entry is mediated by SOCE ([199], [200]). Type 2 InsP_3R ($\text{InsP}_3\text{R}2$), which shows the sharpest dependence on cytosolic Ca^{2+} and has the highest affinity for InsP_3 , is the main oscillatory unit as shown in DT40 cells ([201]) and myocytes ([202]). Stimulation of type 1 receptor ($\text{InsP}_3\text{R}1$) can also lead to oscillations, but most often damped rather than sustained ([203], [201]). In contrast, type 3 receptor ($\text{InsP}_3\text{R}3$) tends to suppress oscillations. This surprising result is because $\text{InsP}_3\text{R}3$, which is not inhibited by Ca^{2+} , provides a constant flux of Ca^{2+} without providing the feedback necessary for oscillations to occur ([196]).

With regard to BBB endothelial cells, intercellular Ca^{2+} waves have been reported in response to mechanical cell stimulation or photoliberation of caged- InsP_3 in primary rat brain capillary ECs or immortalized cells from the same origin (GP8/3.9 and RBE4) ([204], [205]). In bEnd3 mouse BBB ECs, intercellular Ca^{2+} waves were triggered by the production of a localized oxidative insult upon illumination of a photosensitizer probe ([206]). Inter-endothelial Ca^{2+} waves propagating in arterioles are believed to strengthen a conducted vasodilation ([207], [208]) while also being involved in hypoxic preconditioning ([209]). Ca^{2+} oscillations in BBB endothelial cells occur in response to bradykinin, ATP and histamine ([210]) and were inhibited by hypoxia ([211]), which reduced both ER Ca^{2+} levels and SOCE.

Although the observation of Ca^{2+} oscillations and intercellular Ca^{2+} wave propagation in brain capillary endothelial cells indicate that all essential elements of the Ca^{2+} signaling toolkit are available, the molecular architecture of the Ca^{2+} toolkit in brain microvascular endothelial cells are yet to be fully elucidated ([212]). For instance, only $\text{InsP}_3\text{R1}$ has been recently found in human brain ECs ([213]), while there is no report about the other InsP_3R isoforms or RYRs. Moreover, while all PLC subtypes (except $\text{PLC}\zeta$) have been identified in the brain, little is known on their presence and function in brain microvascular ECs ([214]). There is also scarce information as regard to the Ca^{2+} -transporting systems. In rat brain capillary ECs, SERCA provides the major pathway responsible for clearing cytosolic Ca^{2+} , whereas the contribution of NCX in extruding ER-released Ca^{2+} is far less important (around 30%) of the calcium ions mobilized from ER ([215]). Nevertheless, NCX expression *in situ* has been reported in rat brain ECs ([216]).

Surprisingly, while TRP and Orai channels are widely studied in vascular ECs ([31], [217]), little is known about their expression and function in brain ECs. TRPC1 has been found interact with TRPC3 in bovine brain capillary ECs, in which they are responsible for Ca^{2+} entry induced by the application of ATP ([218]). Moreover, TRPV1 is expressed in human brain capillary and microvascular eECs and is involved in EDHF-dependent vasodilation induced by AA derivatives ([219]). Interestingly, TRPV4 and TRPV3 are also expressed in ECs from pial arteries and cerebral parenchymal arterioles and they are responsible for Ca^{2+} influx in response to EETs and carvacrol, respectively; TRPV4- and TRPV3-mediated Ca^{2+} influx can have a robust impact on cerebrovascular tone ([220], [221]). As to SOCE, the genetic down-regulation of Stim1 and Orai1 in a bovine brain endothelial cell line, t-BBEC117, decreases SOCE and reduces cell proliferation. Intriguingly, Orai2 is up-regulated at the G2/M phase of cell cycle and somehow negatively modulates SOCE activity [222]. A subsequent study revealed that hypoxia increases SOCE by inducing the up-regulation of

the Ba²⁺-sensitive inward rectifier K⁺ channel, Kir2.1, thereby causing membrane hyperpolarization and boosting cell proliferation ([223]).

Taking together these information, we could give an important input in elucidating the composition and role of the Ca²⁺ toolkit of brain ECs. In this work, we first will investigate the Ca²⁺ response induced by Ach and Glu in mouse brain endothelial cells (bEND5). Finally, we will compare these results with a human brain cells line (hCMEC/D3).

MATERIALS AND METHODS

Cell culture

The bEND5 (American Type Culture Collection, Manassas, VA, USA) is an immortalized mouse cell line derived from mouse brain endothelium of BALB/c mice. Immortalisation has been carried out by infection of primary cells with retrovirus coding for the Polyoma virus middle T-antigen. bEND5 cells are positive for endothelial specific proteins (PECAM-1, Endoglin, MECA-32, Flk-1) tested by FACS. Inflammatory cytokines induce the expression of proteins such as CAM-1, VCAM-1 and E-selectin [224].

The bEND5 cells were used to investigate the Ca^{2+} and NO response to Ach in mouse brain microvascular endothelial cells. Cells were grown in Dulbecco's modified Eagle's medium (DMEM; Gibco Invitrogen, Carlsbad, CA, USA) supplemented with 10% fetal bovine serum, 2 mmol/L L-glutamine, 1mmol/L sodium pyruvate, 100 Units/mL penicillin, and 10 ng/mL streptomycin, 1% minimal essential medium nonessential amino acids exactly, as originally described previously [224]. Cells were cultured in a humidified cell culture incubator at 37°C and an atmosphere of 5% CO_2 /95% air. The bEND5 cells were used for experiments from passages 15 to 25.

Human brain endothelial cells (hCMEC/D3) were obtained from Institut National de la Santé et de la Recherche Médicale (INSERM, Paris, France). hCMEC/D3 cells cultured between passage 25 and 35 were used. The cells were seeded at a concentration of 27,000 cells/cm² and grown in tissue culture flasks coated with 0.1 mg/mL rat tail collagen type 1, in the following medium: EBM-2 medium (Lonza, Basel, Switzerland) supplemented with 5% fetal bovine serum (FBS), 1% Penicillin–Streptomycin, 1.4 μM hydrocortisone, 5 $\mu\text{g}/\text{mL}$ ascorbic acid, 1/100 chemically defined lipid concentrate (Invitrogen), 10 mM HEPES and 1 ng/mL basic FGF (bFGF). The cells were cultured at 37 °C, 5% CO_2 saturated humidity.

Solutions

Physiological salt solution (PSS) had the following composition (in mM): 150 NaCl, 6 KCl, 1.5 CaCl₂, 1 MgCl₂, 10 Glucose, 10 Hepes. In Ca²⁺-free solution (0Ca²⁺), Ca²⁺ was substituted with 2 mM NaCl, and 0.5 mM EGTA was added. Solutions were titrated to pH 7.4 with NaOH. In Mn²⁺-quenching experiments, 200 μM MnCl₂ was added to the 0Ca²⁺ external solution. The osmolality of the extracellular solution, as measured with an osmometer (Wescor 5500, Logan, UT), was 338 mmol/kg.

Fluorescence microscope

Fluorescence microscopy is probably the most rapidly expanding technique in comparison to the others. The enormous development of fluorescent indicators in the last forty years has contributed to significantly expand the exploration possibilities of this technique. In the biological field its application was initially confined to the localization of structures and/or proteins in cells or tissues and was mainly based on immunofluorescence techniques.

[Ca²⁺]_i measurements

bEND5 or hCMEC/D3 cells were loaded with 4 μM fura-2 acetoxymethyl ester (Fura-2/AM; 1 mM stock in dimethyl sulfoxide) in PSS for 20 min at room temperature. After washing in PSS, the coverslip was fixed to the bottom of a Petri dish and the cells observed by an upright epifluorescence Axiolab microscope (Carl Zeiss, Oberkochen, Germany), usually equipped with a Zeiss ×40 Achromplan objective (water-immersion, 2.0 mm working distance, 0.9 numerical aperture). The cells were excited alternately at 340 and 380 nm, and the emitted light was detected at 510 nm. A first neutral density filter (1 or 0.3 optical density) reduced the overall intensity of the excitation light and a second neutral density filter (optical density=0.3) was coupled to the 380 nm filter to approach the intensity of the 340 nm light. A round diaphragm was used to increase the contrast. The excitation filters were mounted on a filter wheel (Lambda 10, Sutter Instrument, Novato, CA, USA). Custom software, working in the LINUX environment, was used to drive the camera (Extended-ISIS Camera, Photonic Science, Millham, UK) and the filter wheel, and to measure and plot on-line the fluorescence from 30-45 rectangular “regions of interest” (ROI) enclosing 30-45 single cells. Each ROI was identified by a number. Adjacent ROIs never superimposed. [Ca²⁺]_i was monitored by measuring, for each ROI, the ratio of the mean

fluorescence emitted at 510 nm when exciting alternatively at 340 and 380 nm (shortly termed "ratio"). An increase in $[Ca^{2+}]_i$ causes an increase in the ratio. Ratio measurements were performed and plotted on-line every 3 s. The experiments were performed at room temperature (22°C).

Mn^{2+} has been shown to quench Fura-2 fluorescence. Since Mn^{2+} and Ca^{2+} share common entry pathways in the plasmalemma, Fura-2 quenching by Mn^{2+} is regarded as an index of divalent cation influx ([225]). Experiments were carried out at the 360 nm wavelength, the isosbestic wavelength for Fura-2, and in Ca^{2+} -free medium supplemented with 0.5 mM EGTA, as previously described ([226], [128]). This avoids Ca^{2+} competition for Mn^{2+} entry and therefore enhances Mn^{2+} quenching.

NO was measured as described in ([119]) and ([227]). Briefly, bEND5 or hCMEC/D3 were loaded with the membrane permeable NO-sensitive dye 4-Amino-5-methylamino-2',7'-difluorofluorescein (DAF-FM) diacetate (10 μ M) for 60 min at room temperature and washed in PSS for one further hour. DAF-FM fluorescence was measured by using the same equipment described for Ca^{2+} recordings but with a different filter set, i.e. excitation at 480 nm and emission at 535 nm wavelength (emission intensity was shortly termed "NO_i"). The changes in DAF-FM fluorescence induced by Ach were recorded and plotted on-line every 3 s. Again, off-line analysis was performed by using custom-made macros developed by Microsoft Office Excel software. The experiments were performed at room temperature.

RNA isolation and Real Time RT-PCR (qRT-PCR) of Ca^{2+} -permeable channels

Total RNA was extracted using the QIAzol Lysis Reagent (QIAGEN, Italy), as recently shown ([228], [229]). The first cDNA copy was synthesized from 1 μ g total RNA using random hexamers and M-MLV Reverse Transcriptase (Invitrogen S.R.L., Milan, Italy). Real-time PCR was performed using GoTaq qPCR master mix according to manufacturer's instructions (Promega, Milan, Italy) on a SFX96 Real-time system (Biorad, Segrate, Italy). Oligonucleotide primers were obtained from Primer3. Ribosomal S18 subunit was tested as housekeeping gene.

Immunoblotting

Immunoblotting was performed as previously described [230]. Briefly, the cells were lysed in 100 μ l RIPA lysis buffer (Santa Cruz Biotechnology, Inc, CA, USA) for 30 min in ice. Lysates were centrifuged at 14,000 g for 10 min at 4°C. Total cell protein extracts were normalized for concentration by the Bradford assay (Bio-Rad Laboratories Segrate Milan Italy). Two different concentrations respectively of 35 μ g and 20 μ g of proteins were separated by SDS-PAGE and transferred to polyvinylidenedifluoride membrane (Millipore's Corporate, Billerica, MA, USA). Membranes were incubated with two anti-mouse antibody Stim 1 and Orai 2 according to the manufacturer's instructions (Santa Cruz Biotechnology, Inc, CA, USA). Anti-mouse horseradish peroxidase-conjugated secondary antibody was used 1:500 (Amersham Biosciences, Inc., Piscataway, NJ, USA) and visualized by the ECL detection system (Amersham Biosciences, Inc. Piscataway, NJ, USA) according to the manufacturer's instructions. Each membrane was probed with the monoclonal anti-actin antibody (Fitzgerald Industries International, USA) to estimate equal protein loading.

Statistics

All the data have been collected from bEND5 cells deriving from at least three coverslips from three independent experiments. The amplitude of Ca^{2+} release in response to either CPA or Ach (1st spike) was measured as the difference between the ratio at the peak of intracellular Ca^{2+} mobilization and the mean ratio of 1 min baseline before the peak. The magnitude of CPA-evoked SOCE upon Ca^{2+} restoration to the bath was measured as the difference between the ration at the peak of extracellular Ca^{2+} entry and the mean ration of 1 in baseline before Ca^{2+} readdition. The rate of Mn^{2+} influx was evaluated by measuring the slope of the fluorescence intensity curve at 400 sec after Mn^{2+} addition. Pooled data are given as mean \pm SE and statistical significance ($P < 0.05$) was evaluated by the Student's t-test for unpaired observations. Data relative to both Ca^{2+} and NO signals and to Mn^{2+} influx rate are presented as mean \pm SE, while the number of cells analyzed is indicated between parentheses.

RESULTS

Acetylcholine induces intracellular Ca²⁺ oscillations in bEnd5 cells

In order to assess whether Ach was able to induce Ca²⁺ signals, bEND5 were loaded with the Ca²⁺-sensitive dye Fura-2/AM and were initially imaged with conventional epifluorescence microscopy. A fraction (~45%) of cells showed spontaneous Ca²⁺ spikes that arose in the absence of external stimulation. For the following evaluation of Ach-induced Ca²⁺ signals, these cells were discarded from the analysis. When Ach was applied to the quiescent cells, we observed a dose-dependent increase in [Ca²⁺]_i with a different pattern depending on agonist concentration (Fig. 1 and Fig. 2).

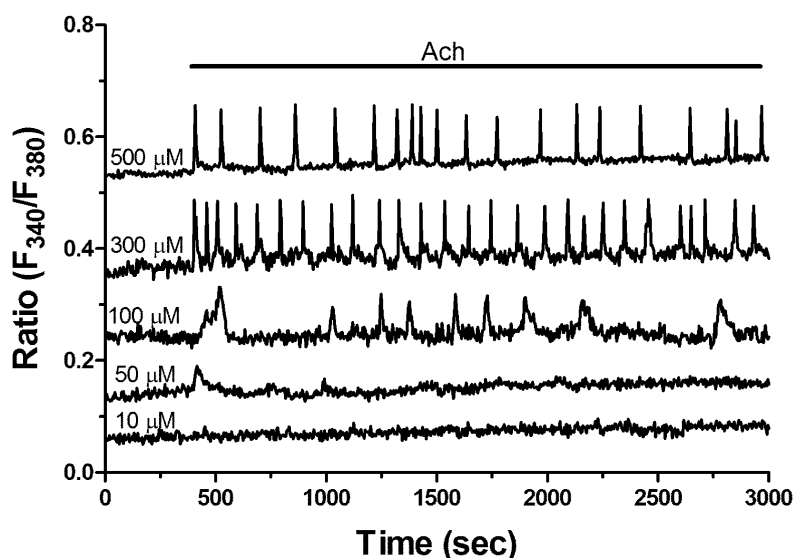


Figure 1. Acetylcholine evokes repetitive Ca²⁺ transients in bEND5 cells. Ach causes the immediate initiation of an oscillatory Ca²⁺ response whose duration, amplitude of the 1st spike and interspike interval (ISI) was a function of agonist concentration. In this and the following figures, Ach was added at the time indicated by the horizontal bar drawn around the Ca²⁺ tracings. The baseline of Ca²⁺ tracings has been shifted to avoid their overlapping for representation purposes.

Ach at 100 μM and above, Ach caused repetitive oscillations in [Ca²⁺]_i, while lower doses of Ach induced only a short Ca²⁺ transient (50 μM) or none (10 μM) (Fig. 1 and Fig. 2). Of note, a slow increase in [Ca²⁺]_i preceded each Ca²⁺ oscillation, giving rise to sub-threshold Ca²⁺ signal known as pacemaker Ca²⁺ ramp ([231]), that led to the regenerative Ca²⁺ upstroke and was a hallmark of InsP₃-driven intracellular Ca²⁺ release. According to the statistical analysis, 300 μM was the most

suitable concentration for Ach to generate a prolonged (up to 1 hour) Ca^{2+} burst in bEND5 cells. Indeed, at this concentration, the frequency of Ca^{2+} transients and the number of oscillations/hour (Fig. 2B) reached their greatest value, while there was no significant ($p < 0.05$) difference in the fraction of responding cells between 100 and 300 μM (Fig. 2A). Notably, while the amplitude of the 1st Ca^{2+} spike was highest at 100 μM (Fig. 2B), there was no statistically relevant difference in the amplitude of the subsequent Ca^{2+} transients at each concentration tested (Fig. 2E). Moreover, the height of the Ca^{2+} peaks significantly ($p < 0.05$) declined from the 1st to the 2nd one, but then it remained constant throughout the Ca^{2+} train at both 100 and 300 μM (Fig. 2E). Conversely, the magnitude of the 2nd Ca^{2+} transient elicited by 500 μM Ach was significantly ($p < 0.05$) lower than the 1st, but higher than the following spikes (Fig. 2E).

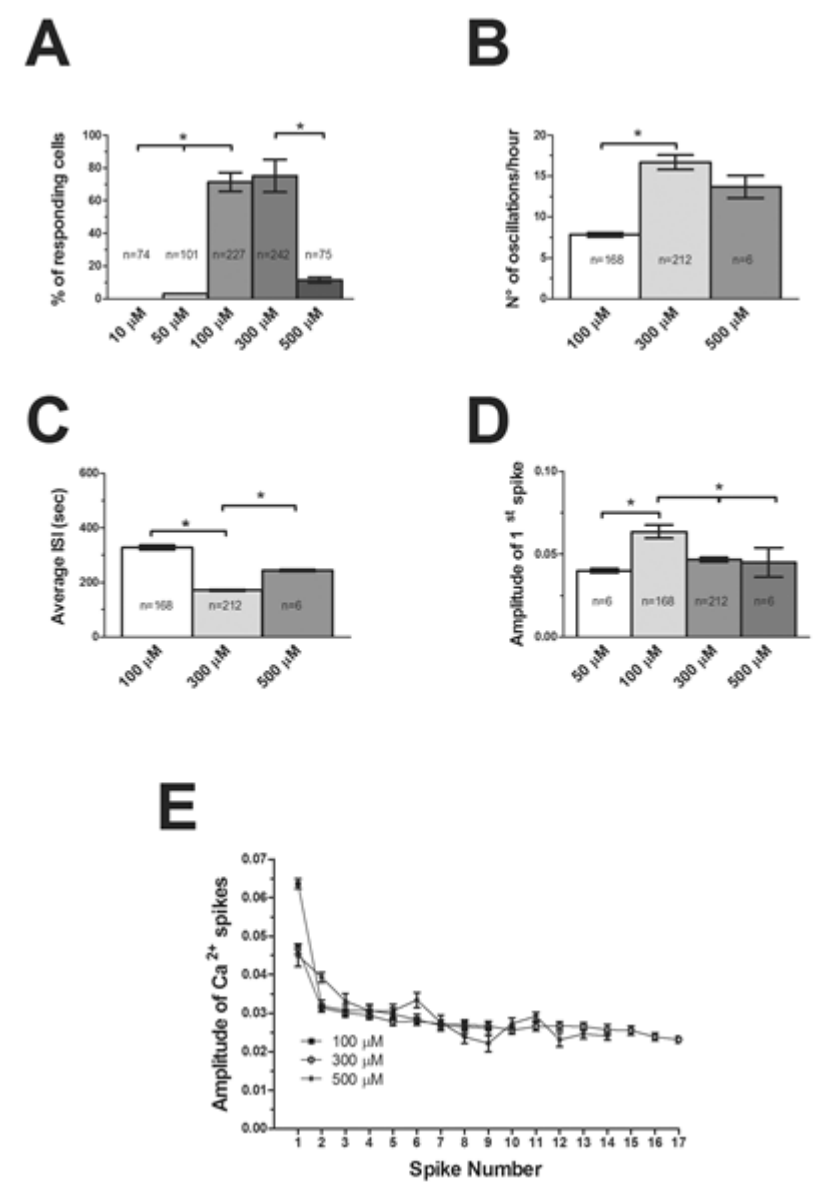


Figure 2. Statistical analysis of Ach-induced intracellular Ca^{2+} oscillations in bEND5 cells. Bar histograms show the average \pm SE of the percentage of responding cells (A), number of oscillations/hour (B), amplitude of the 1st spike (C), average ISI (D) and amplitude of the 2-15th Ca^{2+} spike (E) of Ach-evoked intracellular Ca^{2+} oscillations. The asterisk indicates $p < 0.05$.

Ach-induced intracellular Ca^{2+} oscillations required the continuous presence of the agonist as they were rapidly interrupted upon Ach removal from the perfusate (Fig. 3A). Moreover, they were blocked by atropine (100 μ M, 30 min), a selective mAChR antagonist (Fig. 3B). Conversely, nicotine, a selective agonist of cholinergic nicotinic receptors (nAChRs) ([232]), did not increase $[Ca^{2+}]_i$ in bEND5 cells (Fig. 3C). Taken together, these results suggest that the most frequent Ca^{2+} response induced by Ach in bEND5 consists in Ca^{2+} oscillations that arise upon mAChR activation. Consistently, qRT-PCR revealed that mouse brain microvascular endothelial cells express the transcript encoding for mAChR M3 (M3-mAChR), while those encoding for M1, M2, M4 and M5 are absent (Fig. 3D). The remainder of the experiments was therefore carried out by challenging the cells with 300 μ M, which is within the same range as that shown to induce vasorelaxation in brain intraparenchymal arterioles ([83], [93]).

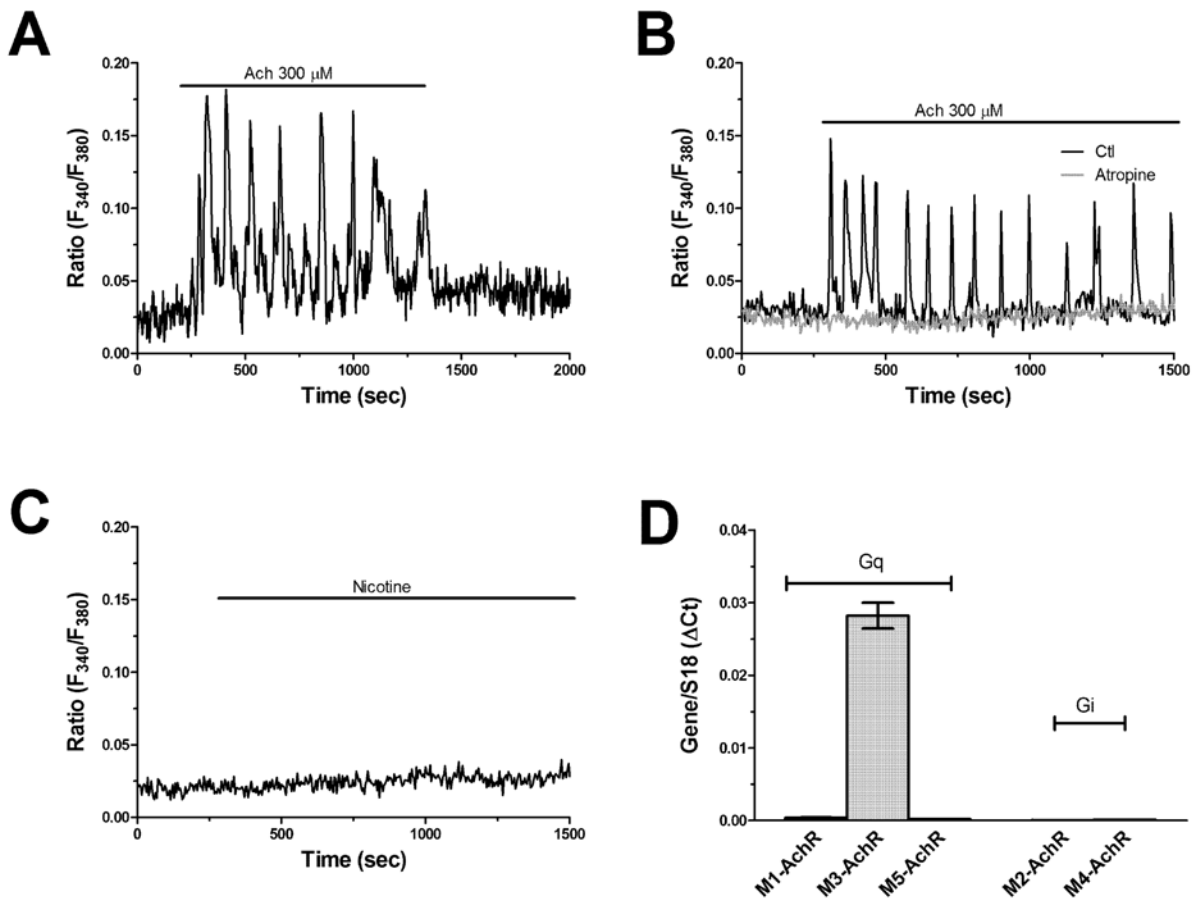


Figure 3. Metabotropic muscarinic receptors drive the onset of acetylcholine-induced intracellular Ca^{2+} oscillations. (A), removal of Ach from the extracellular solution causes the interruption of the ongoing Ca^{2+} burst. (B), atropine (100 μ M, 30 min) prevents the initiation of the Ca^{2+} response to Ach. (C), nicotine (100 μ M) did not increase $[Ca^{2+}]_i$ in bEND5 cells, as also observed in other endothelial cell types. (D), qRT-PCR analysis of metabotropic muscarinic receptors (M-AChRs) revealed that only M3-AChR mRNA is expressed in bEND5. Data are expressed as mean \pm SE of qRT-PCR runs performed in triplicate.

Expression of the components of the Ca²⁺ signaling toolkit in bEND5 cells

As mentioned in the Introduction, the molecular components of the Ca²⁺ toolkit in brain microvascular endothelial cells are largely unknown. Therefore, in order to investigate the signalling machinery that shapes Ach-induced intracellular Ca²⁺ spikes, we first investigated the expression of the components of the endothelial Ca²⁺ toolkit downstream of PLC β activation ([128]). We used qRT-PCR by using the specific primers designed with Primer3. The following transcripts were expressed in bEND5 cells: InsP₃R1 and InsP₃R2 (Fig. 4A); Stim1 and Stim2 (Fig. 4A); Orai2 (Fig. 4A); TRPC1 (Fig. 4B). As observed in many endothelial cell types (Moccia et al., 2012 WJBC), RyRs were absent (Fig. 4A). TRPC2 levels were significantly low as compared to TRPC1, while TRPC4 was almost undetectable (Fig. 4B). Surprisingly, Orai1 (as well as Orai3) transcripts could not be detected (Fig. 4A), which hints at Orai2 as the pore-forming subunit of store-operated channels in bEND5 cells. As anticipated earlier, Orai2 is the major candidate to mediate both constitutive and agonist-stimulated SOCE also in mouse neurons ([231]). Immunoblotting confirmed that both Stim1 and Orai2 were expressed at protein level in bEND5 cells (Fig. 4C). Moreover, the diacylglycerol (DAG)-gated Ca²⁺-permeable Canonical Transient Receptor Potential 3 and 6 (TRPC3 and TRPC6) were not found in bEND5 cells (Fig. 4B). Consistently, oleoyl-acyl-sn-glycerol (OAG; 100 μ M), a membrane-permeable DAG analog that mediates Ach-induced Ca²⁺ entry through TRPC3 and TRPC6 channels ([233], [234]), failed to evoke any detectable Ca²⁺ signal in bEND5 cells (Fig. 4D). Collectively, these results demonstrate that, upon PLC β activation, Ach has the potential to induce ER Ca²⁺ release only via InsP₃Rs and to promote extracellular Ca²⁺ entry through the store-operated Ca²⁺ channel, Orai2.

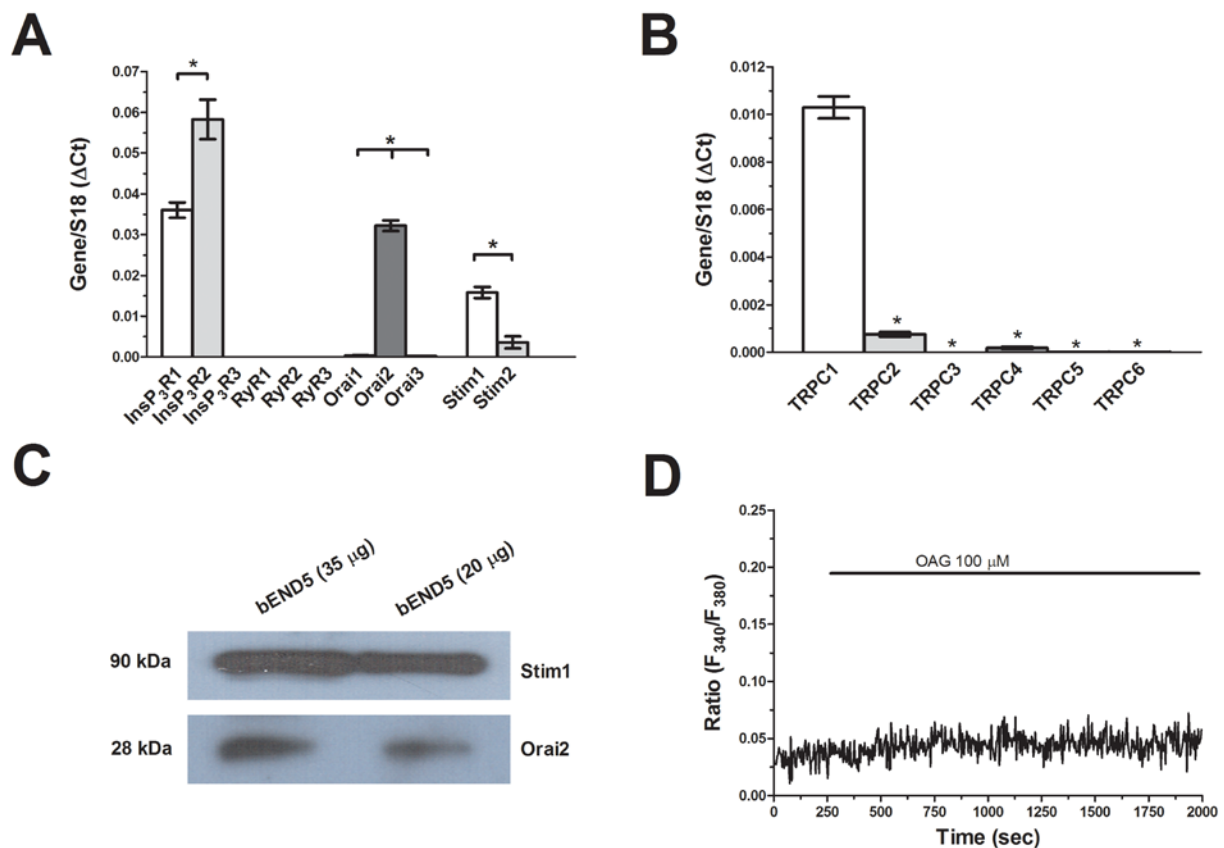


Figure 4. The Ca²⁺ toolkit of bEND5 cells. (A), mRNA levels of InsP₃R1-3, RyR1-3, Orai1-3, and Stim1-2 in bEND5 cells. (B), mRNA levels of TRPC1-6 channels in bEND5 cells. In both (A) and (B), data are expressed as mean±SE of qRT-PCR runs performed in triplicate. (C), Stim1 and Orai2 proteins was detected by immunoblotting, as described in Materials and Methods. Lanes were loaded with 35 or 20 μg of proteins and probed with specific rabbit polyclonal antibodies. A band of about 90 kDa was found for Stim1 and of about 28 kDa for Orai2. Blots representative of three were shown. (D), OAG (100 μM) did not increase [Ca²⁺]_i in bEND5 cells.

Acetylcholine-induced Ca²⁺ oscillations derive from the periodic discharge of intraluminally stored Ca²⁺ through InsP₃Rs

As Ach stimulates Ca²⁺ spiking by activating mAChRs in bEND5 cells, we first assessed the signaling pathway whereby PLCβ triggers the Ca²⁺ response. U73122 (10 μM, 30 min), a rather selective PLCβ inhibitor ([232]), was able to block Ach-induced intracellular Ca²⁺ oscillations, while its inactive structural analog, U73343 (10 μM, 30 min), did not (Fig. 5A-5C). Similarly, the Ca²⁺ response to Ach was abolished by 2-aminoethoxydiphenylborate (2-APB) (50 μM, 30 min), a widely employed InsP₃R inhibitor ([235]), (Fig. 5A-Fig. 5C). Taking together, these results demonstrate that Ach-induced Ca²⁺ oscillations are produced by repetitive cycles of ER Ca²⁺

release via InsP_3Rs . In further support of this conclusion, we probed the effect of cyclopiazonic acid (CPA). CPA is a specific SERCA inhibitor, thereby preventing Ca^{2+} sequestration into ER lumen. Addition of CPA ($10\ \mu\text{M}$) during ongoing spikes caused an abrupt increase in $[\text{Ca}^{2+}]_i$, due to the passive Ca^{2+} leak, followed by complete inhibition of the Ca^{2+} transients (Fig. 5D). This result confirms that recurrent cycles of ER Ca^{2+} release and re-uptake underpin the oscillatory response to Ach.

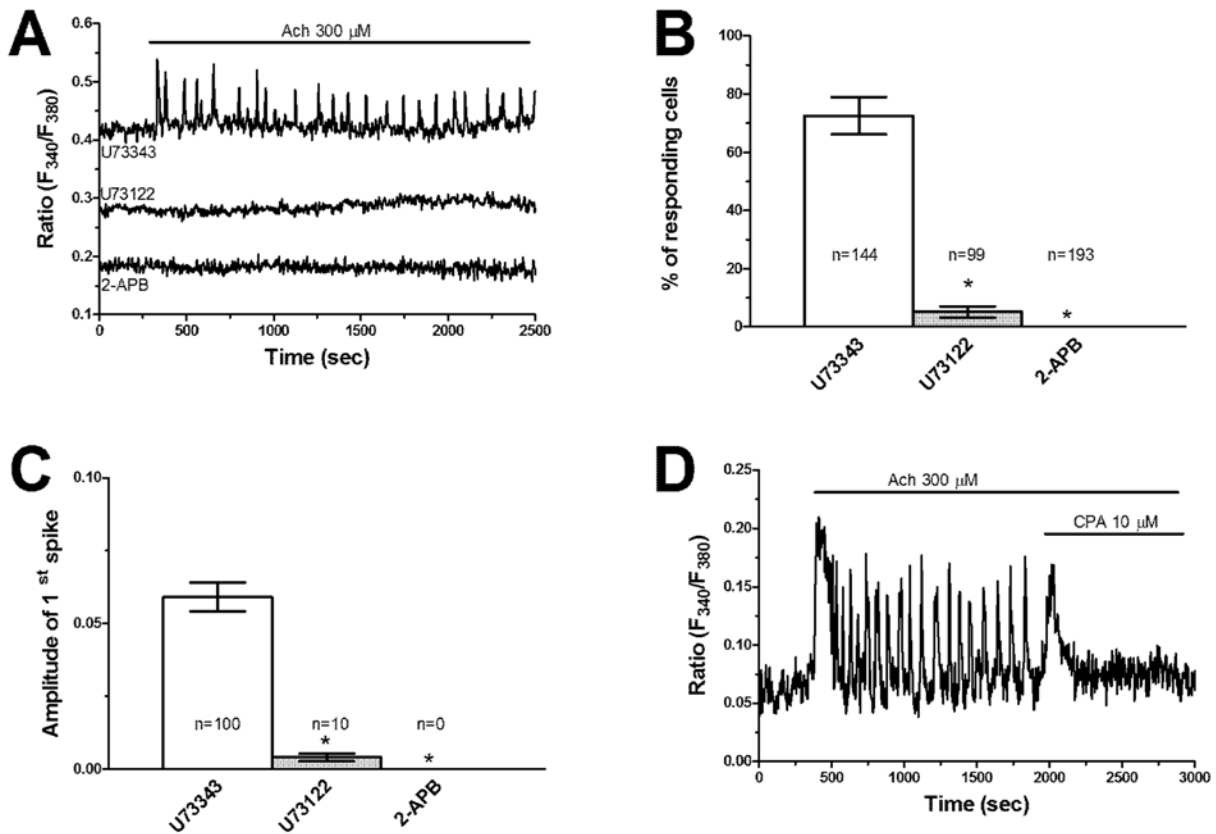


Figure 5. Ach-induced intracellular Ca^{2+} oscillations derived from repetitive Ca^{2+} release from ER via InsP_3Rs . (A), Ach-induced Ca^{2+} oscillations were inhibited by U73122 ($10\ \mu\text{M}$, 30 min), an established PLC inhibitor, but not by structurally inactive analog, U73343 ($10\ \mu\text{M}$, 30 min), and by 2-APB ($50\ \mu\text{M}$, 30 min), which blocks InsP_3Rs . The baseline of Ca^{2+} tracings has been shifted to avoid their overlapping for representation purposes. (B), bar histogram shows the average \pm SE of the percentage of responding cells under the designated treatments. The asterisk indicates $p < 0.05$. (C), bar histogram shows the average \pm SE of the percentage of the amplitude of the 1st spike under the designated treatments. The asterisk indicates $p < 0.05$. (D), addition of CPA ($20\ \mu\text{M}$) during Ach-induced Ca^{2+} spikes causes an immediate increase in $[\text{Ca}^{2+}]_i$ due to passive depletion of the ER Ca^{2+} pool followed by blockade of ongoing oscillations.

The acetylcholine-induced intracellular Ca^{2+} oscillations requires extracellular Ca^{2+} entry

Ach failed to generate any detectable increase in $[\text{Ca}^{2+}]_i$ in the absence of extracellular Ca^{2+} (0Ca^{2+}) in most bEND5 cells (Fig. 6A and Fig. 6B). The oscillatory response to Ach, however, immediately resumed after Ca^{2+} addition to the perfusate (Fig. 6A). Similarly, removal of external Ca^{2+} during ongoing oscillations caused the stop of the Ca^{2+} burst after 1-2 spikes (Fig. 6C). Again, intracellular Ca^{2+} oscillations resumed upon Ca^{2+} restoration to the bathing solution (Fig. 6C). These findings strongly indicate that the extracellular Ca^{2+} entry is required to initiate Ach-induced Ca^{2+} oscillations in bEND5 cells. As the Ca^{2+} response occurs as a consequence of $\text{PLC}\beta$ activation, the underlying plasmalemmal channel must be gated by a second messenger generated upon PIP_2 hydrolysis. Our previous characterization of the Ca^{2+} toolkit revealed that DAG-sensitive endothelial Ca^{2+} channels (TRPC3 and 6) are absent in bEND5 cells, while the molecular components of SOCE (Stim1, Stim2 and Orai2) are largely expressed. Therefore, SOCE is the major candidate to mediate Ach-induced Ca^{2+} entry in bEND5 cells.

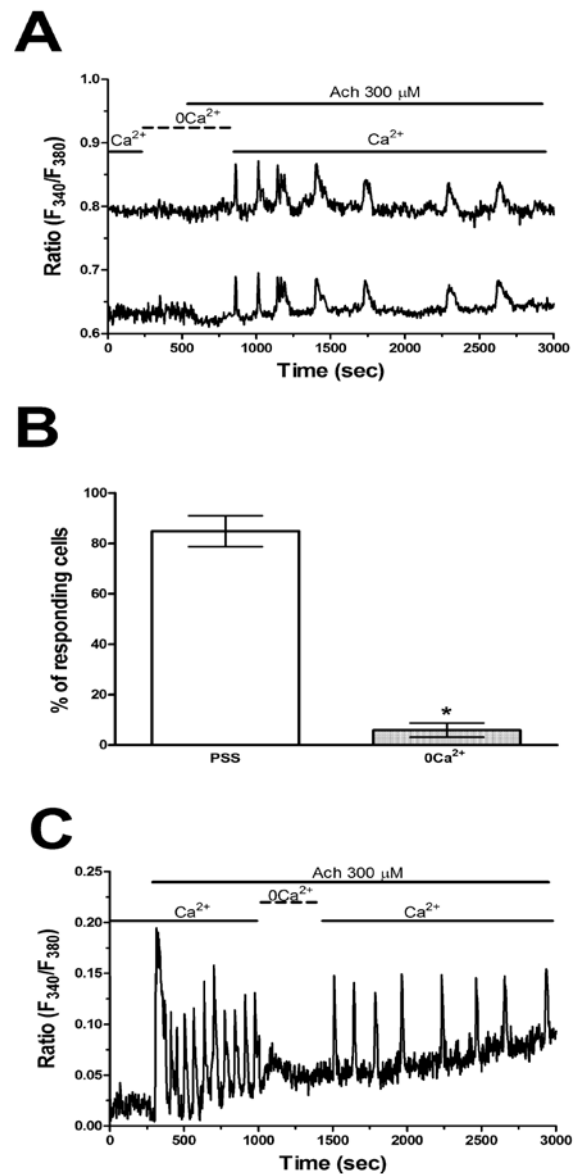


Figure 6. Extracellular Ca^{2+} is necessary for the appearance of Ach-induced intracellular Ca^{2+} oscillations. (A), Ach-evoked Ca^{2+} oscillations did not arise in the absence of external Ca^{2+} (0Ca^{2+}) but rapidly resumed on Ca^{2+} restitution to the bath. (B), bar histogram shows the average \pm SE of the percentage of bEND5 cells displaying an oscillatory response to Ach in the presence and absence of external Ca^{2+} . The asterisk indicates $p < 0.05$.

SOCE is the major Ach-activated Ca^{2+} entry pathway in bEND5 cells

In order to confirm whether a functional SOCE is expressed in bEND5 cells, we exploited the “ Ca^{2+} add-back” protocol ([167], [236]). This protocol consists in stimulating the cells in 0Ca^{2+} with a selective SERCA inhibitor, such as CPA or thapsigargin. This treatment depletes the ER Ca^{2+} reservoir through yet to be identified Ca^{2+} leak pathway and leads to a transient increase in $[\text{Ca}^{2+}]_i$ due to passive Ca^{2+} efflux. Gradually the $[\text{Ca}^{2+}]_i$ recovers to the baseline due to the concerted action of NCX, PMCA and mitochondria. Once the Ca^{2+} reservoir of the ER has been depleted, the ER Ca^{2+} sensor Stim1 detects such fall in intraluminal Ca^{2+} , oligomerizes and rapidly relocates towards ER-plasma membrane junctions. Herein, Stim1 binds to and gates the Ca^{2+} -permeable channel Orai1 to trigger Ca^{2+} entry into the cell. Accordingly, subsequent restitution of Ca^{2+} to the perfusate causes a second increase in $[\text{Ca}^{2+}]_i$ driven by Ca^{2+} entry through open Orai channels. As shown in Fig. 7A, CPA (10 μM) caused a robust SOCE in bEND5 cells. Of note, pre-incubating the cells with powerful Orai blockers, such as La^{3+} (10 μM) and BTP2 (10 μM), prevented both CPA-induced intracellular Ca^{2+} mobilization and CPA-induced SOCE. The statistical analysis of these experiments is illustrated in Fig. 7B and in Fig. 7C. This result suggests that SOCE is partially activated under resting conditions and controls ER Ca^{2+} refilling in bEND5 cells. Not surprisingly, therefore, both La^{3+} (10 μM) and BTP2 (10 μM) prevented the onset of Ach-induced Ca^{2+} oscillations (Fig. 7D and Fig. 7E).

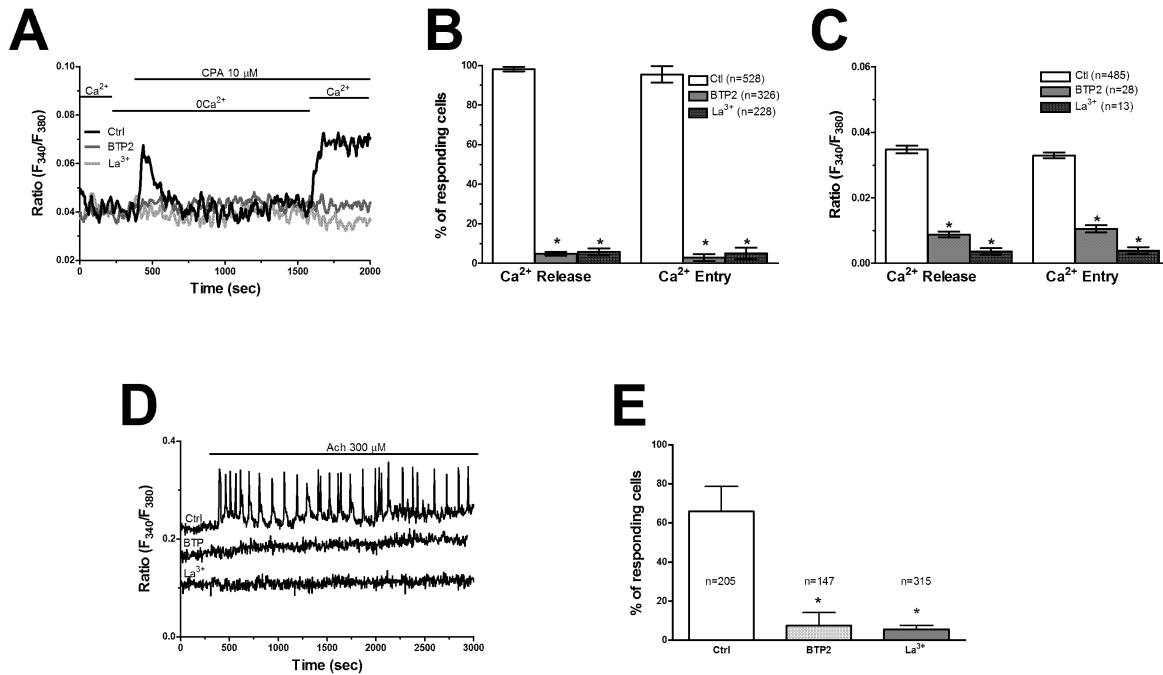


Figure 7. A functional SOCE is present and controls ER Ca²⁺ content in bEND5 cells. (A), the Ca²⁺ “add-back” protocol was applied to assess whether SOCE is active in bEND5 cells. CPA (10 μM) was administered under 0Ca²⁺ conditions to deplete the ER Ca²⁺ pool and activate store-operated Ca²⁺ channels. The following restitution of Ca²⁺ to the external solution caused a second increase in [Ca²⁺]_i due to SOCE activation. However, pre-incubating the cells with either La³⁺ (10 μM, 30 min) or BTP2 (10 μM, 30 min), two rather selective Orai inhibitors, blocked both CPA-induced intracellular Ca²⁺ mobilization and SOCE. (B), bar histogram of the average±SE of the percentage of bEND5 cells responding to CPA in the absence and presence of either La³⁺ (10 μM, 30 min) or BTP2 (10 μM, 30 min). The asterisk indicates p<0.05. (C), bar histogram of the average±SE of the percentage of the amplitude of CPA-induced Ca²⁺ release and SOCE in the absence and presence of either La³⁺ (10 μM, 30 min) or BTP2 (10 μM, 30 min). The asterisk indicates p<0.05. (D), Ach-induced intracellular Ca²⁺ oscillations were prevented by either La³⁺ (10 μM, 30 min) or BTP2 (10 μM, 30 min). (E), bar histogram of the average±SE of the percentage of bEND5 cells displaying a spiking response to Ach in the absence and in the presence of either La³⁺ (10 μM, 30 min) or BTP2 (10 μM, 30 min).

To further corroborate the hypothesis that SOCE is constitutively activated in bEND5 cells, we applied the Mn²⁺-quenching technique. The Mn²⁺ quenching technique is an established tool to monitor both constitutive and agonist-induced Ca²⁺ entry in vascular endothelial cells and EPCs ([226], [128], [237], [238], [239]). As Mn²⁺ and Ca²⁺ share common entry pathways in the plasmalemma, Mn²⁺ can be used as a reliable surrogate of Ca²⁺. As explained in Materials and Methods, Fura-2 quenching by Mn²⁺ is regarded as an index of divalent cation influx. Experiments were carried out at the 360 nm wavelength, the isobestic wavelength for Fura-2, in 0Ca²⁺ medium supplemented with 0.5 mM EGTA (0Ca²⁺ OEGTA). Figure 8A shows that addition of 200 μM Mn²⁺ enhanced the quenching of Fura-2 fluorescence, which is consistent with the expression of a constitutive Ca²⁺ entry pathway in bEND5 cells ([226], [128], [240], [241]). Basal Ca²⁺ influx was

abolished by pre-treating the cells with either La^{3+} (10 μM) or BTP2 (10 μM) (Fig. 8A-8C). These data confirm that SOCE is constitutively active and maintains ER Ca^{2+} load in brain microvascular endothelial cells ([128]), as also recently demonstrated in mouse brain neurons ([178]).

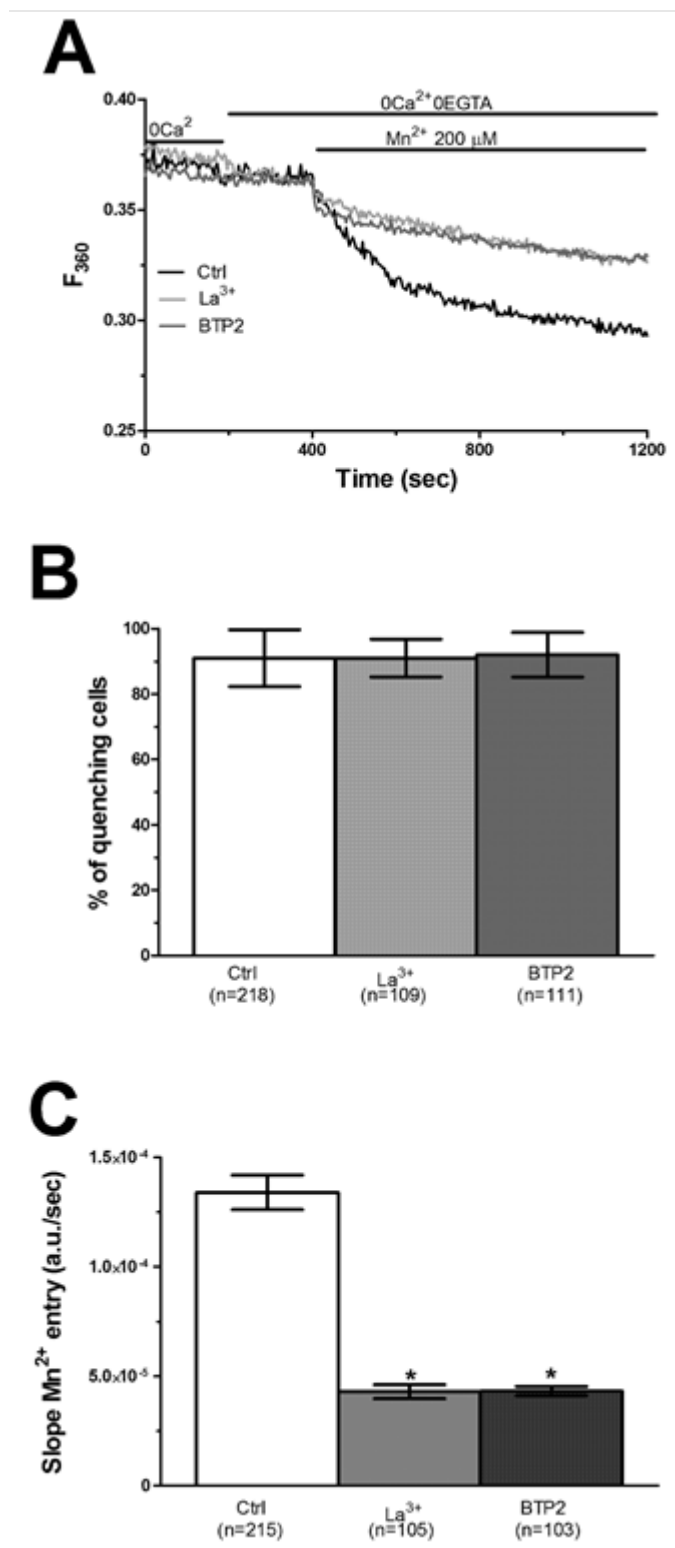


Figure 8. SOCE is constitutively active in bEND5 cells. (A), resting Ca^{2+} entry in mouse brain microvascular endothelial cells was evaluated by using the Mn^{2+} -quenching technique. 200 μM Mn^{2+} was added and they caused an immediate decay in Fura-2 fluorescence. This finding indicates that a basal Ca^{2+} -permeable pathway is active. The rate of fluorescence decay for each individual tracing was calculated as the slope of a linear regression. Pre-incubating the cells with either La^{3+} (10 μM , 30 min) or BTP2 (10 μM , 30 min) caused an evident reduction in rate of Mn^{2+} entry. This finding hints at the store-dependent nature of this constitutive Ca^{2+} influx pathway. (B), mean \pm SE of the percentage of bEND5 cells showing constitutive SOCE in the absence or presence of either La^{3+} (10 μM , 30 min) or BTP2 (10 μM , 30 min). The asterisk indicates $p < 0.05$. (C), mean \pm SE of the quenching rate of Fura-2 fluorescence induced by Mn^{2+} addition in resting bEND5 cells in the absence or presence of either La^{3+} (10 μM , 30 min) or BTP2 (10 μM , 30 min). The asterisk indicates $p < 0.05$.

Moreover, CPA further increased the rate of Fura-2 quenching induced by Mn^{2+} in the absence, but not in the presence, of La^{3+} (10 μM) or BTP2 (10 μM). Therefore, the Mn^{2+} -quenching technique is also a suitable tool to monitor agonist-induced SOCE. According, in a separate set of experiments, once the rate of basal quenching was established, addition of Ach further increased the slope of the quenching curve (Fig. 9A), which reflects the activation of an Ach-sensitive channel. The pharmacological blockade of SOCE with either La^{3+} (10 μM) or BTP2 (10 μM) prevented Ach-induced divalent cation entry (Fig. 9A-9C). Taken together, these findings convincingly suggest that Ach stimulates SOCE in bEND5 cells. We finally challenged the cells with CPA (10 μM) in the presence of external Ca^{2+} (Fig. 9D). The application of CPA induces a rapid elevation in $[Ca^{2+}]_i$ associated to ER emptying followed by a decay phase to a discernible plateau level, due to SOCE activation ([242]). At 30 min after CPA addition, a time interval sufficient for depleting ER Ca^{2+} stores and fully activating SOCE ([243], [244]), Ach failed to induce Ca^{2+} entry (Fig. 9D). This result demonstrates that Ach is unlikely to activate a store-independent channel in brain microvascular endothelial cells ([244], [242]).

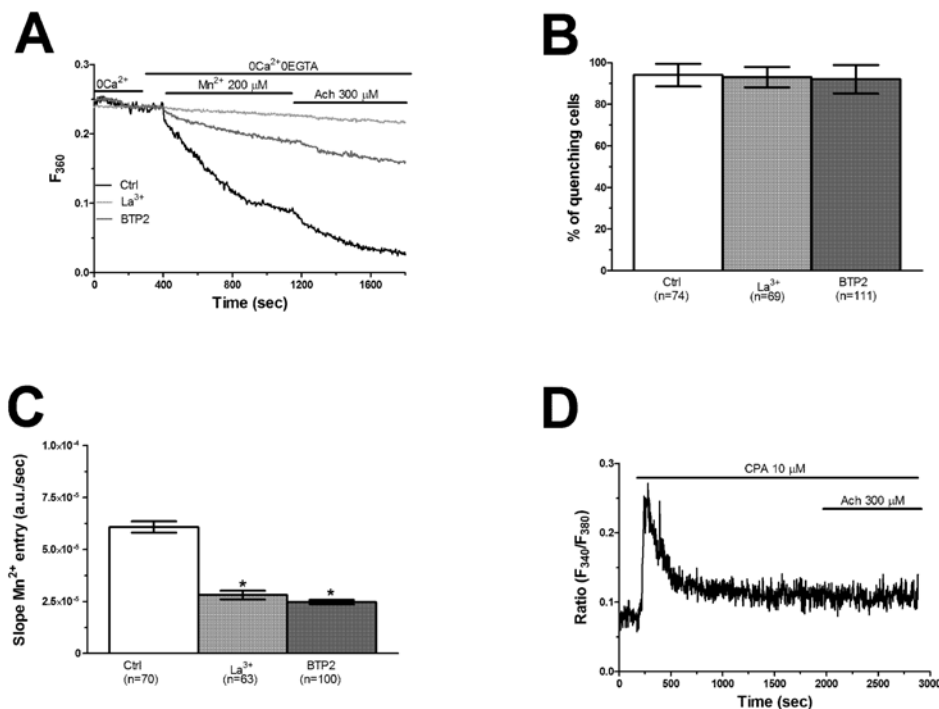


Figure 9. Acetylcholine induces SOCE activation in bEND5 cells. (A), Ach (300 μM) caused a clear increase in the rate of Mn^{2+} entry in bEND5 cells, which was dramatically reduced upon pre-treatment with either La^{3+} (10 μM , 30 min) or BTP2 (10 μM , 30 min). (B), mean \pm SE of the percentage of bEND5 cells displaying Ach-induced Mn^{2+} entry in the absence or presence of either La^{3+} (10 μM , 30 min) or BTP2 (10 μM , 30 min). The asterisk indicates $p < 0.05$. (C), mean \pm SE of the quenching rate of Fura-2 fluorescence signal measured in bEND5 cells before and after Ach addition. The asterisk indicates $p < 0.05$. (D), addition of CPA (10 μM) in the presence of extracellular Ca^{2+} caused a biphasic increase in $[Ca^{2+}]_i$ due to passive Ca^{2+} mobilization followed by SOCE activation. Subsequent administration of Ach at 30 min from CPA application failed to enhance intracellular Ca^{2+} levels.

Acetylcholine-induced intracellular Ca^{2+} oscillations lead to NO synthesis in bEND5 cells

Finally, we assessed whether Ach-induced Ca^{2+} oscillations induced NO release by loading the cells with DAF/FM, a NO-sensitive fluorochrome ([128]). Ach caused an immediate elevation in DAF/FM fluorescence, which then decayed to a plateau level (Fig. 10A). Ach-induced NO production was significantly ($p < 0.05$) reduced by pre-incubating the cells with either L-NG-Nitroarginine methyl ester (L-NAME; 100 μM , 1 h), a widely employed eNOS inhibitor, or 1,2-is(o-aminophenoxy)ethane-N,N,N',N'-tetraacetic acid (BAPTA; 30 μM , 2 h), a membrane-permeable intracellular Ca^{2+} buffer (Fig. 10A and Fig. 10D). These findings clearly show that Ach recruits eNOS in a Ca^{2+} -dependent manner. Of note, NO release did not occur in the absence of external Ca^{2+} (0Ca^{2+}), but rapidly resumed upon restoration of extracellular Ca^{2+} concentration (Fig. 10B and Fig. 10D). Moreover, NO production was severely reduced by inhibiting concomitant Ca^{2+} oscillations with U73122 (10 μM), and 2-APB (50 μM , 30 min) (Fig. 10B and Fig. 10D). As expected, Ach-induced NO synthesis was also prevented by La^{3+} (10 μM) and BTP2 (10 μM) (Fig. 10C and Fig. 10D). These results demonstrate that Ach stimulates NO release from brain microvascular endothelial cells through an oscillatory increase in $[\text{Ca}^{2+}]_i$.

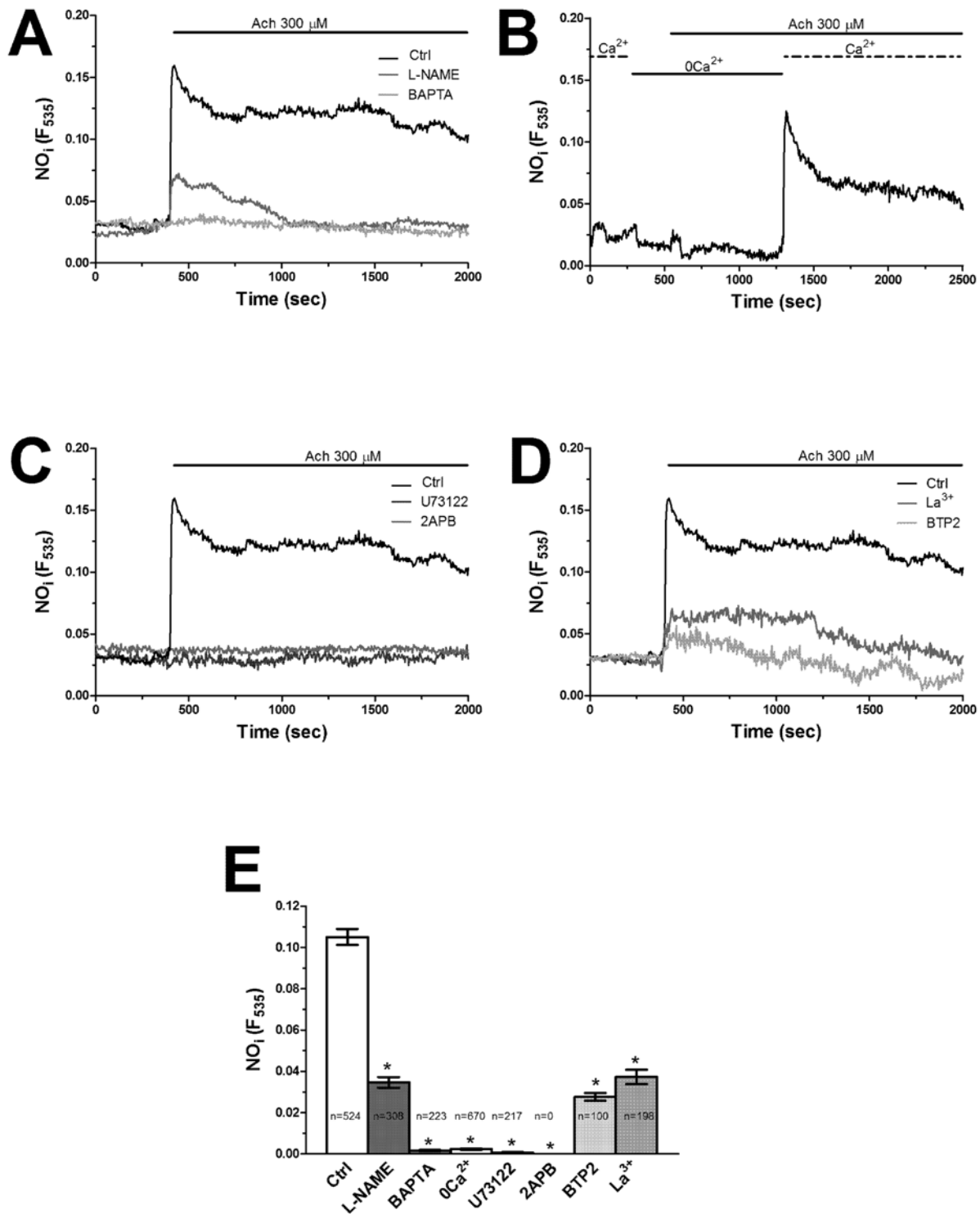


Figure 10. Acetylcholine-induced intracellular Ca^{2+} oscillations lead to NO release in bEND5 cells. (A), in bEND5 cells loaded with the NO-sensitive fluorophore, DAF/FM, Ach (300 μM), caused a robust increase NO-dependent signal, which was strongly reduced by either L-NAME (100 μM , 1 h), a selective NOS blocker, or BAPTA (30 μM , 2 h), a membrane-permeable intracellular Ca^{2+} chelator. (B), Ach failed to induce NO release under 0Ca^{2+} conditions, but caused an immediate increase in NO levels upon restoration of the extracellular Ca^{2+} concentration. (C), Ach-induced NO release was unaffected by U73343 (10 μM ; 30 min), while it was abolished by U73122 (10 μM , 30 min), and 2-APB (50 μM , 30 min). (D), Ach-induced NO production was inhibited by pre-treating the cells with either La^{3+} (10 μM , 30 min) or BTP2 (10 μM , 30 min). (E), mean \pm SE of the magnitude of Ach-induced NO synthesis under the designated treatments. The asterisk indicates $p < 0.05$.

Acetylcholine induces intracellular Ca²⁺ signals in human brain microvascular endothelial cells

In order to assess whether Ach was able to induce Ca²⁺ signals also in a human model, we exploited the hCMEC/D3 cell line, a widely established model of human brain microvascular endothelial cells ([245]). hCMEC/D3 were loaded with the Ca²⁺-sensitive dye Fura-2/AM and Ach was applied at different doses (from 25 μM to 300 μM). As shown in Fig. 11A, Ach caused a dose-dependent increase in [Ca²⁺]_i between 25 μM to 100 μM, while the amplitude of the Ca²⁺ response decreased by raising the agonist concentration up to 200 μM (Fig. 11A and 11C). The fraction of responding cells displayed a similar bell-shaped dose-response relationship, as the percentage of Ach-sensitive cells increased from 25 μM to 50-100 μM and further decreased at 200 μM (Fig. 11B and 11C). Conversely, there was no response at Ach concentrations lower than 25 μM (not shown). Of note, the response to 100 μM Ach displayed biphasic kinetics, consisting of an initial Ca²⁺ which decayed to a plateau level of intermediate amplitude (Fig. 11A), indicative of SOCE activation ([168]). Conversely, at each of the other doses tested, Ach induced only a transient increase in [Ca²⁺]_i, which is likely to reflect ER-dependent InsP₃-mediated intracellular Ca²⁺ mobilization ([31]). Finally, the Ca²⁺ response to Ach did not desensitize after two 30 min-spaced consecutive applications. Taken together, these data suggest that the 100 μM Ach was the most suitable concentration for Ach to induce a Ca²⁺ physiological response in hCMEC/D3 cells.

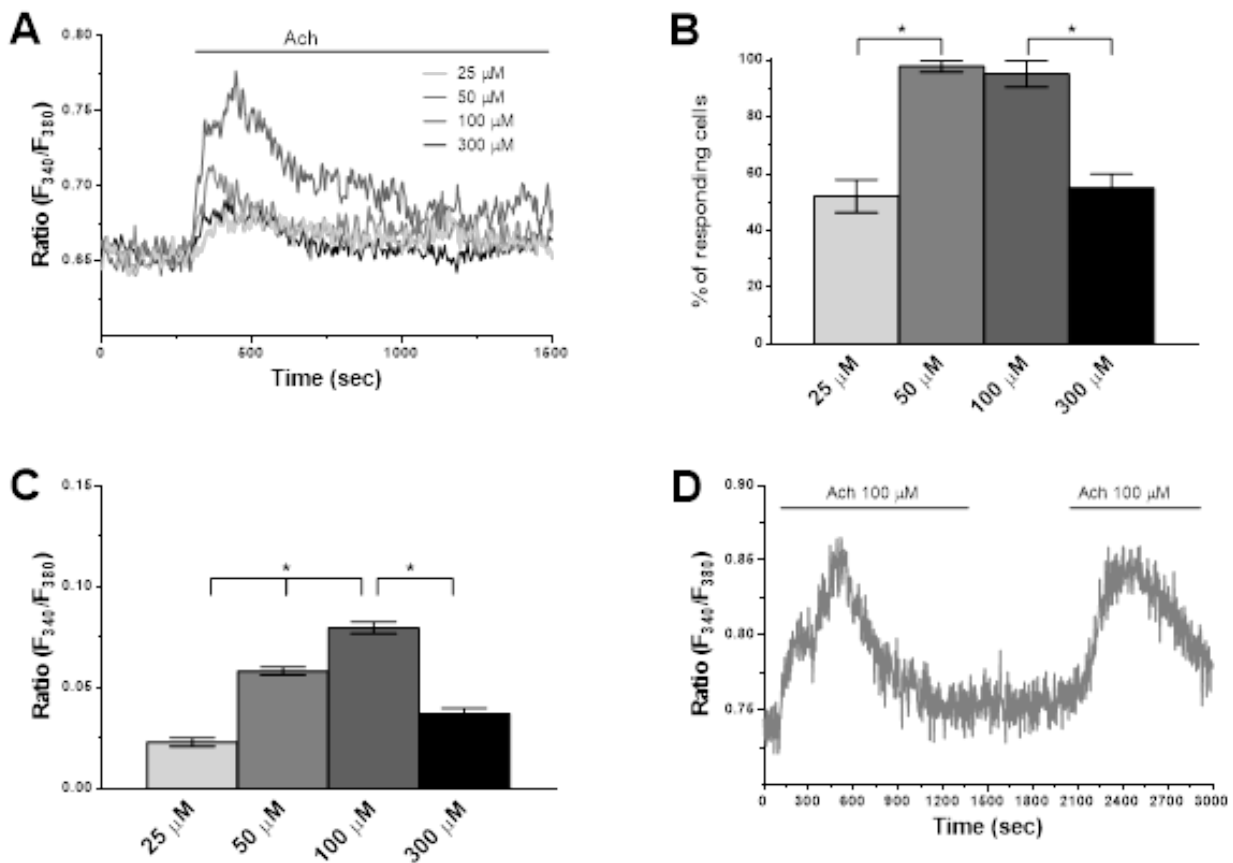


Figure 11: Acetylcholine evokes intracellular Ca^{2+} transient increase in hCMEC/D3 cells. (A), Ach causes the immediate rise in $[\text{Ca}^{2+}]_i$ followed by a rapid decay in a dose-dependent way. Only 100 μM Ach showed a plateau phase. (B), mean \pm SE of the percentage of hCMEC/D3 cells displaying Ach-induced Ca^{2+} response at different agonist concentrations (from 50 μM to 300 μM). The asterisk indicates $p < 0.05$. (C), mean \pm SE of the amplitude of Ach-induced Ca^{2+} mobilization measured in hCMEC/D3 cell. The asterisk indicates $p < 0.05$. In this and the following figures, Ach was added at the time indicated by the horizontal bar drawn around the Ca^{2+} tracings.

Similar to BEND5 cells, Ach-induced Ca^{2+} transient was blocked by atropine (100 μM , 30 min) (Fig. 12A), whereas nicotine did not increase $[\text{Ca}^{2+}]_i$ in hCMEC/D3 cells (Fig. 12B). These results suggest that the Ca^{2+} response induced by Ach arise upon mAChR activation. Consistently, PCR revealed that human brain microvascular endothelial cells express high levels of M4-mAChR, which is coupled to cAMP production, and M5-mAChR (Fig. 12C), which induces InsP_3 synthesis.

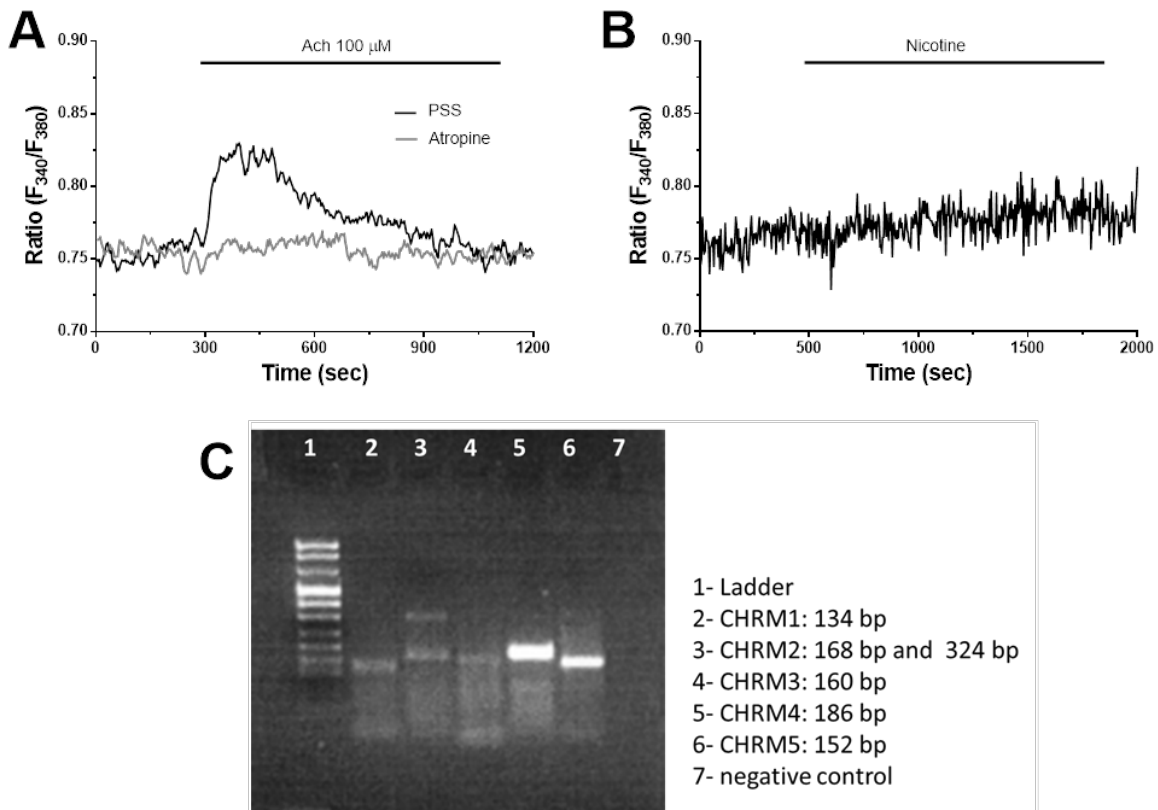


Figure 12. Metabotropic muscarinic receptors drive the acetylcholine-induced Ca^{2+} response. (A), atropine (100 μ M, 30 min) prevents the initiation of the Ca^{2+} response to Ach. (B), nicotine (100 μ M) did not increase $[Ca^{2+}]_i$ in hCMEC/D3 cells. (c), PCR gel of metabotropic muscarinic receptors (M-AChRs) revealed that, among all the five M-AChR mRNAs expressed in hCMEC/D3, M4 and M5 displayed the highest expression.

Expression of the components of the Ca²⁺ signaling toolkit in hCMEC/D3 cells

By using a similar approach to that employed for BEND5 cells, we demonstrated that the following transcripts were expressed in hCMEC/D3 cells: SERCA2b and SERCA3 (Fig. 13A); PMCA1a, PMCAb1, PMCA4a and PMCA4b (Fig. 13A); NCX1.3 and NCX1.7 (Fig. 13B); TPC1 and TPC2 (Fig. 13B); InsP₃R3 (Fig. 13C); Orai 1, 2 and 3 (Fig. 13E); Stim2 (Fig. 13E); and TRPC7 (Fig. 13F).

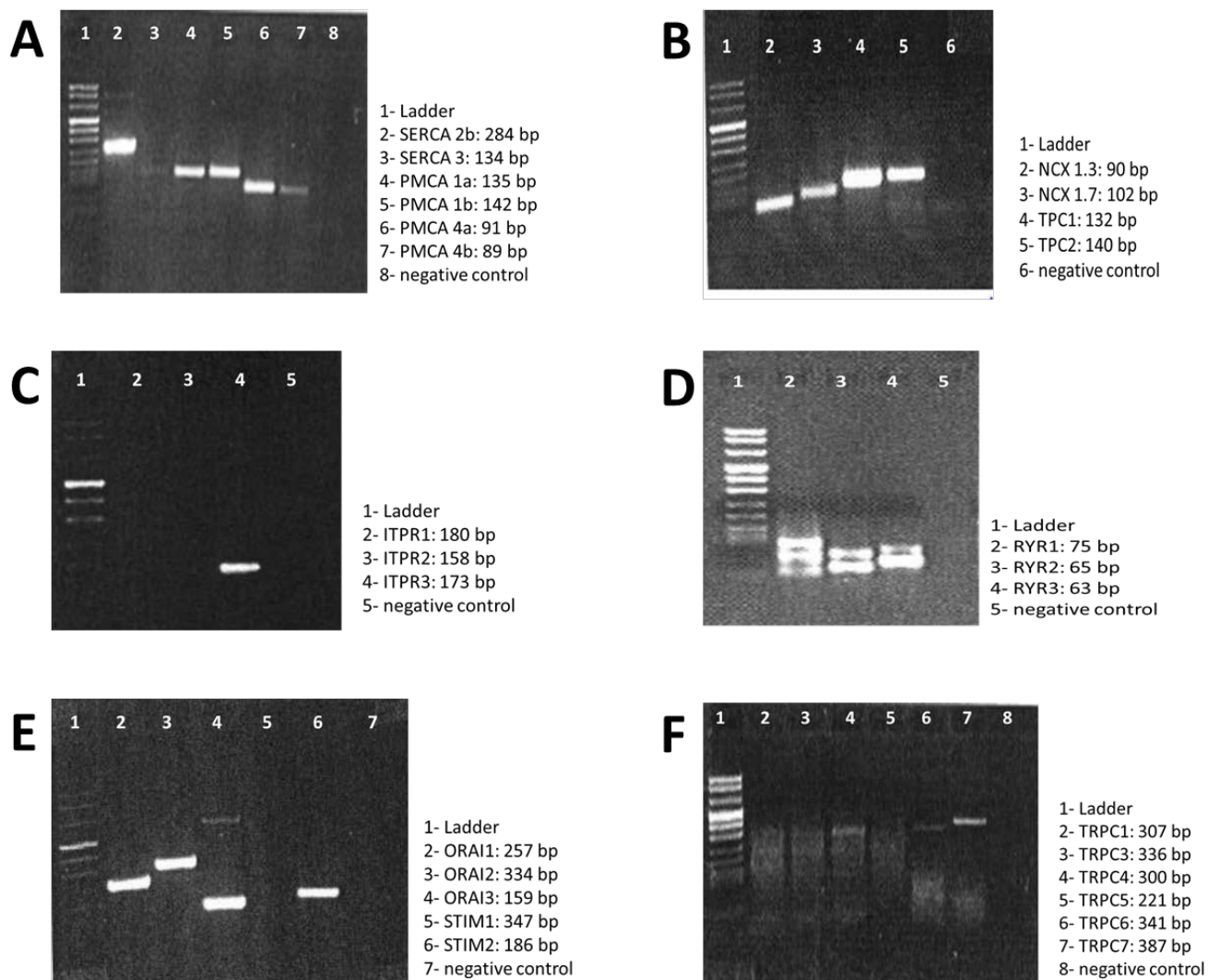


Figure 13. The Ca²⁺ toolkit of hCMEC/D3 cells. qRT-PCR gel of (A) SERCA and PMCA, (B) NCX and TPC, (C) InsP₃R, (D) RyRs, (E) ORAI and STIM isoform, (F) TRPC family.

Of note, $\text{InsP}_3\text{R1-2}$, Stim1 and the endothelial DAG-gated TRPC3 and TRPC6 channels were absent in hCMEC/D3 cells. In agreement with this observation, OAG (100 μM) failed to evoke any detectable Ca^{2+} signal in these cells (Fig. 14A). Likewise, caffeine (5 mM), a selective RyR agonist, failed to increase $[\text{Ca}^{2+}]_i$ in hCMEC/D3 cells (Fig.14B).

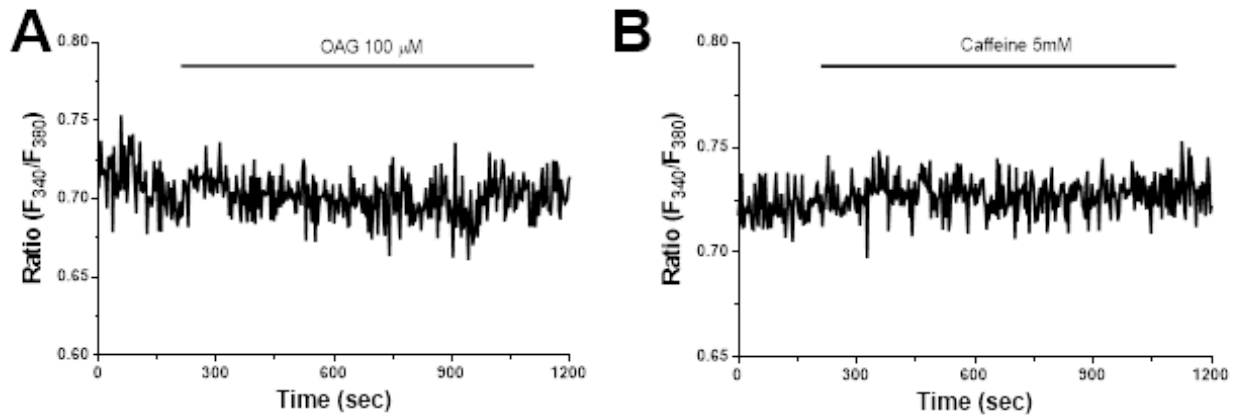


Figure 14. TRPC3,6-mediated Ca^{2+} entry and RyRs-dependent Ca^{2+} release are absent in hCMEC/D3 cells. OAG (100 μM) (A) and caffeine (5 mM) did not increase $[\text{Ca}^{2+}]_i$ in hCMEC/D3 cells.

Acetylcholine-induced intracellular Ca^{2+} response requires intracellular Ca^{2+} release and extracellular Ca^{2+} entry

Interestingly, in absent of extracellular Ca^{2+} (0Ca^{2+}) 100 μM Ach was able to generate a rapid increase in $[\text{Ca}^{2+}]_i$ that rapidly declined to the baseline, lacking the plateau phase that characterized the Ach-induced Ca^{2+} response in presence of extracellular Ca^{2+} (Fig. 15A-C). Taken together these results suggest that Ach-induced intracellular Ca^{2+} signalling is triggered by intracellular Ca^{2+} release and sustained by extracellular Ca^{2+} entry.

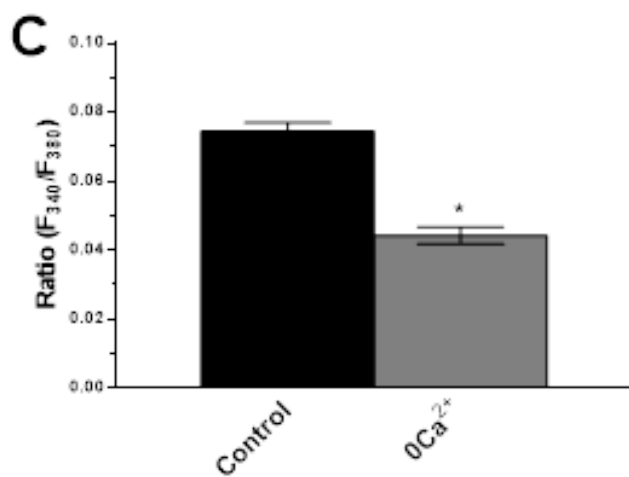
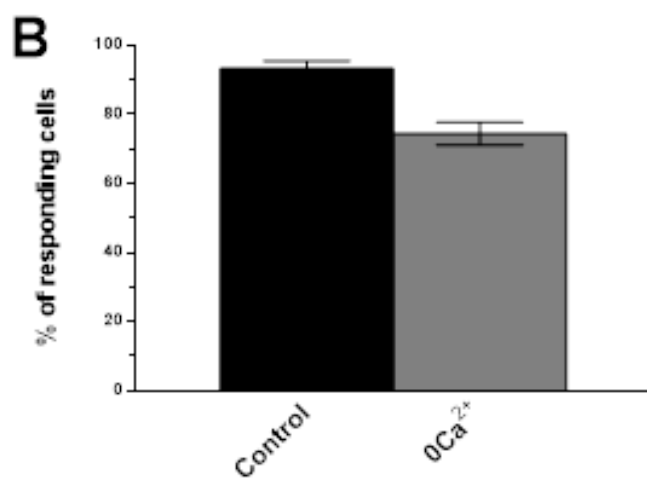
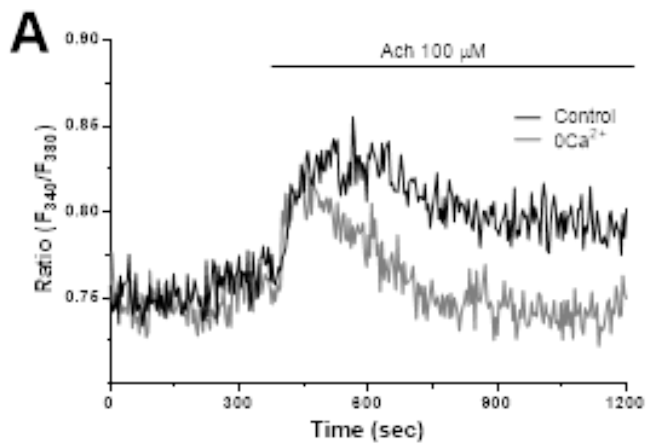


Figure 15. Intracellular Calcium release and extracellular calcium entry are both involved in the Ach-induced Ca^{2+} response in hCMEC/D3. (A), Ach-induced increase in $[Ca^{2+}]_i$ is significantly ($p < 0.05$) lower in $0Ca^{2+}$ compare with control. (B), bar histogram shows the average \pm SE of the percentage of responding cells. The asterisk indicates $p < 0.05$. (C), bar histogram shows the average \pm SE of the amplitude of the response. The asterisk indicates $p < 0.05$.

Acetylcholine-induced intracellular Ca²⁺ release is mediated by the PLCβ/InsP₃ signalling pathway

In order to confirm that the PLCβ/InsP₃ signalling pathway drives Ach-induced intracellular Ca²⁺ release also in hCMEC/D3 cells, we adopted a similar strategy to that illustrated for BEND5 cells. We found that Ach-induced intracellular Ca²⁺ mobilization was abrogated by U73122 (10 μM, 30 min), but not its inactive structural analog, U73343 (10 μM, 30 min), by 2-APB (50 μM, 30 min), and by CPA (Fig. 16A-Fig. 16D). Collectively, these findings demonstrate that M5-mAChRs mediate Ach-induced intracellular Ca²⁺ releases by recruiting the PLCβ/InsP₃ signaling pathway.

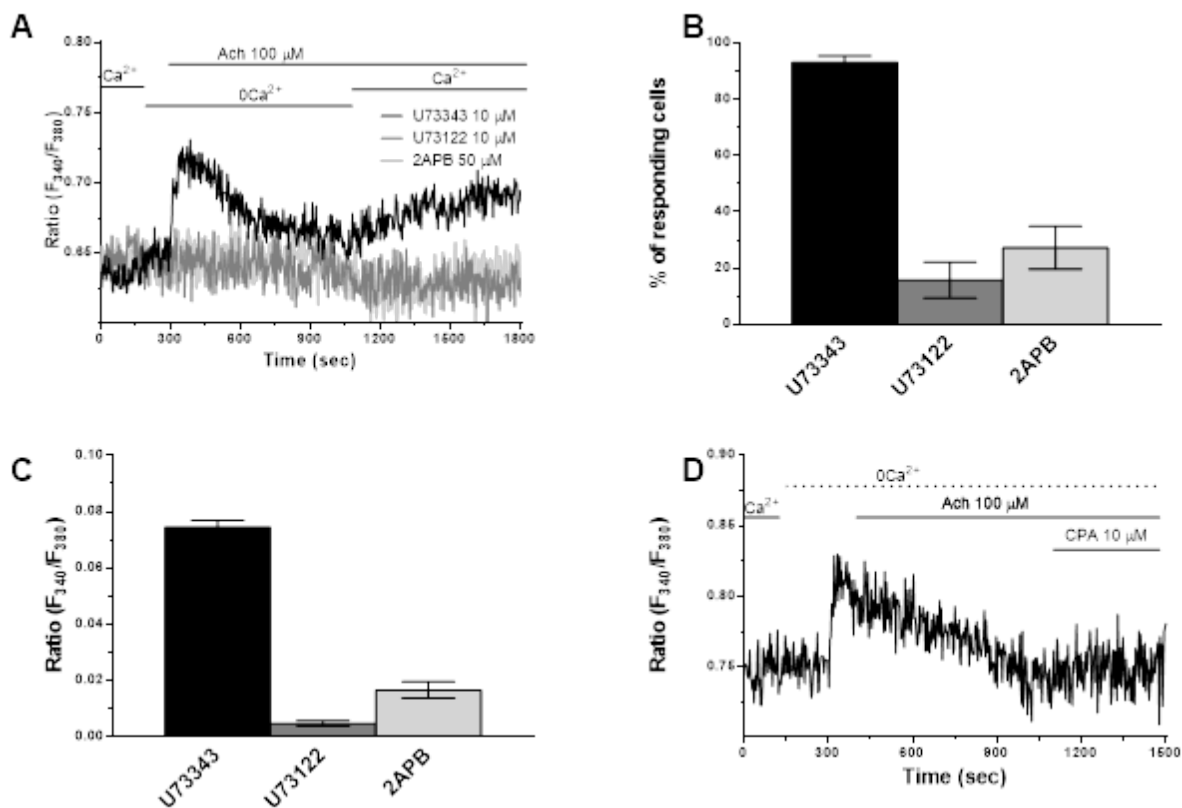


Figure 16. Ach-induced intracellular Ca²⁺ mobilization requires ER-dependent Ca²⁺ release through InsP₃Rs. (A), Ach-induced intracellular Ca²⁺ release was inhibited by U73122 (10 μM, 30 min), but not by its structurally inactive analog, U73343 (10 μM; 30 min), by 2-APB (50 μM, 30 min), and by CPA (to do). (B), bar histogram shows the average±SE of the percentage of responding cells under the designated treatments. The asterisk indicates p<0.05. (C), bar histogram shows the average±SE of the amplitude of the response under the designated treatments. The asterisk indicates p<0.05.

SOCE participates to the Ca^{2+} response to Ach in hCMEC/D3 cells

In order to confirm the involvement of a functional SOCE in hCMEC/D3 cells we exploited the “ Ca^{2+} add-back” protocol ([167], [236]). As shown in Fig. 17A, CPA (10 μM) caused a robust SOCE in hCMEC/D3 cells. Conversely, pre-incubating the cells with Pyr 6 (10 μM , 30 min), a newly synthesized pyrazole compound that inhibits Orai-mediated Ca^{2+} responses, prevented both CPA-induced intracellular Ca^{2+} mobilization and CPA-induced SOCE. The statistical analysis of these experiments is illustrated in Fig. 17B and in Fig. 17C. Not surprisingly Pyr6 (10 μM) also inhibited the Ca^{2+} response to Ach in most hCMEC/D3 cells (Fig. 17D-F). Of note, in the responding cells, the Ca^{2+} signal recorded in the presence of Pyr6 was similar to that measured in the absence of extracellular Ca^{2+} , i.e. it reached lower amplitude as compared to controls and lacked a plateau phase (Fig. 15A). These results suggests that SOCE is activated under resting conditions and controls ER Ca^{2+} levels also in hCMEC/D3 cells and that it could be further activated by cholinergic stimulation.

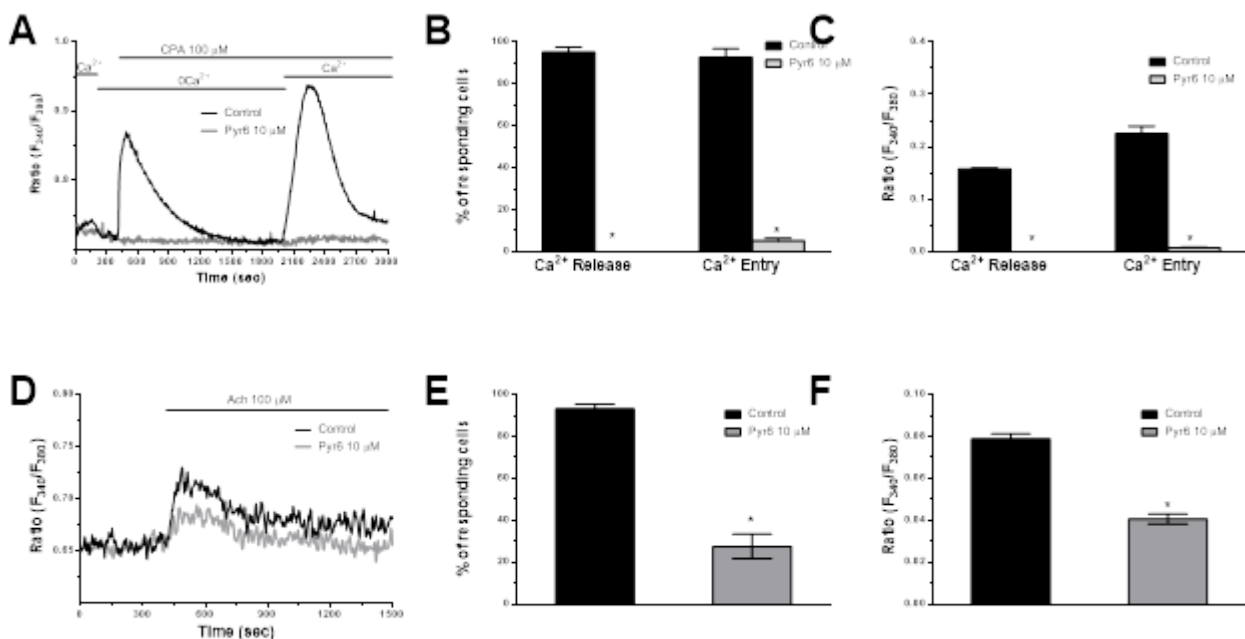


Figure 17. A functional SOCE is present and controls ER Ca^{2+} content in hCMEC/D3 cells. (A), the Ca^{2+} “add-back” protocol was applied to assess whether SOCE was active in these cells. CPA (100 μM) was administered under 0Ca^{2+} conditions to deplete the ER Ca^{2+} pool and activate SOCs. The following restitution of Ca^{2+} to the external solution caused a second increase in $[\text{Ca}^{2+}]_i$ due to SOCE activation. However, pre-incubating the cells with Pyr6 (10 μM , 30 min), an inhibitor of Orai-mediated Ca^{2+} responses, blocked both CPA-induced intracellular Ca^{2+} mobilization and SOCE. (B), bar histogram of the average \pm SE of the percentage of hCMEC/D3 cells responding to CPA in the absence

and presence of Pyr6 (10 μ M, 30 min). The asterisk indicates $p < 0.05$. (C), bar histogram of the average \pm SE of the percentage of the amplitude of CPA-induced Ca^{2+} release and SOCE in the absence and presence of Pyr6 (10 μ M, 30 min). The asterisk indicates $p < 0.05$. (D), Ach-induced intracellular Ca^{2+} response were inhibited by Pyr6 (10 μ M, 30 min). (E), bar histogram of the average \pm SE of the percentage of hCMEC/D3 cells displaying a response to Ach in the absence and in the presence of Pyr6 (10 μ M, 30 min). (F) bar histogram shows the average \pm SE of the amplitude of the response. The asterisk indicates $p < 0.05$.

To further corroborate these hypotheses, we exploited again the Mn^{2+} -quenching technique (see above), which revealed a Pyr6-sensitive basal Ca^{2+} entry also in hCMEC/D3 cells (Fig. 18A-C). Addition of Ach further increased the slope of the quenching curve (Fig. 18A-C), which demonstrated the activation of an Ach-sensitive channel. The pharmacological blockade of SOCE with Pyr6 (10 μ M) prevented Ach-induced divalent cation entry (Fig. 18A-C). Taken together, these findings convincingly show that SOCE maintains the Ca^{2+} response to Ach in hCMEC/D3 cells. We finally challenged the cells with CPA (10 μ M) in the presence of external Ca^{2+} (Fig. 18D). The application of CPA induces a rapid elevation in $[\text{Ca}^{2+}]_i$ associated to ER emptying followed by a decay phase to a discernible plateau level, due to SOCE activation ([242]). At 30 min after CPA addition, a time interval sufficient for depleting ER Ca^{2+} stores and fully activating SOCE ([243], [244]), Ach failed to induce Ca^{2+} entry (Fig. 18D). This result clearly demonstrates that Ach is unlikely to activate a store-independent channel in brain microvascular endothelial cells ([244], [242]).

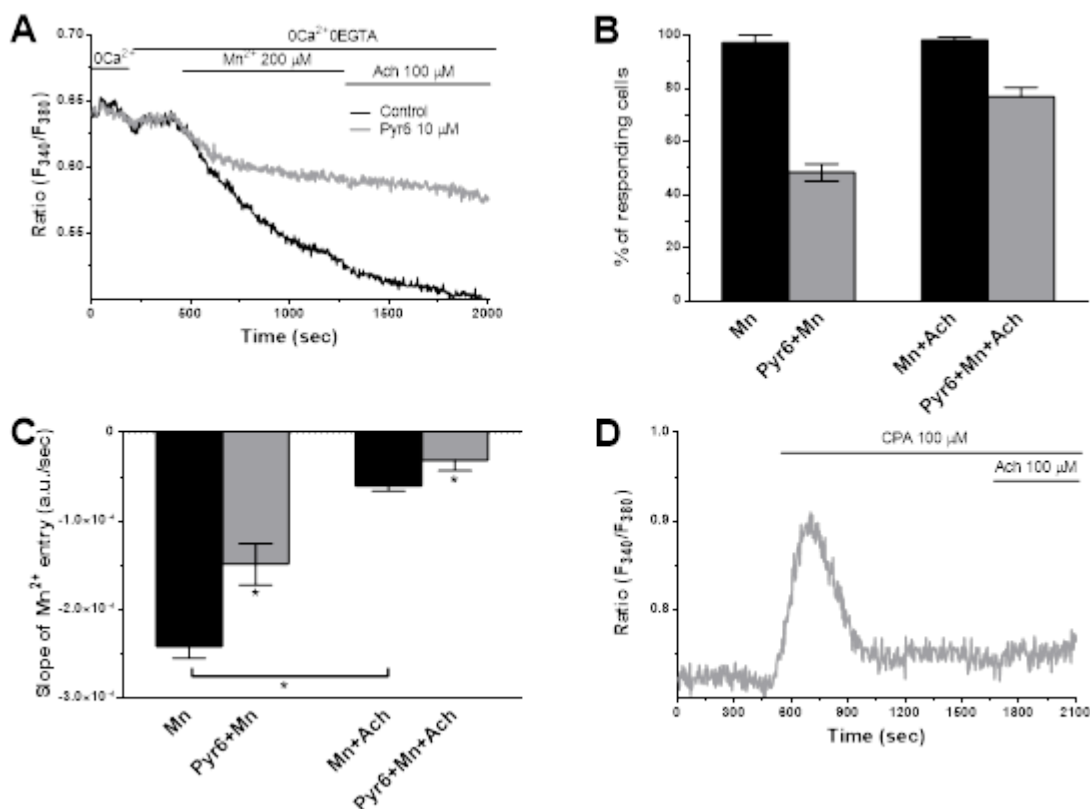


Figure 18. Acetylcholine induces SOCE activation in hCMEC/D3 cells. (A), Ach (100 μM) caused an increase in the rate of Mn^{2+} entry in hCMEC/D3 cells, which was dramatically reduced upon pre-treatment with Pyr6 (10 μM , 30 min). (B), mean \pm SE of the percentage of hCMEC/D3 cells displaying Mn^{2+} entry and Ach-induced Mn^{2+} entry in the absence or presence of Pyr6 (10 μM , 30 min). The asterisk indicates $p < 0.05$. (C), mean \pm SE of the quenching rate of Fura-2 fluorescence signal measured in hCMEC/D3 cells before and after Mn^{2+} and Ach addition in presence and in absence of Pyr6 (10 μM , 30 min). The asterisk indicates $p < 0.05$. (D), addition of CPA (10 μM) in the presence of extracellular Ca^{2+} caused a biphasic increase in $[\text{Ca}^{2+}]_i$ due to passive Ca^{2+} mobilization followed by SOCE activation. Subsequent administration of Ach at 30 min from CPA application failed to enhance intracellular Ca^{2+} levels.

Acetylcholine-induced Ca^{2+} signalling leads to NO synthesis in hCMEC/D3 cells

Finally, we assessed whether Ach-induced Ca^{2+} increase induced NO release by loading the cells with DAF/FM, the NO-sensitive fluorochrome ([128]). Ach (100 μM) caused a sustained increase in NO levels. (Fig. 19A). Ach-induced NO production was significantly ($p < 0.05$) reduced by pre-incubating the cells with either L-NAME (100 μM , 1 h) or BAPTA (30 μM , 2 h). These findings clearly show that Ach recruits eNOS in a Ca^{2+} -dependent manner. Of note, NO release did not occur in the absence of external Ca^{2+} (0Ca^{2+}) (Fig. 19A and Fig. 19C). Moreover, NO production was severely reduced by U73122 (10 μM), 2-APB (50 μM , 30 min) and Pyr6 (10 μM) (Fig. 19B and Fig. 19C). These results demonstrate that both InsP_3Rs and SOCE sustain Ach-induced NO release in hCMEC/D3.

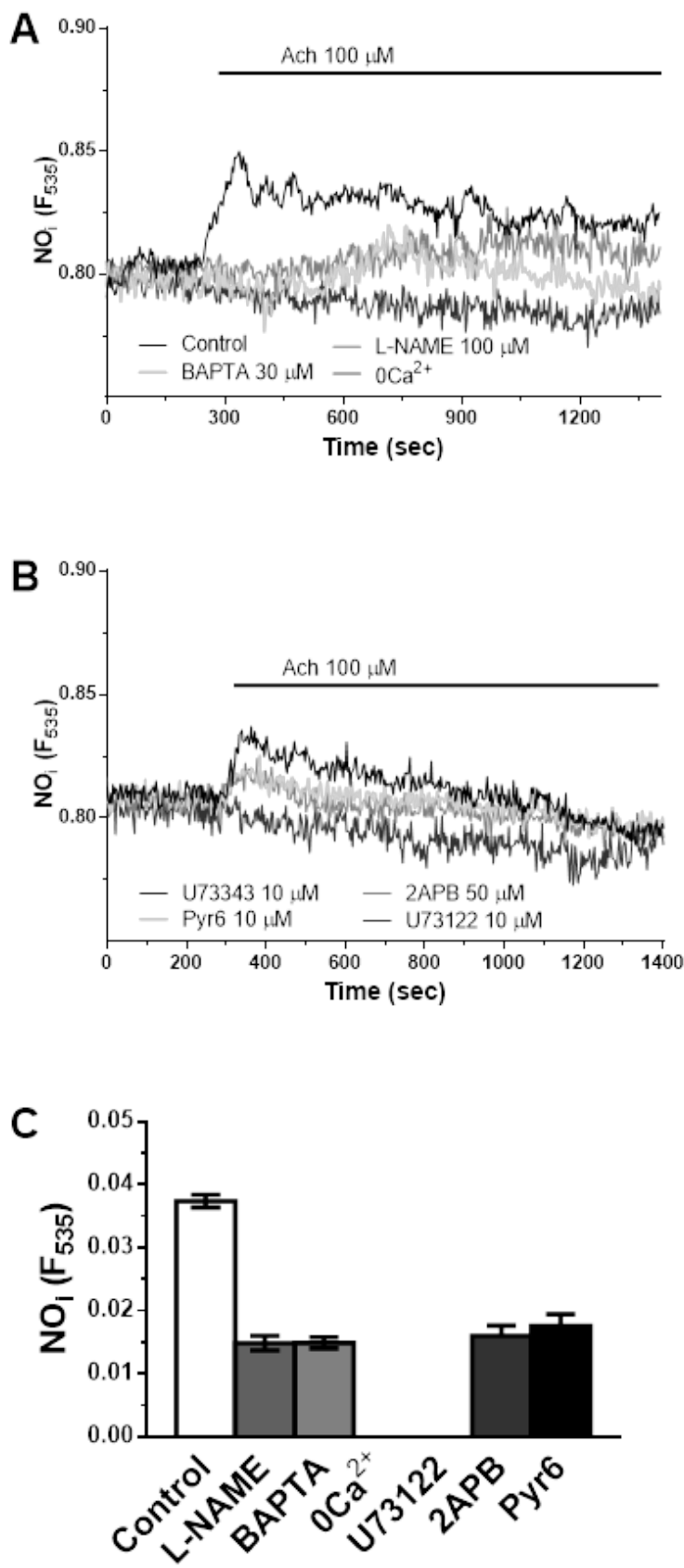


Figure 19. Acetylcholine-induced increase in $[Ca^{2+}]_i$ leads to NO release in hCMEC/D3 cells. (A), Ach (100 μ M) caused a robust increase in DAF/FM fluorescence in hCMEC/D3 cells, that was strongly reduced by either L-NAME (100 μ M, 1 h) or BAPTA (30 μ M, 2 h), a membrane-permeable intracellular Ca^{2+} chelator. Moreover, Ach failed to induce NO release under $0Ca^{2+}$ conditions. (B), Ach-induced NO release was unaffected by U73343 (10 μ M; 30 min), while it was abolished by U73122 (10 μ M, 30 min). 2-APB (50 μ M, 30 min) and Pyr6 (10 μ M, 30 min) were also able to inhibit NO release. (C), mean \pm SE of the magnitude of Ach-induced NO synthesis under the designated treatments. The asterisk indicates $p < 0.05$.

Glutamate induces intracellular Ca²⁺ oscillations in bEnd5 cells

After the characterization of Ach-induced Ca²⁺ and NO signals in murine and human brain microvascular endothelial cells, we focused on Glu. Again, bEND5 cells were loaded with with the Ca²⁺-sensitive fluorochrome, Fura-2/AM, in order to assess whether Glu induces intracellular Ca²⁺ activity. The addition of glutamate to quiescent cells caused a dose-dependent oscillatory increase in [Ca²⁺]_i (Fig. 20 and 21). Similar to Ach, each Ca²⁺ oscillation was preceded by a pacemaker Ca²⁺ elevation, which strongly hints at the involvement of InsP₃-induced ER Ca²⁺ release ([231]).

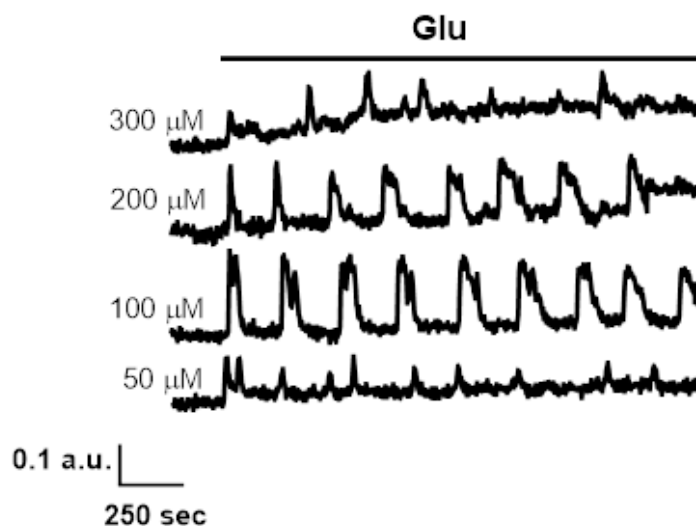


Figura 20: Glutamate evokes repetitive Ca²⁺ transients in bEND5 cells. Glutamate causes the immediate initiation of oscillatory Ca²⁺ spikes whose duration, amplitude of the 1st spike and interspike interval (ISI) was a function of agonist concentration. In this and the following figures, Glut was added at the time indicated by the horizontal bar drawn around the Ca²⁺ tracings. The baseline of Ca²⁺ tracings has been shifted to avoid their overlapping for representation purposes.

The spiking Ca²⁺ response arose at 50 μM and achieved a peak at 200 μM, as the percentage of responding cells (Fig. 21A), the amplitude of the 1st Ca²⁺ transient (Fig. 21B), the number of Ca²⁺ spikes/30 min (Fig. 21C) and the frequency of the Ca²⁺ train (Fig. 21D) reached their highest value at this dose, and decreased by further increasing glutamate concentration to 300 μM.

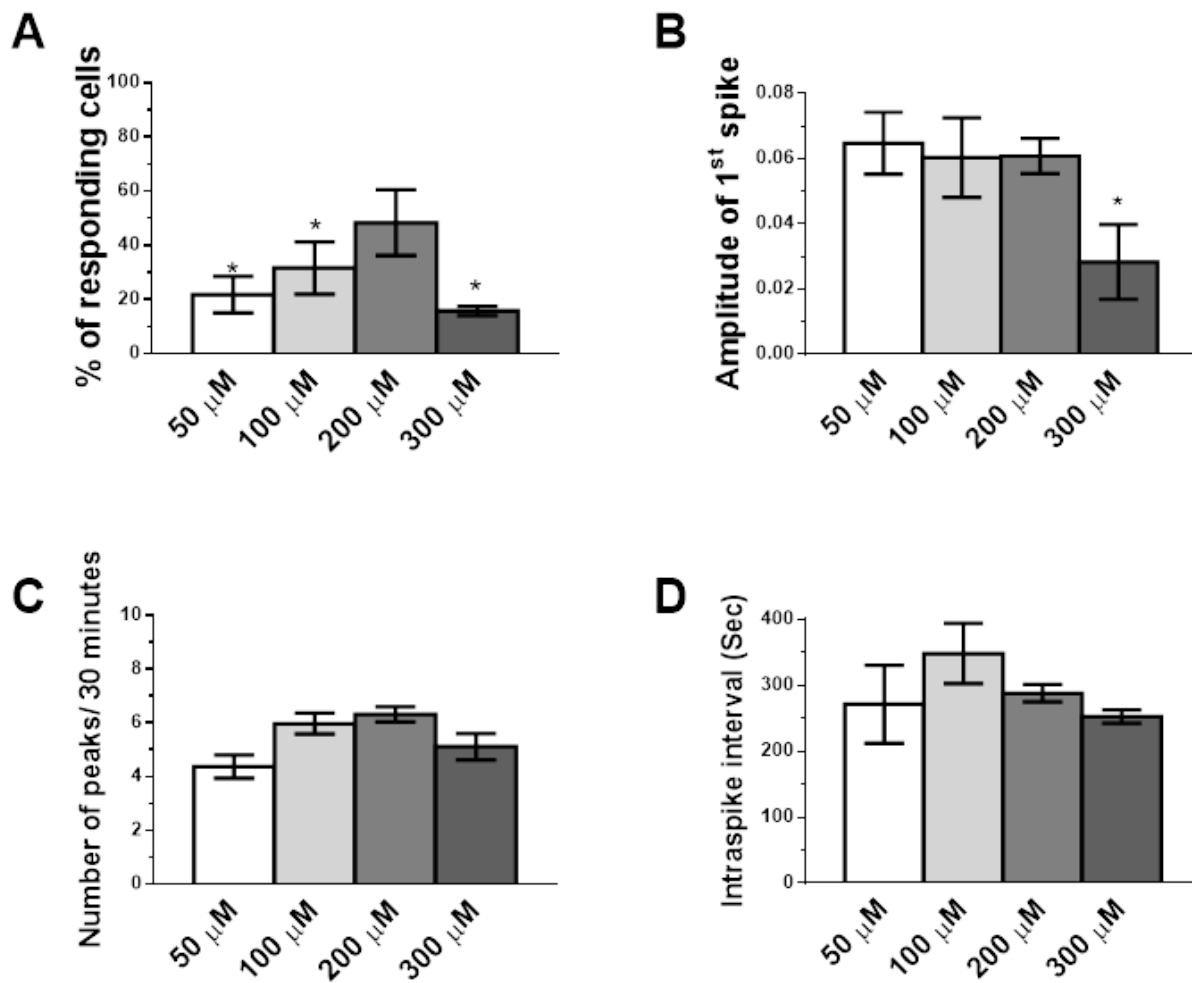


Figure 21. Statistical analysis of Glut-induced intracellular Ca^{2+} oscillations in bEND5 cells. Bar histograms show the average \pm SE of the percentage of responding cells (A), amplitude of the 1st spike, (B), number of oscillations/30 min (C), average ISI. The asterisk indicates $p < 0.05$.

Glutamate-induced intracellular Ca^{2+} oscillations require both intracellular Ca^{2+} release and extracellular Ca^{2+} entry

The analysis of Ach-induced intracellular Ca^{2+} oscillations revealed that intracellular Ca^{2+} signals in bEnd5 cells may involve ER-dependent Ca^{2+} mobilization through InsP_3Rs and SOCE. Therefore, in order to assess the relative contribution of endogenous Ca^{2+} release and Ca^{2+} entry to the evoked response, we first applied glutamate (200 μM) in the absence of extracellular Ca^{2+} (0Ca^{2+}). Glutamate still induced repetitive Ca^{2+} spikes under 0Ca^{2+} conditions, but these Ca^{2+} oscillations rapidly run down (Fig. 22A and Fig. 22C). The subsequent addition of Ca^{2+} to perfusate resumed the oscillatory response (Fig. 22A and Fig. 22C). The amplitude of the 1st Ca^{2+} spike was not different in the presence and absence of external Ca^{2+} (Fig. 22B), thus suggesting that Ca^{2+} entry is not necessary to initiate the oscillations, but is strictly required to maintain them over time ([246]). Likewise, removal of extracellular Ca^{2+} during ongoing oscillations caused the Ca^{2+} oscillatory response to persist only for 1-2 spikes before rapidly returned $[\text{Ca}^{2+}]_i$ to resting levels (Fig. 22D). Again, intracellular Ca^{2+} burst quickly recovered when Ca^{2+} was restored to the extracellular bathing solution (Fig. 22D). Overall, these findings strongly indicate that glutamate-induced intracellular Ca^{2+} oscillations are shaped by the rhythmical mobilization of the intracellular Ca^{2+} reservoir and sustained by extracellular Ca^{2+} entry.

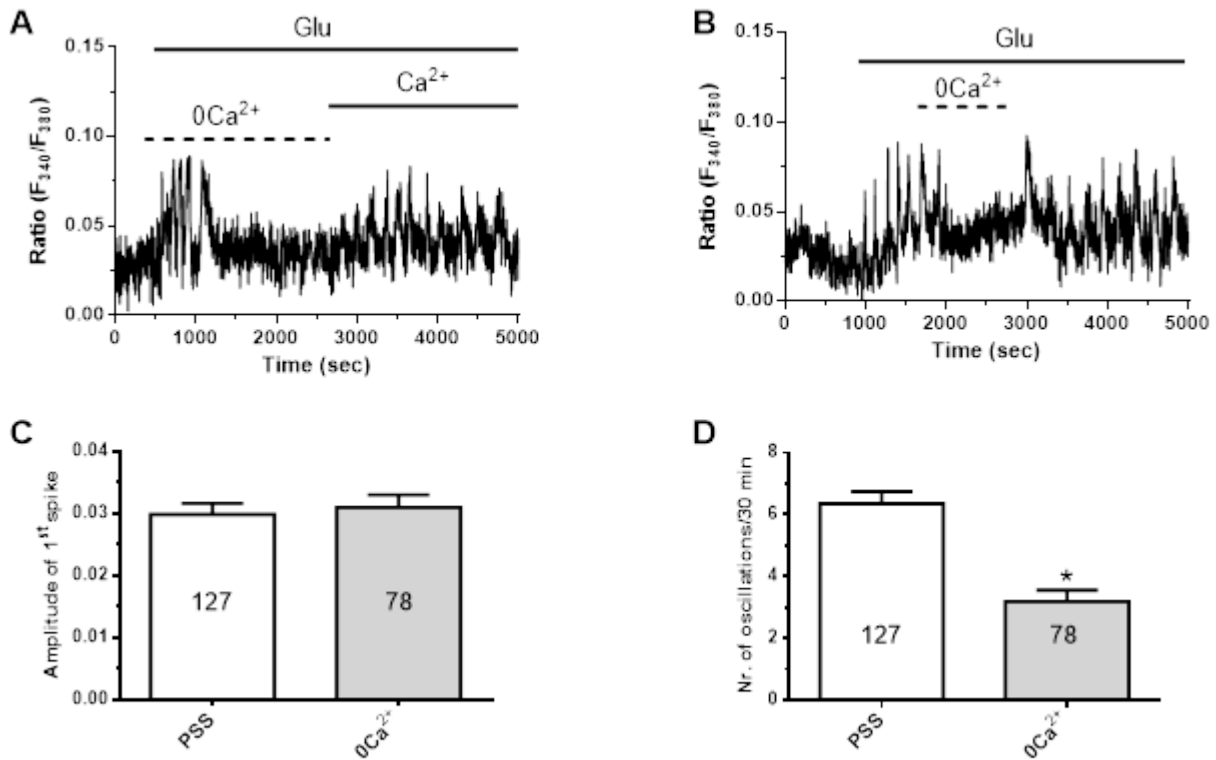


Figure 22. Glut-induced intracellular Ca²⁺ oscillations require Ca²⁺ release and extracellular Ca²⁺ entry. (A), Glut induced repetitive Ca²⁺ spikes under 0Ca²⁺ conditions, but these Ca²⁺ oscillations rapidly run down. Glut-induced Ca²⁺ oscillations resumed when Ca²⁺ was added to perfusate. (B), questa figura dice un'altra cosa, guardala meglio leggendo il testo. (C), bar histogram shows the average±SE of the amplitude of 1st spike induced by Glut in the presence and absence of extracellular Ca²⁺. (D), bar histogram shows the number of oscillation/30 min induced by glutamate in bEND5 cells in the presence and absence of external Ca²⁺. The asterisk indicates p<0.05.

Glutamate-induced intracellular Ca^{2+} oscillations are generated by Ca^{2+} release from the ER

As mentioned earlier, the ER represents the main intracellular Ca^{2+} reservoir in bEnd5 cells and delivers periodic Ca^{2+} spikes in response to extracellular stimulation through InsP_3Rs . Accordingly, Glut-induced intracellular Ca^{2+} oscillations were blocked by U73122 (10 μM , 30 min), while its inactive analogue, U73343 (10 μM , 30 min), had no effect (Fig. 23A and 23D). Likewise, 2-APB (50 μM , 30 min) prevented the initiation of glutamate-induced intracellular Ca^{2+} oscillations under 0Ca^{2+} conditions. Therefore, InsP_3 plays a key role also in the generation of repetitive Ca^{2+} transients induced by Glut in BEND5 cells. To further confirm this hypothesis, we depleted the ER Ca^{2+} store with CPA in the absence of extracellular Ca^{2+} . As expected, Glut failed to trigger any detectable increase in intracellular Ca^{2+} levels under these conditions (Fig. 23B and 23D). According to this model, after each Ca^{2+} spike, Ca^{2+} must be sequestered back by SERCA to allow the ER to continue releasing Ca^{2+} and support the intracellular Ca^{2+} waves. If this hypothesis was true, the pharmacological blockade of SERCA should suppress the Ca^{2+} spikes as the ER can no longer be replenished. Consistently, addition of CPA during ongoing spikes caused an abrupt increase in $[\text{Ca}^{2+}]_i$, due to the passive Ca^{2+} leak, followed by complete inhibition of glutamate-induced intracellular Ca^{2+} transients (Fig. 23C). The $[\text{Ca}^{2+}]_i$, however, decayed to a plateau level which was indicative of SOCE activation. Therefore, these data strongly support the hypothesis that InsP_3Rs mediate the periodic release of ER Ca^{2+} in response to glutamate stimulation in bEnd5 cells.

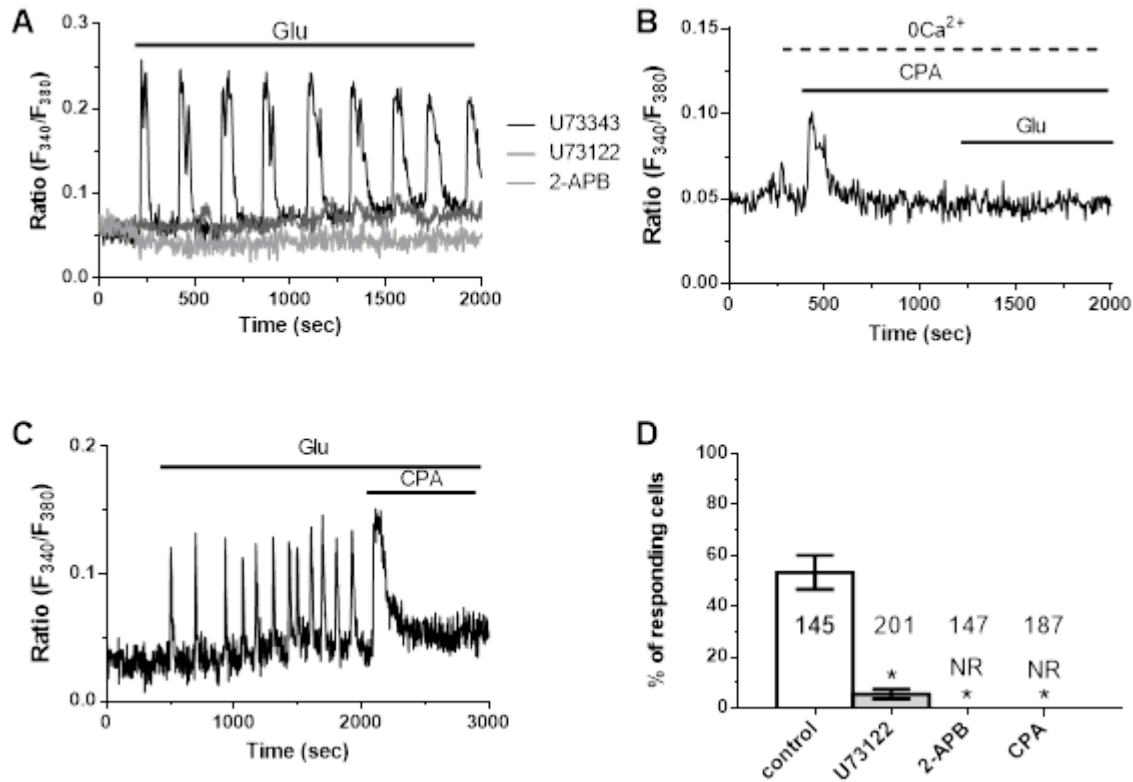


Figure 23. Glut-induced intracellular Ca^{2+} oscillations are mediated by rhythmical ER-dependent Ca^{2+} release through $InsP_3Rs$. (A), Glut-induced Ca^{2+} oscillations were inhibited by U73122 (10 μM , 30 min), but not by structurally inactive analog, U73343 (10 μM ; 30 min), and by 2-APB (50 μM , 30 min). (B), addition of CPA (10 μM) in absence of extracellular Ca^{2+} caused an increase in $[Ca^{2+}]_i$ due to Ca^{2+} leak from ER. Subsequent administration of glutamate failed to enhance intracellular Ca^{2+} levels. (C), addition of CPA (100 μM) during ongoing oscillations caused a complete inhibition of Glut-induced Ca^{2+} transients. (D), bar histogram shows the average \pm SE of the percentage of responding cells under the designated treatments. The asterisk indicates $p < 0.05$.

Glutamate-induced intracellular Ca^{2+} oscillations are maintained by constitutive Ca^{2+} entry

The results described in Figure 25A and Figure 25B demonstrate that extracellular Ca^{2+} entry is necessary to maintain the oscillatory Ca^{2+} response to glutamate over time. As described above, SOCE represents the main pathway for agonist-induced Ca^{2+} entry in bEnd5 cells, but is also heavily activated in the absence of extracellular stimulation to replenish the ER Ca^{2+} content. Therefore, in order to evaluate whether SOCE is the Ca^{2+} -permeable route recruited by glutamate to sustain the intracellular Ca^{2+} oscillations, we could not pre-incubate the cells with any SOCE inhibitor.

Therefore, we turned to the Mn^{2+} -quenching technique, which revealed that Glutamate was not able to enhance the rate of the constitutive Mn^{2+} influx in BEND5 cells (Fig. 24A). As expected, in the same batch of cells, acetylcholine (100 μM) increased the rate of Fura-2 fluorescence decline (Fig. 24B). According to the statistical analysis (Fig. 24C), these data provide a strong evidence that glutamate does not activate metabotropic Ca^{2+} entry in bEnd5 cells. It turns out that it is the constitutive SOCE to maintain glutamate-induced intracellular Ca^{2+} oscillations by providing releasable Ca^{2+} to the InsP_3 -sensitive ER stores ([237]).

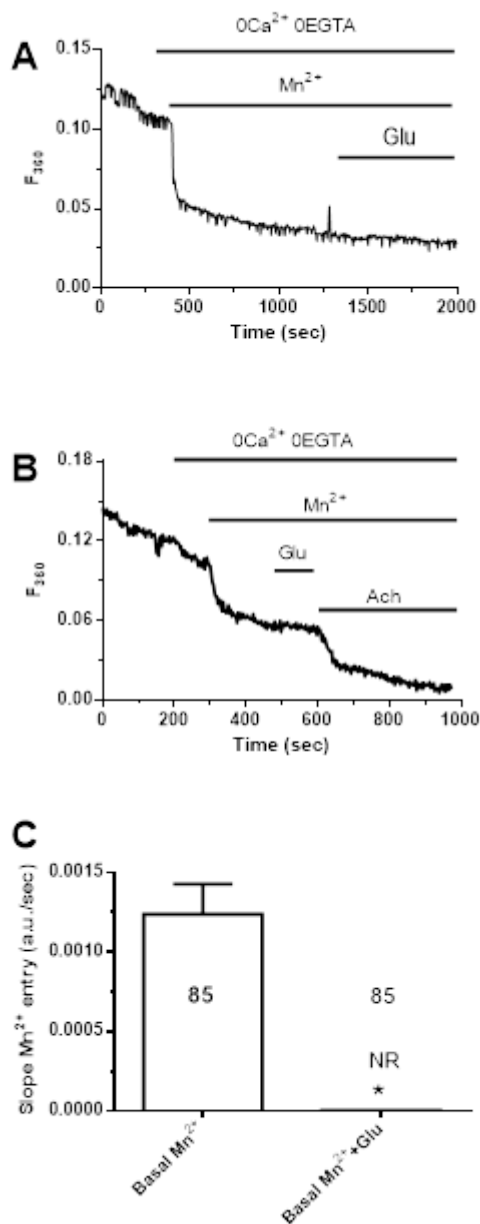


Figure 24. Glutamate induces intracellular calcium entry activation in bEND5 cells. (A), Glut was not able to enhance the rate of constitutive Mn^{2+} influx in BEND5 cells. (B), Acetylcholine (100 μM) increased the rate of Mn^{2+} entry in bEND5 cells. (C), mean \pm SE of the slope of basal and Glut-induced in bEND5 cells. The asterisk indicates $p < 0.05$.

Glutamate-induced intracellular Ca^{2+} oscillations lead to NO release in bEnd5 cells

Finally, we assessed whether Glut-induced intracellular Ca^{2+} oscillations drive NO release by loading the cells with the NO-sensitive fluorochrome, DAF/FM ([13], [119]). Glut caused a slow, but sustained increase in NO levels, which started with a latency of 387 ± 53 sec ($n=143$) and reached a plateau after about 1000 sec (Fig. 25A). This signal was suppressed by MCPG (200 μM , 10 min) (Fig. 25B and 25E). Moreover, glutamate-induced NO release was abolished by pre-incubating the cells with L-NAME (100 μM , 1 h) or BAPTA (30 μM , 2 h) (Fig. 25A and 25E). These findings demonstrate that glutamate engages eNOS in a Ca^{2+} -dependent manner. Also, glutamate failed to elevate NO levels in the presence of either U73122 (10 μM , 30 min), 2-APB (50 μM , 30 min), or CPA (10 μM , 30 min) (Fig. 25C and 25E). Unlike acetylcholine, Glut-induced NO release also occurred in the absence of external Ca^{2+} and was further enhanced by the subsequent addition of Ca^{2+} to the extracellular solution (Fig. 25D), in agreement with the Ca^{2+} imaging data (Fig. 22A). Collectively, these findings clearly show that Glut stimulates NO release by activating intracellular Ca^{2+} oscillations in mouse brain endothelial cells.

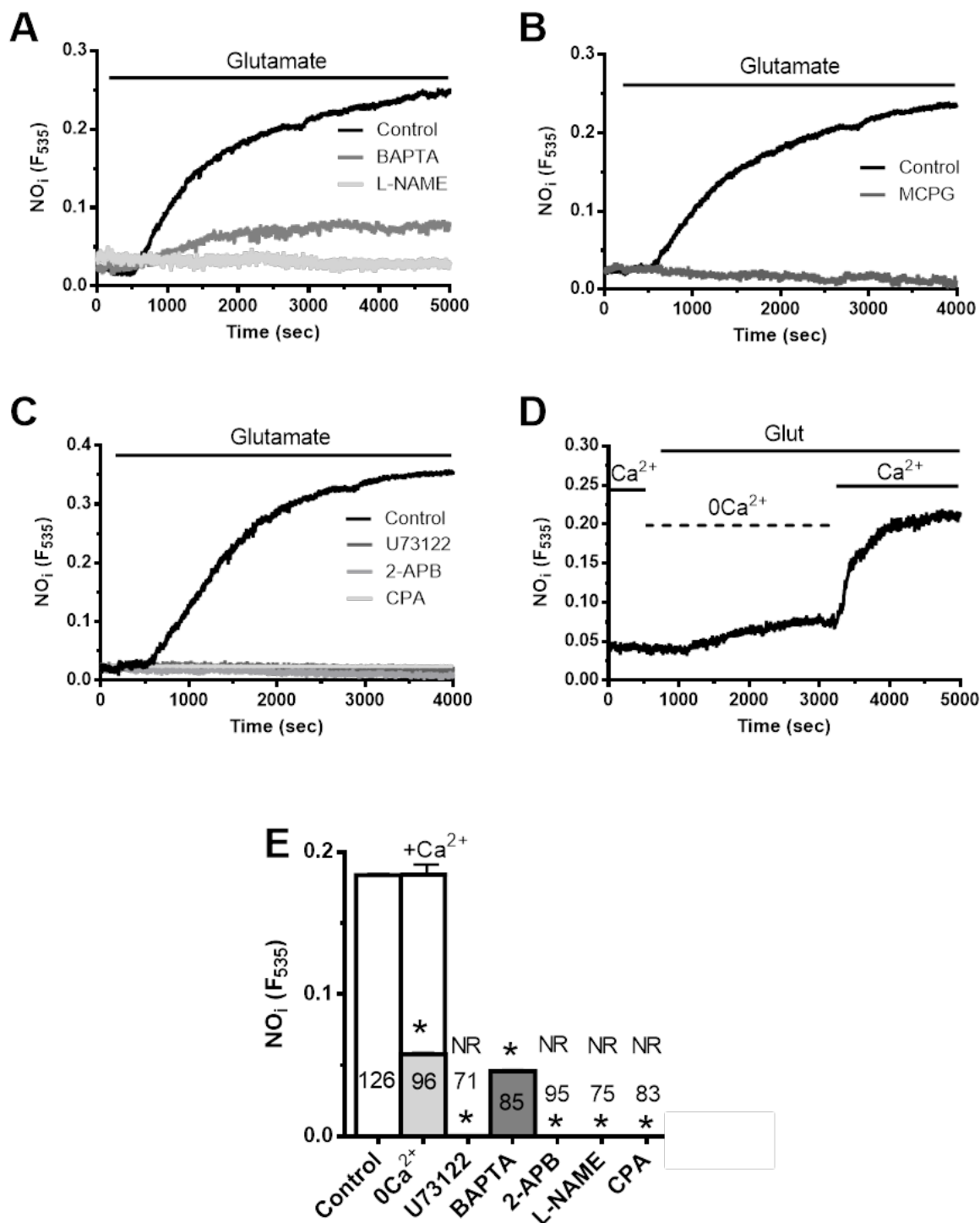


Figure 25. Glut-induced intracellular Ca²⁺ oscillations lead to NO release in bEND5 cells. (A), Glut (200 μM), caused an increase NO-dependent signal in bEND5 cells loaded with the NO-sensitive fluorophore, DAF/FM; this signal was strongly reduced by either L-NAME (100 μM, 1 h) or BAPTA (30 μM, 2 h). (B), Glut-induced NO release was abolished by MCPG (200 μM, 10 min). (C) Glut-induced NO release was also abolished by U73122 (10 μM, 30 min), 2-APB (50 μM, 30 min) and CPA (10 μM, 30 min). (D), Glut induced NO production also in absence of extracellular Ca²⁺ (0Ca²⁺). (E), mean±SE of the magnitude of Glut-induced NO synthesis under the designated treatments. The asterisk indicates p<0.05.

Glutamate induces Ca²⁺-dependent NO synthesis in human brain microvascular endothelial cells

As for Ach, we assessed whether glutamate stimulates NO production in a Ca²⁺-dependent manner also in hCMEC/D3 cells. As shown in Figure 27A, Glut (200 μM) caused a slow increase in [Ca²⁺]_i, which then gradually decayed to the baseline. As observed in bEND5 cells, the Ca²⁺ response to Glut was abolished by MCPG (200 μM, 10 min) (Fig. 26A), which hints at mGluR involvement. Likewise, in hCMEC/D3 cells loaded with DAF/FM, Glut caused a slow and sustained increase in DAF/FM fluorescence that was inhibited by BAPTA (30 μM, 2 h) (Fig. 26B). Therefore, Glut is able to induce NO synthesis in a Ca²⁺-dependent manner also in human microvascular endothelial cells, although with a different mode of Ca²⁺ signalling.

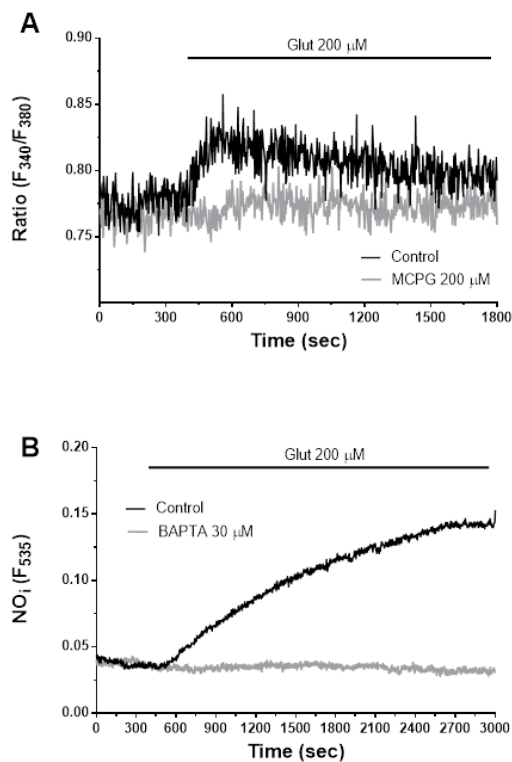


Figure 26. Glutamate causes Ca²⁺-dependent NO release also in human microvascular brain endothelial cells. (A), Glut (200 μM) caused an increase in [Ca²⁺]_i in hCMEC/D3 cells, loaded with Fura-2/AM in the absence, but not in the presence, of MCPG (200 μM, 10 min). (B), Glut (200 μM) caused an increase in DAF/FM fluorescence in hCMEC/D3 cells in the absence, but not in the presence, of BAPTA (30 μM, 2 h).

DISCUSSION

Acetylcholine and glutamate are two of the most important neurotransmitters of the CNS which regulate CBF by releasing NO and causing vasorelaxation. Ach acts through the stimulation of brain microvascular ECs that engage the activation of the eNOS. eNOS is an archetypal Ca^{2+} /Calmodulin-dependent enzyme and the waveform of the Ca^{2+} signals that underlie Ach-induced NO release in many vascular bed is well known. Surprisingly, whether and how acetylcholine evokes an increase in intracellular Ca^{2+} concentration in brain microvascular cells is still unclear. On the other hand, Glu stimulates NMDARs to activate eNOS, but it remains to be elucidated whether mGluRs are able to promote NO release in brain microvascular ECs. The present investigation sought to fill these gaps by analysing bEND5 and hCMEC/D3 cells, two establish brain endothelial cells lines derived from mouse and human, respectively. This information has a potential clinical relevance as increase in cortical CBF is involved in a growing number of neurodegenerative disorder, such as Alzheimer's Disease. Understand the mechanism and the proteins involved could, therefore, be used in the future as target to rescue local blood perfusion in patients affected by neurodegenerative disorders.

Herein, we first demonstrated that Ach induces NO release by triggering two different modes of Ca^{2+} signals in murine (bEND5) and human (hCMEC/D3) brain microvascular endothelial cells. Of note, ER Ca^{2+} release via InsP_3Rs and SOCE shapes the Ca^{2+} response to Ach in both cell types but their different Ca^{2+} toolkits are likely to result in two quite different waveforms, i.e. Ca^{2+} oscillations vs. biphasic Ca^{2+} elevation. Whatever its waveform however, Ach-induced intracellular Ca^{2+} signals lead to robust NO release in both murine and human brain microvascular endothelial cells. Likewise, we demonstrated for the first time that Glut activated mGluRs to trigger intracellular Ca^{2+} oscillation in bEND5 and a biphasic increase in $[\text{Ca}^{2+}]_i$ in hCMEC/D3. We further showed that mGluRs-dependent Ca^{2+} signals drive NO release in both bEND5 and hCMEC/D3. This NO signal is delayed compare to the Ach-induced one and is likely to play a crucial role in the slower vasodilation that often follows brief neuronal activity or that sustains functional hyperemia during persistent synaptic transmission ([247], [16]). The glutamate-induced Ca^{2+} response is likely to play an important role in the generation of additional endothelial vasorelaxing messengers, such as PGE2 and endothelial-dependent hyperpolarizing factor (EDHF) ([8], [248]), that are also involved in NVC during glutamatergic transmission ([16]).

Future experiments will have to assess: 1) the role of other neurotransmitters, such as GABA and glutamate, or neuromodulators, such as catestatine, in modulating Ca^{2+} signaling in bEND5 and hCMEC/D3 cells; and 2) whether Ach- and Glut-induced Ca^{2+} and NO signals are deranged in neurodegenerative disorders, such as Alzheimer's Disease (AD). AD indeed is a severe cortical cholinergic deficiency. This disease process is of particular interest, since it seems to be related to distortion in regional brain capillary structure involving endothelial cell shape changes and impairment of NO release which affects signaling between the immune, cardiovascular and nervous systems ([249]).

Acetylcholine stimulates intracellular Ca^{2+} oscillations in bEND5 in a dose-dependent manner

In bEND5, Ach reliably caused recurrent Ca^{2+} oscillations that appeared at 100 μM and were then maintained at 300 and 500 μM . We could not detect any increase in $[\text{Ca}^{2+}]_i$ at concentrations lower than 50 μM ; however, we cannot rule out the possibility that highly localized sub-cellular Ca^{2+} pulses occur at such doses, but are missed by our epifluorescence system. In this view, 0.1 μM carbachol (a non-selective mAChR agonist) elicits spatially restricted Ca^{2+} puffs that intermittently arise at no more than two discharging sites located at the ends of rat artery tail endothelial cells in situ ([250]). However, Ach induces vasorelaxation of mouse brain intracortical microvessels in vivo in the mid micromolar range([251]), although in one study it induced vasodilation already at 10 μM ([83]). It has long been known that mAChR expression declines rapidly with successive passages of cultured endothelial cells ([86], [252]), which could account for the reduced sensitivity to Ach observed in our investigation as compared to others ([83]). Unfortunately, the isolation of intact brain microvessels from the mouse is extremely technically challenging and we could not investigate the effect of Ach on Ca^{2+} dynamics in brain endothelial cells in situ ([214], [253]). As expected ([254], [248]), Ach-induced Ca^{2+} response were indeed prevented by atropine, a wide spectrum inhibitor of mAChRs, in bEnd5 cells. Moreover qRT-PCR analysis revealed that only M3-mAChRs are expressed in bEND5 cells. This finding concurs with the waveform of Ach-induced Ca^{2+} signal as M3-mAChRs trigger repetitive Ca^{2+} transients in most endothelial preparations studied ([86], [254]). The M3-mAChRs caused ACh-dependent endothelium vasodilation in most vascular preparations studied, although there is evidence implicating a role for M1-mAChRs and M5-mAChRs in some vascular beds ([255]). Accordingly to the statistical analysis, in bEND5 the most suitable concentration for Ach to trigger recurrent Ca^{2+} spikes was 300 μM . Accordingly, while the

percentage of responding cells was similar to that measured at 100 μM , the number of oscillations/hour and the average ISI of the Ca^{2+} train were significantly higher at this dose. This finding strongly suggests that the biological information encoded within Ach-induced Ca^{2+} transients is mainly delivered via frequency rather than amplitude modulation ([256], [257], [258]). Consistent with this hypothesis, while the magnitude of the 1st Ca^{2+} spike was significantly higher at 100 μM , there was no difference in the amplitude of the subsequent Ca^{2+} transients between 100 and 300 μM . A further increase in Ach concentration to 500 μM resulted in the reduction of the percentage of responding cells and in the lengthening of the ISI. This bell-shaped dose-response relationship has also been described for EGF-induced intracellular Ca^{2+} oscillations in rat cardiac microvascular endothelial cells ([233]) and hints at partial mAChR desensitization at high Ach concentrations ([259], [260]). For instance, a high dose (1 mM) of carbachol cause rapid desensitization of M3-mAChR-dependent InsP_3 synthesis and InsP_3 -dependent Ca^{2+} mobilization due to receptor sequestration in chinese hamster ovary (CHO) cells ([259], [261]). Previous studies did not investigate the dose-dependent increase in the endothelial Ca^{2+} response to Ach at concentrations higher than 100 μM ([262], [250], [263]). Intriguingly, bEND5 cells displayed a remarkable propensity to generate spontaneous Ca^{2+} oscillations, which arose in the absence of any agonist in the bathing solution. Spontaneous intracellular Ca^{2+} oscillations are not frequent in vascular endothelial cells, but have also been observed in mouse mesenteric ([264]) and cremasteric arteries ([265]) and in rat lung capillaries ([266]). In most cases, this spontaneous Ca^{2+} activity was triggered by InsP_3 -dependent Ca^{2+} release from the ER and sustained by extracellular Ca^{2+} entry ([264]).

The Ca²⁺ toolkit of mouse brain endothelial cells

Endothelial cells have two main pathways to generate and regulate intracellular Ca²⁺ signals ([87], [31]): Ca²⁺ release from endogenous Ca²⁺ stores and Ca²⁺ entry from the extracellular environment. We performed an extensive qRT-PCR analysis to assess which of the components of the endothelial Ca²⁺ toolkit that can be recruited upon PLC β activation are present in bEND5 cells. According to our screening, ER stored Ca²⁺ could be mobilized via InsP₃R1 and InsP₃R2 in bEND5 cells, in which we could not detect any transcript encoding for RyRs. The pattern of InsP₃R expression in this mouse brain microvascular endothelial cell line supports their propensity to trigger intracellular Ca²⁺ oscillations either under resting conditions or in the presence of an extracellular ligand. Indeed, InsP₃R2, which shows the sharpest dependence on ambient Ca²⁺ and is the most sensitive to InsP₃, has long been regarded as the main oscillatory unit ([201], [267]). As to Ca²⁺ entry, we found that bEND5 cells express both Stim isoforms, i.e. Stim1 and Stim2, but only the Orai2 subtype at both mRNA and protein level. Curiously, Orai2 is also the isoform that mediates SOCE in both resting and synaptically-activated mouse neurons ([178]), while Orai1 mediates SOCE in rat brain ([268]). Vascular endothelial cells are extremely sensitive to their surrounding microenvironment ([269]). Their genomic profile may be reprogrammed by signal inputs delivered by the native tissue ([270]). In this perspective, the evidence that Orai2 is the most likely candidate to underlie SOCE in mouse brain microvascular endothelial cells is not surprising. Moreover, Orai2 represents the pore-forming SOC subunit also in a bovine brain capillary endothelial cell line, t-BBEC117 ([222]). The Mn²⁺-quenching technique revealed that a Ca²⁺ influx pathway with a pharmacological profile compatible with that of SOCE is activated under resting conditions in bEND5. The slope of this basal Ca²⁺ entry was further enhanced by depleting ER Ca²⁺ with CPA, thereby suggesting that SOCE could also be recruited by extracellular stimulation. Again, these data are reminiscent of those described in mouse brain neurons, where Orai2 is tonically active due to the partial emptying of the ER Ca²⁺ store even in quiescent cells ([178], [271]), but may also contribute to synaptic dependent activity ([272]). It is assumed that Stim2, which displays a lower affinity for ER Ca²⁺ levels and may be activated by a modest reduction in intraluminal Ca²⁺ concentration, gates Orai2 in unstimulated bEND5 cells ([178], [271]), [273]), while Stim1 is called into action by a massive ER store depletion ([274]). Among TRPC channels, which represent the TRP sub-family preferentially coupled to PLC β ([275]), only TRPC1 was expressed in mouse brain microvascular endothelial cells. Interestingly, TRPC1 is a polymodal channel which can mediate SOCE in endothelial cells, but mainly in association with Orai1 ([167], [276]).

Acetylcholine-induced Ca^{2+} response is driven by ER Ca^{2+} release via InsP_3Rs and sustained by SOCE in mouse brain endothelial cells

In bEND5, Ach-induced Ca^{2+} oscillations were driven by recurrent cycles of ER Ca^{2+} release via InsP_3Rs followed by SERCA-mediated sequestration. The first evidence that supports this theory is that inhibiting the synthesis of InsP_3 with U73122, which selectively blocks $\text{PLC}\beta$ activity in vascular endothelial cells ([277], [278]), prevents the Ach-induced oscillating Ca^{2+} response. This effect was mimicked by 2-APB, which interferes with InsP_3Rs , but it not highly specific as it could also impede Ca^{2+} entry ([179]). However, the inactive structural analog of U73122, i.e. U73343, did not exert any significant effect on the Ca^{2+} response to Ach. We can therefore conclude that $\text{PLC}\beta$ triggers the repetitive Ca^{2+} oscillations via InsP_3 -dependent Ca^{2+} release. Second, the pharmacological blockade of SERCA activity rapidly interrupted the spiking signal. Indeed, when SERCA activity is blocked, Ca^{2+} cannot be sequestered back into ER lumen to refill the store and this prevents the onset of the next Ca^{2+} spike. Third, RyRs are absent in bEND5 cells, as reported in endothelial cells from other vascular districts ([31]). However, the presence of extracellular Ca^{2+} is a necessary condition to the onset of the regenerative ER Ca^{2+} release. Ach-induced Ca^{2+} oscillations did not reach the threshold for detection by our epifluorescence system under 0Ca^{2+} conditions, but suddenly resumed as soon as we restored Ca^{2+} to the bathing solution. At the same way, removal of external Ca^{2+} led to the rapid decline of the spiking signal, which could not last for longer than 1-2 spikes in the absence of Ca^{2+} influx. Likewise, intracellular Ca^{2+} oscillations were never observed in the absence of extracellular Ca^{2+} in several types of human endothelial colony forming cells ([242], [279]), Ea.hy926 cells ([280]), and bovine atria endothelial cells ([281]).

The Mn^{2+} quenching technique revealed that Ach was able to readily activate a Ca^{2+} permeable pathway with a pharmacological profile compatible with that of SOCE in bEND5 cells. In the presence of either La^{3+} or BTP2, Ach did not cause any significant increase in the slope of the quenching curve, which is a reliable readout of Ca^{2+} influx ([237], [239], [241], [282]). Moreover, Ach failed to induce any detectable Ca^{2+} response after a prolonged application of CPA, which led to the depletion of the ER Ca^{2+} reservoir and to full SOCE activation ([242], [243], [244]). It turns out that a store-independent Ca^{2+} channel is not activated by Ach in bEND5 cells. Overall, these data strongly suggest that SOCE is the main Ca^{2+} entry route engaged by Ach in bEnd5 cells.

The requirement of SOCE for regenerative InsP_3 -dependent Ca^{2+} release may be interpreted within the framework of the luminal loading mechanism originally proposed by Sir Michael J. Berridge ([283], [284]). According to this model, InsP_3 causes a highly restricted sub-membranal Ca^{2+} release which is not able to result in a regenerative Ca^{2+} signal and escapes therefore detection from a conventional epifluorescence system. Nevertheless, local depletion of this peripheral ER sub-compartment is sufficient to promote Stim oligomerization and relocation towards cell periphery, thereby resulting in Orai2 activation. Such a tight coupling between a small superficial compartment of the ER and store-operated Orai channels has been extensively described in many cell types ([274]). Consistently, in bEND5, the ensuing influx of Ca^{2+} results in a SERCA-mediated increase in intraluminal Ca^{2+} concentration ($[\text{Ca}^{2+}]_{\text{ER}}$) that sensitizes InsP_3 Rs to ambient InsP_3 and Ca^{2+} and triggers the first regenerative Ca^{2+} spike. This coordinated sequence of Ca^{2+} fluxes inside the cytosol persists as long as Ca^{2+} is present in the extracellular milieu and preserves $[\text{Ca}^{2+}]_{\text{ER}}$ from depletion. This model is strongly corroborated by the evidence that SOCE maintains ER Ca^{2+} levels in bEND5 cells. Accordingly, the pharmacological blockade of constitutive SOCE induces ER Ca^{2+} depletion and prevents CPA-dependent Ca^{2+} mobilization, as recently shown in EPCs isolated from patients affected by infantile hemangioma ([128]). It is, therefore, conceivable that SOCE is redirected into ER lumen at higher rate following $\text{PLC}\beta$ activation by Ach in mouse brain microvascular endothelial cells, thereby leading to the onset of the Ca^{2+} burst. This model is also supported by a landmark study carried out by Morgan and Jacob twenty years ago, which elegantly demonstrated that agonist-induced SOCE is indispensable for loading up the ER with Ca^{2+} and maintaining InsP_3 R sensitivity from the luminal side during prolonged Ca^{2+} oscillations in human umbilical vein endothelial cells([237]). Once set in motion by Ach administration, the spiking response was not immediately interrupted by extracellular Ca^{2+} removal as it persisted for no more than 1 transient. This observation indicated that the Ca^{2+} pool available for InsP_3 -dependent Ca^{2+} release rapidly depleted in the absence of Ca^{2+} entry and cannot further sustain the Ca^{2+} signal.

Acetylcholine-induced intracellular Ca²⁺ oscillations drive NO production in bEND5 cells

The functional outcome of Ach-induced Ca²⁺ response is the generation of NO in bEND5. The pharmacological inhibition of each signaling pathway involved in the oscillatory signal impaired Ach-induced NO synthesis. This observation suggests that the NO production was driven by Ca²⁺ oscillations in bEND5 cells. A frequency modulated system is more suitable to sustain the prolonged activation of a cellular decoder, such as eNOS, that is regulated by Ca²⁺ in a highly cooperative manner ([256]). Accordingly, Ach-induced Ca²⁺ oscillations have been shown to support NO release in a number of vascular districts ([86]), including rat tail artery ([285]) and mouse aorta ([254]). This information shed further light on the molecular events that take place in the neurovascular unit during neuronal activity ([8]). Moreover, they further highlight the role played by Ca²⁺ pathways in brain endothelium ([214]). A periodic increase in [Ca²⁺]_i has long been known to regulate blood-brain barrier permeability([286], [194]), lymphocyte migration across the blood-brain barrier ([287]) and trypanosome infection ([288]). Taken together these data add NO production to the growing list of functions underlain by intracellular Ca²⁺ response in brain microvascular endothelium.

Acetylcholine driven intracellular Ca²⁺ increase in hCMEC/D3 in a dose-dependent manner

In hCMEC/D3, Ach failed to cause recurrent Ca²⁺ spikes, but induced a transient increase in [Ca²⁺]_i with a different pattern depending on agonist concentration. Similar to bEND5 cells, Ach induced bell-shaped dose-response relationship in human brain ECs, as the amplitude of the initial Ca²⁺ peak increased when Ach concentration was raised from 25 μM to 100 μM and then decreased upon a further rise to 200 μM. These observations indicate that the mAChRs endowed to hCMEC/D3 cells are more sensitive as compared to those expressed in bEnd5 cells. Accordingly, M5-mAChR was the most abundant isoform detectable in hCMEC/D3 cells, which is consistent with previous findings obtained in cerebral arteries of humans, cattle and mice ([83], [84]). These results are quite surprising, as previous studies in ECs located in other vascular districts expressing both M3- and M5-mAChRs demonstrated that the former is more sensitive to cholinergic stimulation ([255]). We speculate that the signalling coupling between M5-mAChR and PLC is more efficient in bEnd5 cells as compared to that between M3-mAChRs and PLC.

The Ca²⁺ toolkit of human brain endothelial cells

We have screened the components of the Ca²⁺ toolkit also in hCMEC/D3 cells. Unlike their murine counterparts, they only expressed InsP₃R3, which displays the lowest affinity to InsP₃ and Ca²⁺ ([267]), tends to curtail the spiking response and therefore functions as an anti Ca²⁺ oscillatory unit ([201], [267], [203]). This finding, therefore, could explain why Ach (as well as Glut, as discussed below) does not trigger a spiking Ca²⁺ response in hCMEC/D3 cells. Moreover, RYRs are absent, thereby confirming that ER Ca²⁺ mobilization is only mediated by InsP₃R3. As to the Ca²⁺ entry pathways, hCMEC/D3 cells only express Stim2, although they are endowed with all the three Orai subtypes. These data suggest that Stim2 is the ER Ca²⁺ sensor that drives both constitutive and Ach-induced SOCE, while Orai1 and Orai2 are the most likely candidate to provide the pore-forming subunits of SOCs. Quite surprisingly, hCMEC/D3 cells lack all TRPC channel subtypes with the exception of TRPC7, whose endothelial expression has only barely been reported ([31]). TRPC7 is a DAG-sensitive channel, but OAG failed to cause any evident increase in [Ca²⁺]_i. Therefore, TRPC7 is unlikely to contribute to Ach-induced Ca²⁺ entry in hCMEC/D3 cells.

Acetylcholine-induced Ca²⁺ response are driven by ER Ca²⁺ release via InsP₃Rs and SOCE in human brain endothelial cells

Unlike bEND5, the Ca²⁺ response to Ach was detectable also under 0Ca²⁺ conditions in hCMEC/D3 cells. Ach was still able to generate a rapid increase in [Ca²⁺]_i that rapidly went back to the basal line, lacking the SOCE-dependent plateau phase. It is, therefore, possible that hCMEC/D3 possess a higher intraluminal ER Ca²⁺ concentration as compared to bEND5 cells, that more InsP₃ is synthesized in response to M5-mAChR activation, or that newly-synthesized InsP₃ is more efficiently transmitted to InsP₃Rs. These hypotheses are not mutually exclusive among each other. It should, however, be pointed out that the amplitude of CPA-induced ER Ca²⁺ leakage was higher in hCMEC/D3 than in bEND5 cells (Fig. 7 and 17). This observation strongly suggests that the Ca²⁺ pool available for InsP₃-dependent Ca²⁺ release (see below) is higher in hCMEC/D3 than in bEND5 cells and can give rise to the Ca²⁺ signal in absence of extracellular Ca²⁺. Clearly, future experiments with genetic Ca²⁺ indicators targeted to ER lumen are necessary to confirm this mechanism. Indeed, we first found that the Ca²⁺ response to Ach was inhibited by preventing InsP₃ synthesis with U73122 and by interfering with InsP₃Rs with 2-APB. Of note, U73343 did not exert

any significant effect on the Ca^{2+} response to Ach. Secondly, after the complete emptying of ER Ca^{2+} stores obtained after 30 min of treatment with CPA, the Ca^{2+} response to Ach was absent. This data further confirms that Ach needs Ca^{2+} released from ER to induce the intracellular Ca^{2+} response in hCMEC/D3. We can, therefore, conclude that Ach-induced intracellular Ca^{2+} release was triggered by $\text{PLC}\beta$ activation and mediated by InsP_3Rs .

The “ Ca^{2+} add-back” protocol revealed that Ach was able to activate a SOCE pathway that was completely blocked by Pyr6; similar to bEnd5 cells, Pyr6 was also able to prevent CPA- and Ach-induced intracellular Ca^{2+} release. These data indicate that SOCE was also constitutively open in human brain microvascular ECs and could be further recruited upon agonist (i.e. Ach)-induced depletion of the ER Ca^{2+} store. Of note, in a minor fraction of hCMEC/D3 cells responding to Ach despite for the presence of Pyr6, the Ca^{2+} signal was similar to that measured under 0Ca^{2+} conditions, i.e. displayed lower amplitude and lacked the plateau phase. This observation corroborates the notion that SOCE sustains Ach-induced Ca^{2+} signaling in these cells.

Acetylcholine-induced intracellular Ca^{2+} mobilization drive NO production in hCMEC/D3 cells

Also in hCMEC/D3 cells, the Ca^{2+} response to Ach was able to induce NO synthesis. Accordingly, the pharmacological blockade of InsP_3 -dependent Ca^{2+} release and NO prevented Ach-induced NO release. This effect was mimicked by BAPTA, thereby reinforcing the evidence that cytosolic Ca^{2+} is required to recruit the eNOS in Ach-stimulated hCMEC/D3 cells.

Glutamate stimulates intracellular Ca^{2+} oscillations in bEND5 cells

In bEND5, glutamate caused Ca^{2+} oscillations that appeared at 50 μM and were then maintained at 100, 200 and 300 μM . We could not detect any increase in $[\text{Ca}^{2+}]_i$ at concentrations lower than 50 μM ; however, we cannot rule out the possibility that highly localized sub-cellular Ca^{2+} pulses occur at such doses, but are missed by our epifluorescence system. The dose-response relationship revealed that 200 μM Glut was the most efficient dose to evoke intracellular Ca^{2+} oscillations. This observation gains a strong functional relevance as glutamate concentration rapidly raise well beyond this range in the synaptic cleft in response to high frequency stimulation ([289], [290]). Considering that glutamatergic terminals establish close contacts with parenchymal microvessels ([247], [4]), it is highly conceivable that brain microvascular endothelial cells are exposed to a concentration of glutamate which is able to induce robust Ca^{2+} oscillations during neuronal activity.

Glutamate has long been known to induce an NMDARs-mediated increase in $[\text{Ca}^{2+}]_i$ in different types of brain microvascular endothelial cells, such as ECV304 ([291]), primary mouse brain endothelial cells ([292]), and human brain endothelial cells ([293]). However, this increase in $[\text{Ca}^{2+}]_i$ has always been observed at a rather high glutamate concentration, i.e. 1 mM, as the recording solutions were lacking the glutamate co-agonists, glycine or D-serine, which are strictly required by NMDARs to mediate Ca^{2+} entry at physiological glutamate levels also in non-neuronal tissues ([294]). Accordingly, a recent series of studies demonstrated that, in the presence of D-serine, 100 μM was sufficient to cause NMDARs-mediated NO-dependent vasodilation in mouse brain microvessels ([30]). In the present investigation, we did not add either glycine or D-serine to prevent NMDAR activation and rule out any contribution from ionotropic glutamate receptors. We found that glutamate was able to trigger a dose-dependent oscillatory increase in $[\text{Ca}^{2+}]_i$ that was, therefore, most likely to due to mGluR activation. The following observations strongly support this conclusion. First, glutamate-induced intracellular Ca^{2+} oscillations were inhibited by the broad-spectrum mGluR antagonist, MCPG. Second, the oscillatory response to glutamate arose in the absence of extracellular Ca^{2+} , which reflects the engagement of metabotropic receptors ([295]). Third, mGluRs were previously found in brain endothelium ([296], [297], [298]). Unfortunately, qRT-PCR, immunoblotting and immunofluorescence could not confirm mGluR expression in bEnd5 cells. We speculate that, similar to brain neurons, mGluRs could be confined within discrete,

extremely localized, membrane areas, which does not enable their detection with the resolution of our immunofluorescence and immunoblotting assays.

Glutamate-induced Ca^{2+} oscillations are driven by ER Ca^{2+} release via InsP_3Rs and SOCE in bEND5 cells

In bEND5 cells, Glutamate-induced Ca^{2+} oscillations were driven by rhythmical cycles of ER Ca^{2+} release via InsP_3Rs followed by SERCA-mediated sequestration and maintained by constitutive SOCE. The first evidence that supports this model is that Glut-induced Ca^{2+} spikes were inhibited by preventing InsP_3 synthesis with U73122 and by interfering with InsP_3Rs with 2-APB ([234]). Again, the inactive structural analog of U73122, i.e. U73343, did not exert any significant effect on Glut-induced Ca^{2+} oscillations. We can therefore, conclude, that $\text{PLC}\beta$ triggers the repetitive Ca^{2+} oscillations via InsP_3 -dependent Ca^{2+} release. Second, the pharmacological blockade of SERCA activity prevented the subsequent Ca^{2+} response to Glut. Likewise, the application of CPA to ongoing glutamate-induced intracellular Ca^{2+} waves resulted in the complete suppression of Ca^{2+} activity. Unlike Ach, however, Glut still induced repetitive Ca^{2+} spikes under 0Ca^{2+} conditions, but these Ca^{2+} oscillations rapidly run down. The subsequent addition of Ca^{2+} to perfusate resumed the oscillatory response. The amplitude of the 1st Ca^{2+} spike was not different in the presence and absence of external Ca^{2+} , thus suggesting that Ca^{2+} entry is not necessary to initiate the oscillations, but is strictly required to maintain them over time ([246]). Likewise, removal of extracellular Ca^{2+} during ongoing oscillations caused the Ca^{2+} oscillatory response to persist only for 1-2 spikes before rapidly returned $[\text{Ca}^{2+}]_i$ to resting levels. Overall, these findings strongly indicate that glutamate-induced intracellular Ca^{2+} oscillations are shaped by the rhythmical mobilization of the intracellular Ca^{2+} reservoir and sustained by extracellular Ca^{2+} entry. However, the Mn^{2+} quenching technique revealed that Glut was not able to activate a Ca^{2+} permeable pathway in bEND5 cells. Therefore, we speculate that Glut-induced intracellular Ca^{2+} oscillations were maintained over time by the constitutive SOCE. Overall, these findings strongly suggest that the InsP_3 -dependent ER pools upon which Ach and Glut impinge are quite different. Accordingly, the InsP_3 -dependent Ca^{2+} response to Glut is manifest even in the absence of extracellular Ca^{2+} and is maintained by resting Ca^{2+} influx, which indicates that the local ER Ca^{2+} concentration does not fall below the threshold for Stim activation. Conversely, intraluminal Ca^{2+} levels within the ER

sub-region targeted by Ach must be so low that SOCE is required to both trigger and maintain the oscillations over time.

Glutamate-induced intracellular Ca^{2+} oscillations drive NO production in bEND5 cells

Similar to Ach, glutamate-induced intracellular Ca^{2+} oscillations were able to induce NO synthesis in bEND5 cells. Glut-evoked NO release was abrogated by inhibiting Group I mGluRs with MCPG and by blocking each component of the Ca^{2+} toolkit involved in the generation of the Ca^{2+} spikes. Unlike Ach (see above), however, the increase in NO levels was detectable at around 300 sec after the onset of glutamate-induced Ca^{2+} waves and reached its peak with rather slow kinetics. Therefore, although both agonists induce intracellular Ca^{2+} oscillations, eNOS sensitivity to the Ca^{2+} -dependent stimulation differs between acetylcholine and glutamate. This difference has already been reported in the endothelial cells *ex vivo* covering pig aortic valves, in which, for a given increase in $[\text{Ca}^{2+}]_i$, the extent NO production varied depending on the extracellular agonist (thrombin>ATP>bradykinin>ionomycin) ([299]). The highest frequency of glutamate-induced intracellular Ca^{2+} oscillations falls within the same range as that described for acetylcholine (≈ 0.0045 Hz vs. ≈ 0.0047 Hz). Therefore, as suggested for endothelial cells *ex vivo* ([299]), we speculate that Ca^{2+} transients interact with other signalling pathways to boost eNOS activation in glutamate-stimulated cells ([136]). For instance, Akt/protein kinase B (PKB) promotes NO releases independently on Ca^{2+} by phosphorylating eNOS (ref). Interestingly, Group 1 mGluRs may enhance angiogenesis by recruiting the phosphoinositide 3-kinase (PI3K)/PKB pathway ([300]). It should, however, be recalled that DAF/FM is not a true NO detector, but is rather sensitive to several nitrogen derivatives, such as N_2O_3 , NO_2 or ONOO ([301]). More specifically, NO seems to react with the NH radical of the fluorophore which is generated by its non-specific oxidation ([301]). Therefore, NO levels could start to increase before they become detectable through an increase in DAF/FM fluorescence. An additional caveat that should be taken in consideration is that replacing the extracellular perfusate with a glutamate-containing solution does not faithfully mimic the physiological conditions during which glutamate is delivered onto brain microvascular endothelial cells, i.e. synaptic activity. Glutamatergic terminals are in close proximity and functionally coupled to adjoining parenchymal microvessels ([247], [4]). Therefore, brain microvascular endothelial cells are in the most suitable location to directly sense neuronal activity provided that they are

endowed with mGluRs (or NMDARs), as we have shown here. The frequency of the Ca^{2+} spikes we observed was even lower of the slow (0.5-1 Hz) brain oscillations that occur during deep sleep ([97]) (but see below). However, we envisage that high frequency (80-100 Hz) synaptic transmission *in vivo* could accelerate the frequency of the endothelial Ca^{2+} waves, thereby anticipating the onset of the ensuing NO signal. Nevertheless, glutamate-induced endothelial NO release is unlikely to mediate the fast NO-dependent vasodilation that follows neuronal activity in cerebellum and hippocampus ([247], [13]). Conversely, the delayed endothelial NO signal could underpin the slower component of the vasodilating response to brief neuronal activity in these latter structures ([114], [115], [13]) or play a permissive role in the PGE₂- or EET-dependent vasodilation that occurs during sustained (up to 1 min) synaptic activation in the cortex ([247]). Future *in vivo* experiments, involving the use of transgenic mice expressing genetic Ca^{2+} biosensors (such as GCaMP2) in vascular endothelium ([221]) and of more sensitive tools for NO detection (such as electrochemical probes) ([302]), will be necessary to address the exact role of glutamate-induced eNOS activation in NVC. In must, however, be pointed out that very slow or infra-slow oscillations (ISOs) well below 0.1 Hz (0.005-0.1 Hz) occur in the thalamus, as well as in other cortical structures, and are driven by mGluR activation ([303]). Of note, these ISOs have been associated to the spontaneous <0.1 Hz blood-oxygen-dependent level (BOLD) signals recorded with functional magnetic resonance imaging (fMRI) in resting individuals ([304]). The cellular and biochemical underpinnings of such low frequency BOLD fluctuations, which provide one of the most efficient tools to map brain connectivity, are yet to be elucidated. Intriguingly, the novel observation that low frequency glutamate-induced intracellular Ca^{2+} waves in brain microvascular endothelial cells lead to robust NO release could shed new light on the underlying mechanism. Finally, we have to recall that intracellular Ca^{2+} drives the synthesis of a plethora of endothelial-derived vasorelaxing messengers, including PGE₂, EETs, EDHF and hydrogen sulphide ([8], [305], [31]). Therefore, future experiments will be necessary to assess whether the signalling pathway we described in the present investigation contributes to generate PGE₂ and/or EETs in the brain areas, such as the cortex, in which these vasoactive factors trigger the vasodilating response to glutamatergic transmission ([247], [306]).

Glutamate induces intracellular Ca^{2+} signals and NO release in hCMEC/D3 cells

The data obtained from bEND5 cells were partially confirmed in hCMEC/D3 cells. Indeed, Glut was able to trigger an elevation in $[\text{Ca}^{2+}]_i$ and NO release also in human brain microvascular ECs. Similar to their murine counterparts, MCPG blocked both signals, thereby hinting at the involvement of mGluRs. As expected from the lack of $\text{InsP}_3\text{R1}$ and $\text{InsP}_3\text{R2}$, the Ca^{2+} signal lacked an oscillatory component, but displayed transient kinetics. Our preliminary data, not shown here, suggest that Glut-induced increase in $[\text{Ca}^{2+}]_i$ was mainly mediated by $\text{InsP}_3\text{R3}$ -mediated Ca^{2+} release from the ER with no or only scarce contribution by extracellular Ca^{2+} entry.

CONCLUSIONS

This work showed for the first time the Ca^{2+} -dependent mechanisms whereby acetylcholine and glutamate, the two major excitatory neurotransmitters, cause NO release in brain microvascular ECs. This information will shed novel light on the cellular and biochemical pathways that regulate NA-induced CBF.

Ach triggered two different modes of Ca^{2+} signals in murine (bEND5) and human (hCMEC/D3) brain microvascular ECs, i.e. Ca^{2+} oscillations and biphasic Ca^{2+} elevation respectively. The Ach-induced Ca^{2+} response involved ER Ca^{2+} release via InsP_3Rs and SOCE in both cell types. Interestingly, Ach-induced intracellular Ca^{2+} signals lead to robust NO release in both murine and human brain microvascular ECs. These results have a remarkable patho-physiological relevance because as NO release drives vasorelaxation upon cholinergic synaptic transmission in the brain. Recent work has shown that the neurovascular coupling between basal forebrain cholinergic nerve fibers and intraparenchymal microvessels declines with aging and in subjects with Alzheimer's type dementia ([94]). Understanding the signaling pathway whereby Ach induces NO synthesis in intracortical arterioles and capillaries could prove essential to design alternative pharmacological approaches to prevent or limit the decline in higher cognitive functions.

Likewise, we demonstrated for the first time that Glut triggered intracellular Ca^{2+} oscillations in bEND5 cells and a biphasic increase in $[\text{Ca}^{2+}]_i$ in hCMEC/D3 cells. We further showed that Glut-dependent Ca^{2+} signals drive NO release in both cell types. This NO signal is delayed as compared to the Ach-induced one and is likely to play a crucial role in the slower vasodilation that often follows brief neuronal activity or that sustains functional hyperemia during persistent synaptic transmission ([247], [16]). We also obtained the pharmacological evidence that mGluRs drive the Ca^{2+} response to Glut, although future experiment will be necessary to confirm their expression in both types of cells. Nevertheless this data lent further support to the recent observation that glutamate increases CBF by directly activating vascular endothelium, which adds a new layer of complexity to the mechanisms of CBF regulation by NA.

References

1. Attwell D, Laughlin SB. An energy budget for signaling in the grey matter of the brain. *J Cereb Blood Flow Metab* 2001; 21: 1133-1145.
2. Peters A, Schweiger U, Pellerin L et al. The selfish brain: competition for energy resources. *Neurosci Biobehav Rev* 2004; 28: 143-180.
3. Peters A. The selfish brain: Competition for energy resources. *Am J Hum Biol* 2011; 23: 29-34.
4. Iadecola C. Neurovascular regulation in the normal brain and in Alzheimer's disease. *Nat Rev Neurosci* 2004; 5: 347-360.
5. Moore CI, Cao R. The hemo-neural hypothesis: on the role of blood flow in information processing. *J Neurophysiol* 2008; 99: 2035-2047.
6. del Zoppo GJ. The neurovascular unit in the setting of stroke. *J Intern Med* 2010; 267: 156-171.
7. Zlokovic BV. Neurovascular pathways to neurodegeneration in Alzheimer's disease and other disorders. *Nat Rev Neurosci* 2011; 12: 723-738.
8. Attwell D, Buchan AM, Charpak S et al. Glial and neuronal control of brain blood flow. *Nature* 2010; 468: 232-243.
9. Kisler K, Nelson AR, Montagne A, Zlokovic BV. Cerebral blood flow regulation and neurovascular dysfunction in Alzheimer disease. *Nat Rev Neurosci* 2017; 18: 419-434.
10. Kim KJ, Ramiro Diaz J, Iddings JA, Filosa JA. Vasculo-Neuronal Coupling: Retrograde Vascular Communication to Brain Neurons. *J Neurosci* 2016; 36: 12624-12639.
11. Kim KJ, Iddings JA, Stern JE et al. Astrocyte contributions to flow/pressure-evoked parenchymal arteriole vasoconstriction. *J Neurosci* 2015; 35: 8245-8257.
12. Hall CN, Reynell C, Gesslein B et al. Capillary pericytes regulate cerebral blood flow in health and disease. *Nature* 2014; 508: 55-60.
13. Mapelli L, Gagliano G, Soda T et al. Granular Layer Neurons Control Cerebellar Neurovascular Coupling Through an NMDA Receptor/NO-Dependent System. *J Neurosci* 2017; 37: 1340-1351.
14. Mishra A, Reynolds JP, Chen Y et al. Astrocytes mediate neurovascular signaling to capillary pericytes but not to arterioles. *Nat Neurosci* 2016; 19: 1619-1627.
15. Dalkara T, Alarcon-Martinez L. Cerebral microvascular pericytes and neurogliovascular signaling in health and disease. *Brain Res* 2015; 1623: 3-17.
16. Hillman EM. Coupling mechanism and significance of the BOLD signal: a status report. *Annu Rev Neurosci* 2014; 37: 161-181.
17. Chen BR, Kozberg MG, Bouchard MB et al. A critical role for the vascular endothelium in functional neurovascular coupling in the brain. *J Am Heart Assoc* 2014; 3: e000787.
18. Andresen J, Shafi NI, Bryan RM, Jr. Endothelial influences on cerebrovascular tone. *J Appl Physiol (1985)* 2006; 100: 318-327.
19. Behringer EJ. Calcium and electrical signaling in arterial endothelial tubes: New insights into cellular physiology and cardiovascular function. *Microcirculation* 2017; 24.
20. Duncker DJ, Bache RJ. Regulation of coronary blood flow during exercise. *Physiol Rev* 2008; 88: 1009-1086.
21. Harder DR, Zhang C, Gebremedhin D. Astrocytes function in matching blood flow to metabolic activity. *News Physiol Sci* 2002; 17: 27-31.
22. Armstead WM, Raghupathi R. Endothelin and the neurovascular unit in pediatric traumatic brain injury. *Neurol Res* 2011; 33: 127-132.

23. Abbott NJ, Friedman A. Overview and introduction: the blood-brain barrier in health and disease. *Epilepsia* 2012; 53 Suppl 6: 1-6.
24. Abbott NJ, Ronnback L, Hansson E. Astrocyte-endothelial interactions at the blood-brain barrier. *Nat Rev Neurosci* 2006; 7: 41-53.
25. Rennels ML, Nelson E. Capillary innervation in the mammalian central nervous system: an electron microscopic demonstration. *Am J Anat* 1975; 144: 233-241.
26. Simard M, Arcuino G, Takano T et al. Signaling at the gliovascular interface. *J Neurosci* 2003; 23: 9254-9262.
27. del Zoppo GJ. The neurovascular unit, matrix proteases, and innate inflammation. *Ann N Y Acad Sci* 2010; 1207: 46-49.
28. Figley CR, Stroman PW. The role(s) of astrocytes and astrocyte activity in neurometabolism, neurovascular coupling, and the production of functional neuroimaging signals. *Eur J Neurosci* 2011; 33: 577-588.
29. Stobart JL, Lu L, Anderson HD et al. Astrocyte-induced cortical vasodilation is mediated by D-serine and endothelial nitric oxide synthase. *Proc Natl Acad Sci U S A* 2013; 110: 3149-3154.
30. LeMaistre JL, Sanders SA, Stobart MJ et al. Coactivation of NMDA receptors by glutamate and D-serine induces dilation of isolated middle cerebral arteries. *J Cereb Blood Flow Metab* 2012; 32: 537-547.
31. Moccia F, Berra-Romani R, Tanzi F. Update on vascular endothelial Ca²⁺ signalling: A tale of ion channels, pumps and transporters. *World J Biol Chem* 2012; 3: 127-158.
32. Girouard H, Iadecola C. Neurovascular coupling in the normal brain and in hypertension, stroke, and Alzheimer disease. *J Appl Physiol* (1985) 2006; 100: 328-335.
33. Leffler H, Masiarz FR, Barondes SH. Soluble lactose-binding vertebrate lectins: a growing family. *Biochemistry* 1989; 28: 9222-9229.
34. Baptiste DC, Fehlings MG. Pharmacological approaches to repair the injured spinal cord. *J Neurotrauma* 2006; 23: 318-334.
35. Joo F. Endothelial cells of the brain and other organ systems: some similarities and differences. *Prog Neurobiol* 1996; 48: 255-273.
36. Deli MA, Abraham CS, Kataoka Y, Niwa M. Permeability studies on in vitro blood-brain barrier models: physiology, pathology, and pharmacology. *Cell Mol Neurobiol* 2005; 25: 59-127.
37. Cecchelli R, Berezowski V, Lundquist S et al. Modelling of the blood-brain barrier in drug discovery and development. *Nat Rev Drug Discov* 2007; 6: 650-661.
38. Brightman MW, Kadota Y. Nonpermeable and permeable vessels of the brain. *NIDA Res Monogr* 1992; 120: 87-107.
39. Petty MA, Lo EH. Junctional complexes of the blood-brain barrier: permeability changes in neuroinflammation. *Prog Neurobiol* 2002; 68: 311-323.
40. Weiss N, Miller F, Cazaubon S, Couraud PO. The blood-brain barrier in brain homeostasis and neurological diseases. *Biochim Biophys Acta* 2009; 1788: 842-857.
41. Bechmann I, Galea I, Perry VH. What is the blood-brain barrier (not)? *Trends Immunol* 2007; 28: 5-11.
42. Ge S, Song L, Pachter JS. Where is the blood-brain barrier ... really? *J Neurosci Res* 2005; 79: 421-427.
43. Wolburg H, Lippoldt A. Tight junctions of the blood-brain barrier: development, composition and regulation. *Vascul Pharmacol* 2002; 38: 323-337.
44. del Zoppo GJ, Mabuchi T. Cerebral microvessel responses to focal ischemia. *J Cereb Blood Flow Metab* 2003; 23: 879-894.
45. Zlokovic BV. The blood-brain barrier in health and chronic neurodegenerative disorders. *Neuron* 2008; 57: 178-201.

46. Harder DR, Alkayed NJ, Lange AR et al. Functional hyperemia in the brain: hypothesis for astrocyte-derived vasodilator metabolites. *Stroke* 1998; 29: 229-234.
47. Iadecola C. Regulation of the cerebral microcirculation during neural activity: is nitric oxide the missing link? *Trends Neurosci* 1993; 16: 206-214.
48. Kuschinsky W. Neuronal-vascular coupling. A unifying hypothesis. *Adv Exp Med Biol* 1997; 413: 167-176.
49. Lou HC, Edvinsson L, MacKenzie ET. The concept of coupling blood flow to brain function: revision required? *Ann Neurol* 1987; 22: 289-297.
50. Villringer A, Dirnagl U. Coupling of brain activity and cerebral blood flow: basis of functional neuroimaging. *Cerebrovasc Brain Metab Rev* 1995; 7: 240-276.
51. Wahl M, Schilling L. Regulation of cerebral blood flow--a brief review. *Acta Neurochir Suppl (Wien)* 1993; 59: 3-10.
52. Magistretti PJ, Pellerin L. Cellular mechanisms of brain energy metabolism and their relevance to functional brain imaging. *Philos Trans R Soc Lond B Biol Sci* 1999; 354: 1155-1163.
53. Fillenz M, Lowry JP, Boutelle MG, Fray AE. The role of astrocytes and noradrenaline in neuronal glucose metabolism. *Acta Physiol Scand* 1999; 167: 275-284.
54. Hertz L, Yu AC, Kala G, Schousboe A. Neuronal-astrocytic and cytosolic-mitochondrial metabolite trafficking during brain activation, hyperammonemia and energy deprivation. *Neurochem Int* 2000; 37: 83-102.
55. Tsacopoulos M, Magistretti PJ. Metabolic coupling between glia and neurons. *J Neurosci* 1996; 16: 877-885.
56. Chih CP, Roberts Jr EL. Energy substrates for neurons during neural activity: a critical review of the astrocyte-neuron lactate shuttle hypothesis. *J Cereb Blood Flow Metab* 2003; 23: 1263-1281.
57. Bryan RM, Jr., Hawkins RA, Mans AM et al. Cerebral glucose utilization in awake unstressed rats. *Am J Physiol* 1983; 244: C270-275.
58. Ginsburg H, Jehuda-Cohen T, Kinarty A et al. Does stem cell self renewal and progenitor cell commitment operate through an effector-memory cell mechanism? *Immunol Lett* 1986; 13: 107-119.
59. Hawkins RA, Mans AM, Davis DW et al. Cerebral glucose use measured with [14C]glucose labeled in the 1, 2, or 6 position. *Am J Physiol* 1985; 248: C170-176.
60. Sokoloff L. Relation between physiological function and energy metabolism in the central nervous system. *J Neurochem* 1977; 29: 13-26.
61. Paulson HL, Claudio T. Temperature-sensitive expression of all-Torpedo and Torpedo-rat hybrid AChR in mammalian muscle cells. *J Cell Biol* 1990; 110: 1705-1717.
62. Prewitt RL, Rice DC, Dobrian AD. Adaptation of resistance arteries to increases in pressure. *Microcirculation* 2002; 9: 295-304.
63. Attwell D, Iadecola C. The neural basis of functional brain imaging signals. *Trends Neurosci* 2002; 25: 621-625.
64. Lauritzen M. Reading vascular changes in brain imaging: is dendritic calcium the key? *Nat Rev Neurosci* 2005; 6: 77-85.
65. Busija DW, Bari F, Domoki F, Louis T. Mechanisms involved in the cerebrovascular dilator effects of N-methyl-d-aspartate in cerebral cortex. *Brain Res Rev* 2007; 56: 89-100.
66. Anderson CM, Nedergaard M. Astrocyte-mediated control of cerebral microcirculation. *Trends Neurosci* 2003; 26: 340-344; author reply 344-345.
67. Zonta M, Angulo MC, Gobbo S et al. Neuron-to-astrocyte signaling is central to the dynamic control of brain microcirculation. *Nat Neurosci* 2003; 6: 43-50.

68. Schipke CG, Kettenmann H. Astrocyte responses to neuronal activity. *Glia* 2004; 47: 226-232.
69. Newman EA. Calcium increases in retinal glial cells evoked by light-induced neuronal activity. *J Neurosci* 2005; 25: 5502-5510.
70. Amruthesh SC, Boerschel MF, McKinney JS et al. Metabolism of arachidonic acid to epoxyeicosatrienoic acids, hydroxyeicosatetraenoic acids, and prostaglandins in cultured rat hippocampal astrocytes. *J Neurochem* 1993; 61: 150-159.
71. Alkayed NJ, Birks EK, Hudetz AG et al. Inhibition of brain P-450 arachidonic acid epoxygenase decreases baseline cerebral blood flow. *Am J Physiol* 1996; 271: H1541-1546.
72. Zeldin DC. Epoxygenase pathways of arachidonic acid metabolism. *J Biol Chem* 2001; 276: 36059-36062.
73. Roman RJ. P-450 metabolites of arachidonic acid in the control of cardiovascular function. *Physiol Rev* 2002; 82: 131-185.
74. Hamilton NB, Attwell D, Hall CN. Pericyte-mediated regulation of capillary diameter: a component of neurovascular coupling in health and disease. *Front Neuroenergetics* 2010; 2.
75. Shepro D, Morel NM. Pericyte physiology. *FASEB J* 1993; 7: 1031-1038.
76. Peppiatt CM, Howarth C, Mobbs P, Attwell D. Bidirectional control of CNS capillary diameter by pericytes. *Nature* 2006; 443: 700-704.
77. Yemisci M, Gursoy-Ozdemir Y, Vural A et al. Pericyte contraction induced by oxidative-nitrative stress impairs capillary reflow despite successful opening of an occluded cerebral artery. *Nat Med* 2009; 15: 1031-1037.
78. Puro DG. Physiology and pathobiology of the pericyte-containing retinal microvasculature: new developments. *Microcirculation* 2007; 14: 1-10.
79. Lovick TA, Brown LA, Key BJ. Neurovascular relationships in hippocampal slices: physiological and anatomical studies of mechanisms underlying flow-metabolism coupling in intraparenchymal microvessels. *Neuroscience* 1999; 92: 47-60.
80. Adapala RK, Talasila PK, Bratz IN et al. PKC α mediates acetylcholine-induced activation of TRPV4-dependent calcium influx in endothelial cells. *Am J Physiol Heart Circ Physiol* 2011; 301: H757-765.
81. Faraci FM, Heistad DD. Regulation of the cerebral circulation: role of endothelium and potassium channels. *Physiol Rev* 1998; 78: 53-97.
82. Golding NL, Staff NP, Spruston N. Dendritic spikes as a mechanism for cooperative long-term potentiation. *Nature* 2002; 418: 326-331.
83. Elhousseiny A, Hamel E. Muscarinic--but not nicotinic--acetylcholine receptors mediate a nitric oxide-dependent dilation in brain cortical arterioles: a possible role for the M5 receptor subtype. *J Cereb Blood Flow Metab* 2000; 20: 298-305.
84. Yamada M, Lamping KG, Duttaroy A et al. Cholinergic dilation of cerebral blood vessels is abolished in M(5) muscarinic acetylcholine receptor knockout mice. *Proc Natl Acad Sci U S A* 2001; 98: 14096-14101.
85. Zhang F XS, Iadecola C. Role of nitric oxide and acetylcholine in neocortical hyperemia elicited by basal forebrain stimulation: evidence for an involvement of endothelial nitric oxide. *Neuroscience* 1995; 69(4): 1195-1204.
86. Sandow SL, Senadheera S, Grayson TH et al. Calcium and endothelium-mediated vasodilator signaling. *Adv Exp Med Biol* 2012; 740: 811-831.
87. Moccia F, Tanzi F, Munaron L. Endothelial Remodelling and Intracellular Calcium Machinery. *Curr Mol Med* 2013.
88. Sato A, Sato Y. Cholinergic neural regulation of regional cerebral blood flow. *Alzheimer Dis Assoc Disord* 1995; 9: 28-38.

89. Uutela P, Reinila R, Piepponen P et al. Analysis of acetylcholine and choline in microdialysis samples by liquid chromatography/tandem mass spectrometry. *Rapid Commun Mass Spectrom* 2005; 19: 2950-2956.
90. Nirogi R, Mudigonda K, Kandikere V, Ponnamaneni R. Quantification of acetylcholine, an essential neurotransmitter, in brain microdialysis samples by liquid chromatography mass spectrometry. *Biomed Chromatogr* 2010; 24: 39-48.
91. Furchgott RF, Zawadzki JV. The obligatory role of endothelial cells in the relaxation of arterial smooth muscle by acetylcholine. *Nature* 1980; 288: 373-376.
92. Faraci FM, Sigmund CD. Vascular biology in genetically altered mice : smaller vessels, bigger insight. *Circ Res* 1999; 85: 1214-1225.
93. Hamel E. Cholinergic modulation of the cortical microvascular bed. *Prog Brain Res* 2004; 145: 171-178.
94. Hotta H. Neurogenic control of parenchymal arterioles in the cerebral cortex. *Prog Brain Res* 2016; 225: 3-39.
95. Suszkiw JB, Pilar G. Selective localization of a high affinity choline uptake system and its role in ACh formation in cholinergic nerve terminals. *J Neurochem* 1976; 26: 1133-1138.
96. Amenta F, Tayebati SK. Pathways of acetylcholine synthesis, transport and release as targets for treatment of adult-onset cognitive dysfunction. *Curr Med Chem* 2008; 15: 488-498.
97. Berridge MJ. Calcium regulation of neural rhythms, memory and Alzheimer's disease. *J Physiol* 2014; 592: 281-293.
98. Bari F, Louis TM, Busija DW. Kainate-induced cerebrovascular dilation is resistant to ischemia in piglets. *Stroke* 1997; 28: 1272-1276; discussion 1277.
99. Busija DW, Leffler CW. Dilator effects of amino acid neurotransmitters on piglet pial arterioles. *Am J Physiol* 1989; 257: H1200-1203.
100. Faraci FM, Breese KR. Nitric oxide mediates vasodilatation in response to activation of N-methyl-D-aspartate receptors in brain. *Circ Res* 1993; 72: 476-480.
101. Faraci FM, Breese KR, Heistad DD. Responses of cerebral arterioles to kainate. *Stroke* 1994; 25: 2080-2083; discussion 2084.
102. Fergus A, Lee KS. Regulation of cerebral microvessels by glutamatergic mechanisms. *Brain Res* 1997; 754: 35-45.
103. Meng W, Tobin JR, Busija DW. Glutamate-induced cerebral vasodilation is mediated by nitric oxide through N-methyl-D-aspartate receptors. *Stroke* 1995; 26: 857-862; discussion 863.
104. G.J.; S, B.W.; A, R.W.; A et al. *Basic neurochemistry*. 6th ed Philadelphia, PA: Lippincott-Raven. 1998.
105. Hawkins RA, Mokashi A, DeJoseph MR et al. Glutamate permeability at the blood-brain barrier in insulinopenic and insulin-resistant rats. *Metabolism* 2010; 59: 258-266.
106. Dzubay JA, Jahr CE. The concentration of synaptically released glutamate outside of the climbing fiber-Purkinje cell synaptic cleft. *J Neurosci* 1999; 19: 5265-5274.
107. Burger PM, Mehl E, Cameron PL et al. Synaptic vesicles immunisolated from rat cerebral cortex contain high levels of glutamate. *Neuron* 1989; 3: 715-720.
108. Hertz L, Dringen R, Schousboe A, Robinson SR. Astrocytes: glutamate producers for neurons. *J Neurosci Res* 1999; 57: 417-428.
109. Kew JN, Kemp JA. Ionotropic and metabotropic glutamate receptor structure and pharmacology. *Psychopharmacology (Berl)* 2005; 179: 4-29.
110. Nakanishi S. Molecular diversity of glutamate receptors and implications for brain function. *Science* 1992; 258: 597-603.
111. Schoepp DD, Conn PJ. Metabotropic glutamate receptors in brain function and pathology. *Trends Pharmacol Sci* 1993; 14: 13-20.

112. Snyder SH, Ferris CD. Novel neurotransmitters and their neuropsychiatric relevance. *Am J Psychiatry* 2000; 157: 1738-1751.
113. Yang G, Iadecola C. Glutamate microinjections in cerebellar cortex reproduce cerebrovascular effects of parallel fiber stimulation. *Am J Physiol* 1996; 271: R1568-1575.
114. Lauritzen M, Mathiesen C, Schaefer K, Thomsen KJ. Neuronal inhibition and excitation, and the dichotomic control of brain hemodynamic and oxygen responses. *Neuroimage* 2012; 62: 1040-1050.
115. Lourenco CF, Ledo A, Barbosa RM, Laranjinha J. Neurovascular-neuroenergetic coupling axis in the brain: master regulation by nitric oxide and consequences in aging and neurodegeneration. *Free Radic Biol Med* 2017; 108: 668-682.
116. Alderton WK, Cooper CE, Knowles RG. Nitric oxide synthases: structure, function and inhibition. *Biochem J* 2001; 357: 593-615.
117. Brenman JE, Christopherson KS, Craven SE et al. Cloning and characterization of postsynaptic density 93, a nitric oxide synthase interacting protein. *J Neurosci* 1996; 16: 7407-7415.
118. Dedkova EN, Blatter LA. Nitric oxide inhibits capacitative Ca²⁺ entry and enhances endoplasmic reticulum Ca²⁺ uptake in bovine vascular endothelial cells. *J Physiol* 2002; 539: 77-91.
119. Berra-Romani R, Avelino-Cruz JE, Raqeeb A et al. Ca²⁺-dependent nitric oxide release in the injured endothelium of excised rat aorta: a promising mechanism applying in vascular prosthetic devices in aging patients. *BMC Surg* 2013; 13 Suppl 2: S40.
120. Haul S, Godecke A, Schrader J et al. Impairment of neocortical long-term potentiation in mice deficient of endothelial nitric oxide synthase. *J Neurophysiol* 1999; 81: 494-497.
121. Doreulee N, Sergeeva OA, Yanovsky Y et al. Cortico-striatal synaptic plasticity in endothelial nitric oxide synthase deficient mice. *Brain Res* 2003; 964: 159-163.
122. Hyman BT, Van Hoesen GW, Damasio AR, Barnes CL. Alzheimer's disease: cell-specific pathology isolates the hippocampal formation. *Science* 1984; 225: 1168-1170.
123. Son H, Hawkins RD, Martin K et al. Long-term potentiation is reduced in mice that are doubly mutant in endothelial and neuronal nitric oxide synthase. *Cell* 1996; 87: 1015-1023.
124. Hopper RA, Garthwaite J. Tonic and phasic nitric oxide signals in hippocampal long-term potentiation. *J Neurosci* 2006; 26: 11513-11521.
125. Seidel B, Stanarius A, Wolf G. Differential expression of neuronal and endothelial nitric oxide synthase in blood vessels of the rat brain. *Neurosci Lett* 1997; 239: 109-112.
126. Stanarius A, Topel I, Schulz S et al. Immunocytochemistry of endothelial nitric oxide synthase in the rat brain: a light and electron microscopical study using the tyramide signal amplification technique. *Acta Histochem* 1997; 99: 411-429.
127. Bon CL, Garthwaite J. On the role of nitric oxide in hippocampal long-term potentiation. *J Neurosci* 2003; 23: 1941-1948.
128. Zuccolo E, Bottino C, Diofano F et al. Constitutive Store-Operated Ca(2+) Entry Leads to Enhanced Nitric Oxide Production and Proliferation in Infantile Hemangioma-Derived Endothelial Colony-Forming Cells. *Stem Cells Dev* 2016; 25: 301-319.
129. Adams DJ, Barakeh J, Laskey R, Van Breemen C. Ion channels and regulation of intracellular calcium in vascular endothelial cells. *FASEB J* 1989; 3: 2389-2400.
130. Himmel HM, Whorton AR, Strauss HC. Intracellular calcium, currents, and stimulus-response coupling in endothelial cells. *Hypertension* 1993; 21: 112-127.
131. Feletou M, Vanhoutte PM. Endothelium-derived hyperpolarizing factor: where are we now? *Arterioscler Thromb Vasc Biol* 2006; 26: 1215-1225.

132. Nilius B, Droogmans G. Ion channels and their functional role in vascular endothelium. *Physiol Rev* 2001; 81: 1415-1459.
133. Moccia F, Tanzi F, Munaron L. Endothelial remodelling and intracellular calcium machinery. *Curr Mol Med* 2014; 14: 457-480.
134. Dora KA. Coordination of vasomotor responses by the endothelium. *Circ J* 2010; 74: 226-232.
135. Hu QH, Deshpande S, Irani K, Ziegelstein RC. Ca²⁺ (i) oscillation frequency regulates agonist-stimulated NF-kappa B transcriptional activity. *Journal of Biological Chemistry* 1999; 274: 33995-33998.
136. Mancardi D, Pla AF, Moccia F et al. Old and new gasotransmitters in the cardiovascular system: focus on the role of nitric oxide and hydrogen sulfide in endothelial cells and cardiomyocytes. *Curr Pharm Biotechnol* 2011; 12: 1406-1415.
137. Moccia F, Avelino-Cruz JE, Sanchez-Hernandez Y, Tanzi F. Ca²⁺ signalling in damaged endothelium: Do connexin hemichannels aid in filling the gap? *Curr Drug Ther* 2010; 5: 277-287.
138. Tirupathi C, Ahmmed GU, Vogel SM, Malik AB. Ca²⁺ signaling, TRP channels, and endothelial permeability. *Microcirculation* 2006; 13: 693-708.
139. Munaron L. Intracellular calcium, endothelial cells and angiogenesis. *Recent Pat Anticancer Drug Discov* 2006; 1: 105-119.
140. Tran QK, Watanabe H. Calcium signalling in the endothelium. *Handb Exp Pharmacol* 2006; 145-187.
141. Tang EHC, Vanhoutte PM. Gap junction inhibitors reduce endothelium-dependent contractions in the aorta of spontaneously hypertensive rats. *Journal of Pharmacology and Experimental Therapeutics* 2008; 327: 148-153.
142. Berridge MJ, Bootman MD, Roderick HL. Calcium signalling: Dynamics, homeostasis and remodelling. *Nat Rev Mol Cell Biol* 2003; 4: 517-529.
143. Moccia F, Berra-Romani R, Baruffi S et al. Ca²⁺ uptake by the endoplasmic reticulum Ca²⁺-ATPase in rat microvascular endothelial cells. *Biochem J* 2002; 364: 235-244.
144. Abdullaev IF, Bisailon JM, Potier M et al. Stim1 and Orai1 mediate CRAC currents and store-operated calcium entry important for endothelial cell proliferation. *Circ Res* 2008; 103: 1289-1299.
145. Parekh AB. Store-operated CRAC channels: function in health and disease. *Nat Rev Drug Discov* 2010; 9: 399-410.
146. Smyth JT, Hwang S-Y, Tomita T et al. Activation and regulation of store-operated calcium entry. *Journal of Cellular and Molecular Medicine* 2010; 14: 2337-2349.
147. Rebecchi MJ, Pentylala SN. Structure, function, and control of phosphoinositide-specific phospholipase C. *Physiol Rev* 2000; 80: 1291-1335.
148. Vines CM. Phospholipase C. *Adv Exp Med Biol* 2012; 740: 235-254.
149. Nilius B, Szallasi A. Transient receptor potential channels as drug targets: from the science of basic research to the art of medicine. *Pharmacol Rev* 2014; 66: 676-814.
150. Yamada N, Makino Y, Clark RA et al. Human inositol 1,4,5-trisphosphate type-1 receptor, InsP3R1: structure, function, regulation of expression and chromosomal localization. *Biochem J* 1994; 302 (Pt 3): 781-790.
151. Meyer T, Holowka D, Stryer L. Highly cooperative opening of calcium channels by inositol 1,4,5-trisphosphate. *Science* 1988; 240: 653-656.
152. Foskett JK, White C, Cheung KH, Mak DOD. Inositol trisphosphate receptor Ca²⁺ release channels. *Physiol Rev* 2007; 87: 593-658.
153. Kushnir A, Marks AR. The ryanodine receptor in cardiac physiology and disease. *Adv Pharmacol* 2010; 59: 1-30.

154. Amador FJ, Stathopoulos PB, Enomoto M, Ikura M. Ryanodine receptor calcium release channels: lessons from structure-function studies. *FEBS J* 2013; 280: 5456-5470.
155. Fill M, Copello JA. Ryanodine receptor calcium release channels. *Physiol Rev* 2002; 82: 893-922.
156. Otun H, Aidulis DM, Yang JM, Gillespie JI. Interactions between inositol trisphosphate and Ca²⁺ dependent Ca²⁺ release mechanisms on the endoplasmic reticulum of permeabilised bovine aortic endothelial cells. *Cell Calcium* 1996; 19: 315-325.
157. West DJ, Williams AJ. Pharmacological regulators of intracellular calcium release channels. *Curr Pharm Des* 2007; 13: 2428-2442.
158. Morgan AJ, Platt FM, Lloyd-Evans E, Galione A. Molecular mechanisms of endolysosomal Ca²⁺ signalling in health and disease. *Biochem J* 2011; 439: 349-374.
159. Parrington J, Tunn R. Ca(2+) signals, NAADP and two-pore channels: role in cellular differentiation. *Acta Physiol (Oxf)* 2014; 211: 285-296.
160. Galione A, Parrington J, Funnell T. Physiological roles of NAADP-mediated Ca²⁺ signaling. *Sci China Life Sci* 2011; 54: 725-732.
161. Moccia F, Lim D, Kyojuka K, Santella L. NAADP triggers the fertilization potential in starfish oocytes. *Cell Calcium* 2004; 36: 515-524.
162. Di Nezza F, Zuccolo E, Poletto V et al. Liposomes as a Putative Tool to Investigate NAADP Signaling in Vasculogenesis. *J Cell Biochem* 2017.
163. Patel S, Ramakrishnan L, Rahman T et al. The endo-lysosomal system as an NAADP-sensitive acidic Ca(2+) store: role for the two-pore channels. *Cell Calcium* 2011; 50: 157-167.
164. Zhu MX, Ma J, Parrington J et al. Calcium signaling via two-pore channels: local or global, that is the question. *Am J Physiol Cell Physiol* 2010; 298: C430-441.
165. Clapham DE. Calcium signaling. *Cell* 2007; 131: 1047-1058.
166. Feske S. ORAI1 and STIM1 deficiency in human and mice: roles of store-operated Ca²⁺ entry in the immune system and beyond. *Immunol Rev* 2009; 231: 189-209.
167. Lodola F, Laforenza U, Bonetti E et al. Store-operated Ca²⁺ entry is remodelled and controls in vitro angiogenesis in endothelial progenitor cells isolated from tumoral patients. *PLoS One* 2012; 7: e42541.
168. Sánchez-Hernández Y, Laforenza U, Bonetti E et al. Store-operated Ca(2+) entry is expressed in human endothelial progenitor cells. *Stem Cells Dev* 2010; 19: 1967-1981.
169. Somasundaram A, Shum AK, McBride HJ et al. Store-operated CRAC channels regulate gene expression and proliferation in neural progenitor cells. *J Neurosci* 2014; 34: 9107-9123.
170. Cahalan MD. STIMulating store-operated Ca(2+) entry. *Nat Cell Biol* 2009; 11: 669-677.
171. Varnai P, Hunyady L, Balla T. STIM and Orai: the long-awaited constituents of store-operated calcium entry. *Trends in Pharmacological Sciences* 2009; 30: 118-128.
172. Zhou Y, Meraner P, Kwon HT et al. STIM1 gates the store-operated calcium channel ORAI1 in vitro. *Nat Struct Mol Biol* 2010; 17: 112-116.
173. Potier M, Trebak M. New developments in the signaling mechanisms of the store-operated calcium entry pathway. *Pflugers Arch* 2008; 457: 405-415.
174. Shim AH, Tirado-Lee L, Prakriya M. Structural and Functional Mechanisms of CRAC Channel Regulation. *J Mol Biol* 2015; 427: 77-93.
175. Fasolato C, Nilius B. Store depletion triggers the calcium release-activated calcium current (ICRAC) in macrovascular endothelial cells: a comparison with Jurkat and embryonic kidney cell lines. *Pflugers Arch* 1998; 436: 69-74.
176. Hoth M, Penner R. Calcium release-activated calcium current in rat mast cells. *J Physiol* 1993; 465: 359-386.

177. Zweifach A, Lewis RS. Mitogen-regulated Ca²⁺ current of T lymphocytes is activated by depletion of intracellular Ca²⁺ stores. *Proc Natl Acad Sci U S A* 1993; 90: 6295-6299.
178. Moccia F, Zuccolo E, Soda T et al. Stim and Orai proteins in neuronal Ca(2+) signaling and excitability. *Front Cell Neurosci* 2015; 9: 153.
179. Moccia F, Zuccolo E, Poletto V et al. Targeting Stim and Orai proteins as an alternative approach in anticancer therapy. *Curr Med Chem* 2016.
180. Sundivakkam PC, Freichel M, Singh V et al. The Ca(2+) sensor stromal interaction molecule 1 (STIM1) is necessary and sufficient for the store-operated Ca(2+) entry function of transient receptor potential canonical (TRPC) 1 and 4 channels in endothelial cells. *Mol Pharmacol* 2012; 81: 510-526.
181. Cioffi DL, Wu S, Chen H et al. Orai1 determines calcium selectivity of an endogenous TRPC heterotetramer channel. *Circ Res* 2012; 110: 1435-1444.
182. Hamdollah Zadeh MA, Glass CA, Magnussen A et al. VEGF-Mediated Elevated Intracellular Calcium and Angiogenesis in Human Microvascular Endothelial Cells In Vitro are Inhibited by Dominant Negative TRPC6. *Microcirculation* 2008; 15: 605-614.
183. Cheng HW, James AF, Foster RR et al. VEGF activates receptor-operated cation channels in human microvascular endothelial cells. *Arterioscler Thromb Vasc Biol* 2006; 26: 1768-1776.
184. Filosa JA, Yao X, Rath G. TRPV4 and the regulation of vascular tone. *J Cardiovasc Pharmacol* 2013; 61: 113-119.
185. Munaron L. Shuffling the cards in signal transduction: Calcium, arachidonic acid and mechanosensitivity. *World J Biol Chem* 2011; 2: 59-66.
186. Moccia F, Berra-Romani R, Tanzi F. Ca²⁺ signalling in damaged endothelium and arterial remodelling: Do connexin hemichannels provide a suitable target to prevent in-stent restenosis? *Curr Drug Ther* 2012; 7: 268-280.
187. AbouAlaiwi WA, Takahashi M, Mell BR et al. Ciliary polycystin-2 is a mechanosensitive calcium channel involved in nitric oxide signaling cascades. *Circ Res* 2009; 104: 860-869.
188. Li J, Hou B, Tumova S et al. Piezo1 integration of vascular architecture with physiological force. *Nature* 2014; 515: 279-282.
189. Berrout J, Jin M, O'Neil RG. Critical role of TRPP2 and TRPC1 channels in stretch-induced injury of blood-brain barrier endothelial cells. *Brain Res* 2012; 1436: 1-12.
190. Redzic Z. Molecular biology of the blood-brain and the blood-cerebrospinal fluid barriers: similarities and differences. *Fluids Barriers CNS* 2011; 8: 3.
191. Hess J, Jensen CV, Diemer NH. Calcium-imaging with Fura-2 in isolated cerebral microvessels. *Acta Histochem* 1989; 87: 107-114.
192. Koenig H, Goldstone AD, Lu CY, Trout JJ. Polyamines and Ca²⁺ mediate hyperosmolal opening of the blood-brain barrier: in vitro studies in isolated rat cerebral capillaries. *J Neurochem* 1989; 52: 1135-1142.
193. Wilhelm I, Farkas AE, Nagyoszi P et al. Regulation of cerebral endothelial cell morphology by extracellular calcium. *Phys Med Biol* 2007; 52: 6261-6274.
194. De Bock M, Culot M, Wang N et al. Low extracellular Ca²⁺ conditions induce an increase in brain endothelial permeability that involves intercellular Ca²⁺ waves. *Brain Res* 2012; 1487: 78-87.
195. Leybaert L, Sanderson MJ. Intercellular Ca(2+) waves: mechanisms and function. *Physiol Rev* 2012; 92: 1359-1392.
196. Dupont G, Combettes L, Leybaert L. Calcium dynamics: spatio-temporal organization from the subcellular to the organ level. *Int Rev Cytol* 2007; 261: 193-245.
197. Bohr DF. Vascular smooth muscle updated. *Circ Res* 1973; 32: 665-672.
198. Putney JW, Jr., Poggioli J, Weiss SJ. Receptor regulation of calcium release and calcium permeability in parotid gland cells. *Philos Trans R Soc Lond B Biol Sci* 1981; 296: 37-45.

199. Berridge MJ. The Inositol Trisphosphate/Calcium Signaling Pathway in Health and Disease. *Physiol Rev* 2016; 96: 1261-1296.
200. Dupont G, Combettes L, Bird GS, Putney JW. Calcium Oscillations. *Cold Spring Harb Perspect Biol* 2011; 3: 18.
201. Miyakawa T, Maeda A, Yamazawa T et al. Encoding of Ca²⁺ signals by differential expression of IP₃ receptor subtypes. *Embo j* 1999; 18: 1303-1308.
202. Morel JL, Fritz N, Lavie JL, Mironneau J. Crucial role of type 2 inositol 1,4,5-trisphosphate receptors for acetylcholine-induced Ca²⁺ oscillations in vascular myocytes. *Arterioscler Thromb Vasc Biol* 2003; 23: 1567-1575.
203. Hattori M, Suzuki AZ, Higo T et al. Distinct roles of inositol 1,4,5-trisphosphate receptor types 1 and 3 in Ca²⁺ signaling. *J Biol Chem* 2004; 279: 11967-11975.
204. Paemeleire K, de Hemptinne A, Leybaert L. Chemically, mechanically, and hyperosmolarity-induced calcium responses of rat cortical capillary endothelial cells in culture. *Exp Brain Res* 1999; 126: 473-481.
205. Vandamme W, Braet K, Cabooter L, Leybaert L. Tumour necrosis factor alpha inhibits purinergic calcium signalling in blood-brain barrier endothelial cells. *J Neurochem* 2004; 88: 411-421.
206. Feine I, Pinkas I, Salomon Y, Scherz A. Local oxidative stress expansion through endothelial cells--a key role for gap junction intercellular communication. *PLoS One* 2012; 7: e41633.
207. Socha MJ, Behringer EJ, Segal SS. Calcium and electrical signalling along endothelium of the resistance vasculature. *Basic Clin Pharmacol Toxicol* 2012; 110: 80-86.
208. Tallini YN, Brekke JF, Shui B et al. Propagated endothelial Ca²⁺ waves and arteriolar dilation in vivo: measurements in Cx40BAC GCaMP2 transgenic mice. *Circ Res* 2007; 101: 1300-1309.
209. Rath G, Saliez J, Behets G et al. Vascular hypoxic preconditioning relies on TRPV4-dependent calcium influx and proper intercellular gap junctions communication. *Arterioscler Thromb Vasc Biol* 2012; 32: 2241-2249.
210. Revest PA, Abbott NJ, Gillespie JI. Receptor-mediated changes in intracellular [Ca²⁺] in cultured rat brain capillary endothelial cells. *Brain Res* 1991; 549: 159-161.
211. Kimura C, Oike M, Ito Y. Hypoxia-induced alterations in Ca(2+) mobilization in brain microvascular endothelial cells. *Am J Physiol Heart Circ Physiol* 2000; 279: H2310-2318.
212. De Bock M, Vandembroucke RE, Decrock E et al. A new angle on blood-CNS interfaces: a role for connexins? *FEBS Lett* 2014; 588: 1259-1270.
213. Haorah J, Knipe B, Gorantla S et al. Alcohol-induced blood-brain barrier dysfunction is mediated via inositol 1,4,5-triphosphate receptor (IP₃R)-gated intracellular calcium release. *J Neurochem* 2007; 100: 324-336.
214. De Bock M, Wang N, Decrock E et al. Endothelial calcium dynamics, connexin channels and blood-brain barrier function. *Prog Neurobiol* 2013; 108: 1-20.
215. Domotor E, Abbott NJ, Adam-Vizi V. Na⁺-Ca²⁺ exchange and its implications for calcium homeostasis in primary cultured rat brain microvascular endothelial cells. *J Physiol* 1999; 515 (Pt 1): 147-155.
216. Gobbi P, Castaldo P, Minelli A et al. Mitochondrial localization of Na⁺/Ca²⁺ exchangers NCX1-3 in neurons and astrocytes of adult rat brain in situ. *Pharmacol Res* 2007; 56: 556-565.
217. Brayden JE, Earley S, Nelson MT, Reading S. Transient receptor potential (TRP) channels, vascular tone and autoregulation of cerebral blood flow. *Clin Exp Pharmacol Physiol* 2008; 35: 1116-1120.
218. Yamazaki D, Aoyama M, Ohya S et al. Novel functions of small conductance Ca²⁺-activated K⁺ channel in enhanced cell proliferation by ATP in brain endothelial cells. *J Biol Chem* 2006; 281: 38430-38439.

219. Golech SA, McCarron RM, Chen Y et al. Human brain endothelium: coexpression and function of vanilloid and endocannabinoid receptors. *Brain Res Mol Brain Res* 2004; 132: 87-92.
220. Pires PW, Sullivan MN, Pritchard HA et al. Unitary TRPV3 channel Ca²⁺ influx events elicit endothelium-dependent dilation of cerebral parenchymal arterioles. *Am J Physiol Heart Circ Physiol* 2015; 309: H2031-2041.
221. Sonkusare SK, Bonev AD, Ledoux J et al. Elementary Ca²⁺ signals through endothelial TRPV4 channels regulate vascular function. *Science* 2012; 336: 597-601.
222. Kito H, Yamamura H, Suzuki Y et al. Regulation of store-operated Ca²⁺ entry activity by cell cycle dependent up-regulation of Orai2 in brain capillary endothelial cells. *Biochem Biophys Res Commun* 2015; 459: 457-462.
223. Yamamura H, Suzuki Y, Yamamura H et al. Hypoxic stress up-regulates Kir2.1 expression and facilitates cell proliferation in brain capillary endothelial cells. *Biochem Biophys Res Commun* 2016; 476: 386-392.
224. Reiss Y, Hoch G, Deutsch U, Engelhardt B. T cell interaction with ICAM-1-deficient endothelium in vitro: essential role for ICAM-1 and ICAM-2 in transendothelial migration of T cells. *Eur J Immunol* 1998; 28: 3086-3099.
225. Hallam TJ, Jacob R, Merritt JE. Evidence that agonists stimulate bivalent-cation influx into human endothelial cells. *Biochem J* 1988; 255: 179-184.
226. Moccia F, Berra-Romani R, Baruffi S et al. Basal nonselective cation permeability in rat cardiac microvascular endothelial cells. *Microvasc Res* 2002; 64: 187-197.
227. Zuccolo E, Dragoni S, Poletto V et al. Arachidonic acid-evoked Ca²⁺ signals promote nitric oxide release and proliferation in human endothelial colony forming cells. *Vascul Pharmacol* 2016; 87: 159-171.
228. Poletto V, Dragoni S, Lim D et al. Endoplasmic Reticulum Ca²⁺ Handling and Apoptotic Resistance in Tumor-Derived Endothelial Colony Forming Cells. *J Cell Biochem* 2016.
229. Ronco V, Grolla AA, Glasnov TN et al. Differential deregulation of astrocytic calcium signalling by amyloid-beta, TNFalpha, IL-1beta and LPS. *Cell Calcium* 2014; 55: 219-229.
230. Perna A, Lucariello A, Sellitto C et al. Different Cell Cycle Modulation in SKOV-3 Ovarian Cancer Cell Line by Anti-HIV Drugs. *Oncol Res* 2017.
231. Bootman MD, Berridge MJ, Lipp P. Cooking with calcium: The recipes for composing global signals from elementary events. *Cell* 1997; 91: 367-373.
232. Moccia F, Frost C, Berra-Romani R et al. Expression and function of neuronal nicotinic ACh receptors in rat microvascular endothelial cells. *Am J Physiol Heart Circ Physiol* 2004; 286: H486-491.
233. Moccia F, Berra-Romani R, Tritto S et al. Epidermal growth factor induces intracellular Ca²⁺ oscillations in microvascular endothelial cells. *J Cell Physiol* 2003; 194: 139-150.
234. Dragoni S, Laforenza U, Bonetti E et al. Vascular endothelial growth factor stimulates endothelial colony forming cells proliferation and tubulogenesis by inducing oscillations in intracellular Ca²⁺ concentration. *Stem Cells* 2011; 29: 1898-1907.
235. Dragoni S, Turin I, Laforenza U et al. Store-operated Ca²⁺ entry does not control proliferation in primary cultures of human metastatic renal cellular carcinoma. *Biomed Res Int* 2014; 2014: 739494.
236. Dragoni S, Laforenza U, Bonetti E et al. Enhanced expression of Stim, Orai, and TRPC transcripts and proteins in endothelial progenitor cells isolated from patients with primary myelofibrosis. *PLoS One* 2014; 9: e91099.
237. Morgan AJ, Jacob R. Ca²⁺ influx does more than provide releasable Ca²⁺ to maintain repetitive spiking in human umbilical vein endothelial cells. *Biochem J* 1996; 320 (Pt 2): 505-517.

238. Jacob R. Agonist-stimulated divalent cation entry into single cultured human umbilical vein endothelial cells. *J Physiol* 1990; 421: 55-77.
239. Wang X, van Breemen C. Multiple mechanisms of activating Ca²⁺ entry in freshly isolated rabbit aortic endothelial cells. *J Vasc Res* 1997; 34: 196-207.
240. Chen Q, van Breemen C. The superficial buffer barrier in venous smooth muscle: sarcoplasmic reticulum refilling and unloading. *Br J Pharmacol* 1993; 109: 336-343.
241. Sasajima H, Wang X, van Breemen C. Fractional Ca²⁺ release from the endoplasmic reticulum activates Ca²⁺ entry in freshly isolated rabbit aortic endothelial cells. *Biochem Biophys Res Commun* 1997; 241: 471-475.
242. Dragoni S, Laforenza U, Bonetti E et al. Canonical transient receptor potential 3 channel triggers vascular endothelial growth factor-induced intracellular Ca²⁺ oscillations in endothelial progenitor cells isolated from umbilical cord blood. *Stem Cells Dev* 2013; 22: 2561-2580.
243. Kwan HY, Cheng KT, Ma Y et al. CNGA2 contributes to ATP-induced noncapacitative Ca²⁺ influx in vascular endothelial cells. *J Vasc Res* 2010; 47: 148-156.
244. Leung PC, Cheng KT, Liu C et al. Mechanism of non-capacitative Ca²⁺ influx in response to bradykinin in vascular endothelial cells. *J Vasc Res* 2006; 43: 367-376.
245. Re F, Cambianica I, Sesana S et al. Functionalization with ApoE-derived peptides enhances the interaction with brain capillary endothelial cells of nanoliposomes binding amyloid-beta peptide. *J Biotechnol* 2011; 156: 341-346.
246. Bird GS, Putney JW, Jr. Capacitative calcium entry supports calcium oscillations in human embryonic kidney cells. *J Physiol* 2005; 562: 697-706.
247. Cauli B, Hamel E. Revisiting the role of neurons in neurovascular coupling. *Front Neuroenergetics* 2010; 2: 9.
248. Behringer EJ, Segal SS. Membrane potential governs calcium influx into microvascular endothelium: integral role for muscarinic receptor activation. *J Physiol* 2015; 593: 4531-4548.
249. de la Torre JC, Stefano GB. Evidence that Alzheimer's disease is a microvascular disorder: the role of constitutive nitric oxide. *Brain Res Brain Res Rev* 2000; 34: 119-136.
250. Mumtaz S. Spatial and temporal characteristics of Ca²⁺ signaling in endothelial cells of intact rat tail artery. *Artery Research* 2013; 7: 84-92.
251. Rosenblum WI, McDonald M, Wormley B. Calcium ionophore and acetylcholine dilate arterioles on the mouse brain by different mechanisms. *Stroke* 1989; 20: 1391-1395.
252. Tracey WR, Peach MJ. Differential muscarinic receptor mRNA expression by freshly isolated and cultured bovine aortic endothelial cells. *Circ Res* 1992; 70: 234-240.
253. Neuwelt EA, Bauer B, Fahlke C et al. Engaging neuroscience to advance translational research in brain barrier biology. *Nat Rev Neurosci* 2011; 12: 169-182.
254. Boittin FX, Alonso F, Le Gal L et al. Connexins and M3 muscarinic receptors contribute to heterogeneous Ca²⁺ signaling in mouse aortic endothelium. *Cell Physiol Biochem* 2013; 31: 166-178.
255. Gericke A, Sniatecki JJ, Mayer VG et al. Role of M1, M3, and M5 muscarinic acetylcholine receptors in cholinergic dilation of small arteries studied with gene-targeted mice. *Am J Physiol Heart Circ Physiol* 2011; 300: H1602-1608.
256. Parekh AB. Decoding cytosolic Ca²⁺ oscillations. *Trends Biochem Sci* 2011; 36: 78-87.
257. Smedler E, Uhlén P. Frequency decoding of calcium oscillations. *Biochim Biophys Acta* 2014; 1840: 964-969.
258. Berridge MJ. The AM and FM of calcium signalling. *Nature* 1997; 386: 759-760.
259. Detjen K, Yang J, Logsdon CD. Muscarinic acetylcholine receptor down-regulation limits the extent of inhibition of cell cycle progression in Chinese hamster ovary cells. *Proc Natl Acad Sci U S A* 1995; 92: 10929-10933.

260. Schimerlik MI. Structure and regulation of muscarinic receptors. *Annu Rev Physiol* 1989; 51: 217-227.
261. Yang J, Williams JA, Yule DI, Logsdon CD. Mutation of carboxyl-terminal threonine residues in human m3 muscarinic acetylcholine receptor modulates the extent of sequestration and desensitization. *Mol Pharmacol* 1995; 48: 477-485.
262. Mumtaz S, Burdyga G, Borisova L et al. The mechanism of agonist induced Ca(2+) signalling in intact endothelial cells studied confocally in in situ arteries. *Cell Calcium* 2011; 49: 66-77.
263. Huang TY, Chu TF, Chen HI, Jen CJ. Heterogeneity of [Ca(2+)](i) signaling in intact rat aortic endothelium. *Faseb j* 2000; 14: 797-804.
264. Kansui Y, Garland CJ, Dora KA. Enhanced spontaneous Ca2+ events in endothelial cells reflect signalling through myoendothelial gap junctions in pressurized mesenteric arteries. *Cell Calcium* 2008; 44: 135-146.
265. Duza T, Sarelius IH. Localized transient increases in endothelial cell Ca2+ in arterioles in situ: implications for coordination of vascular function. *Am J Physiol Heart Circ Physiol* 2004; 286: H2322-2331.
266. Ying X, Minamiya Y, Fu C, Bhattacharya J. Ca2+ waves in lung capillary endothelium. *Circ Res* 1996; 79: 898-908.
267. Zhang S, Fritz N, Ibarra C, Uhlén P. Inositol 1,4,5-trisphosphate receptor subtype-specific regulation of calcium oscillations. *Neurochem Res* 2011; 36: 1175-1185.
268. Gruszczynska-Biegala J, Pomorski P, Wisniewska MB, Kuznicki J. Differential roles for STIM1 and STIM2 in store-operated calcium entry in rat neurons. *PLoS One* 2011; 6: e19285.
269. Aird WC. Endothelial cell heterogeneity. *Cold Spring Harb Perspect Med* 2012; 2: a006429.
270. Regan ER, Aird WC. Dynamical systems approach to endothelial heterogeneity. *Circ Res* 2012; 111: 110-130.
271. Berna-Erro A, Braun A, Kraft R et al. STIM2 regulates capacitive Ca2+ entry in neurons and plays a key role in hypoxic neuronal cell death. *Sci Signal* 2009; 2: ra67.
272. Emptage NJ, Reid CA, Fine A. Calcium stores in hippocampal synaptic boutons mediate short-term plasticity, store-operated Ca2+ entry, and spontaneous transmitter release. *Neuron* 2001; 29: 197-208.
273. Brandman O, Liou J, Park WS, Meyer T. STIM2 is a feedback regulator that stabilizes basal cytosolic and endoplasmic reticulum Ca2+ levels. *Cell* 2007; 131: 1327-1339.
274. Prakriya M, Lewis RS. Store-Operated Calcium Channels. *Physiol Rev* 2015; 95: 1383-1436.
275. Putney JW, Tomita T. Phospholipase C signaling and calcium influx. *Adv Biol Regul* 2012; 52: 152-164.
276. Sundivakkam PC, Kwiatek AM, Sharma TT et al. Caveolin-1 scaffold domain interacts with TRPC1 and IP(3)R3 to regulate Ca(2+) store release-induced Ca(2+) entry in endothelial cells. *Am J Physiol Cell Physiol* 2009; 296: C403-C413.
277. Berra-Romani R, Raqeeb A, Laforenza U et al. Cardiac microvascular endothelial cells express a functional Ca2+-sensing receptor. *J Vasc Res* 2009; 46: 73-82.
278. Asmat TM, Tenenbaum T, Jonsson AB et al. Impact of calcium signaling during infection of *Neisseria meningitidis* to human brain microvascular endothelial cells. *PLoS One* 2014; 9: e114474.
279. Dragoni S, Reforgiato M, Zuccolo E et al. Dysregulation of VEGF-induced pro-angiogenic Ca(2+) oscillations in primary myelofibrosis-derived endothelial colony forming cells. *Exp Hematol* 2015.
280. Paltauf-Doburzynska J, Frieden M, Spitaler M, Graier WF. Histamine-induced Ca2+ oscillations in a human endothelial cell line depend on transmembrane ion flux, ryanodine receptors and endoplasmic reticulum Ca2+-ATPase. *J Physiol* 2000; 524 Pt 3: 701-713.

281. Laskey RE, Adams DJ, Cannell M, van Breemen C. Calcium entry-dependent oscillations of cytoplasmic calcium concentration in cultured endothelial cell monolayers. *Proc Natl Acad Sci U S A* 1992; 89: 1690-1694.
282. Morgan AJ, Jacob R. Ionomycin enhances Ca²⁺ influx by stimulating store-regulated cation entry and not by a direct action at the plasma membrane. *Biochem J* 1994; 300 (Pt 3): 665-672.
283. Berridge MJ. Inositol trisphosphate and calcium oscillations. In Wakelam MJO (ed) *Cell Biology of Inositol Lipids and Phosphates*. London: Portland Press Ltd 2007; 1-7.
284. Berridge MJ. Inositol trisphosphate and calcium signalling mechanisms. *Biochimica Et Biophysica Acta-Molecular Cell Research* 2009; 1793: 933-940.
285. Kasai Y, Yamazawa T, Sakurai T et al. Endothelium-dependent frequency modulation of Ca²⁺ signalling in individual vascular smooth muscle cells of the rat. *J Physiol* 1997; 504 (Pt 2): 349-357.
286. Scharbrodt W, Abdallah Y, Kasseckert SA et al. Cytosolic Ca²⁺ oscillations in human cerebrovascular endothelial cells after subarachnoid hemorrhage. *J Cereb Blood Flow Metab* 2009; 29: 57-65.
287. Etienne-Manneville S, Manneville JB, Adamson P et al. ICAM-1-coupled cytoskeletal rearrangements and transendothelial lymphocyte migration involve intracellular calcium signaling in brain endothelial cell lines. *J Immunol* 2000; 165: 3375-3383.
288. Nikolskaia OV, de ALAP, Kim YV et al. Blood-brain barrier traversal by African trypanosomes requires calcium signaling induced by parasite cysteine protease. *J Clin Invest* 2006; 116: 2739-2747.
289. Clements JD, Lester RA, Tong G et al. The time course of glutamate in the synaptic cleft. *Science* 1992; 258: 1498-1501.
290. Lee KH, Kristic K, van Hoff R et al. High-frequency stimulation of the subthalamic nucleus increases glutamate in the subthalamic nucleus of rats as demonstrated by in vivo enzyme-linked glutamate sensor. *Brain Res* 2007; 1162: 121-129.
291. Kuhlmann CR, Gerigk M, Bender B et al. Fluvastatin prevents glutamate-induced blood-brain-barrier disruption in vitro. *Life Sci* 2008; 82: 1281-1287.
292. Legros H, Launay S, Roussel BD et al. Newborn- and adult-derived brain microvascular endothelial cells show age-related differences in phenotype and glutamate-evoked protease release. *J Cereb Blood Flow Metab* 2009; 29: 1146-1158.
293. Sharp CD, Hines I, Houghton J et al. Glutamate causes a loss in human cerebral endothelial barrier integrity through activation of NMDA receptor. *Am J Physiol Heart Circ Physiol* 2003; 285: H2592-2598.
294. Hogan-Cann AD, Anderson CM. Physiological Roles of Non-Neuronal NMDA Receptors. *Trends Pharmacol Sci* 2016; 37: 750-767.
295. He L, Linden DJ, Sapirstein A. Astrocyte inositol triphosphate receptor type 2 and cytosolic phospholipase A2 alpha regulate arteriole responses in mouse neocortical brain slices. *PLoS One* 2012; 7: e42194.
296. Beard RS, Jr., Reynolds JJ, Bearden SE. Metabotropic glutamate receptor 5 mediates phosphorylation of vascular endothelial cadherin and nuclear localization of beta-catenin in response to homocysteine. *Vascul Pharmacol* 2012; 56: 159-167.
297. Collard CD, Park KA, Montalto MC et al. Neutrophil-derived glutamate regulates vascular endothelial barrier function. *J Biol Chem* 2002; 277: 14801-14811.
298. Gillard SE, Tzaferis J, Tsui HC, Kingston AE. Expression of metabotropic glutamate receptors in rat meningeal and brain microvasculature and choroid plexus. *J Comp Neurol* 2003; 461: 317-332.

299. Mizuno O, Kobayashi S, Hirano K et al. Stimulus-specific alteration of the relationship between cytosolic Ca(2+) transients and nitric oxide production in endothelial cells ex vivo. *Br J Pharmacol* 2000; 130: 1140-1146.
300. Wen Y, Li J, Koo J et al. Activation of the glutamate receptor GRM1 enhances angiogenic signaling to drive melanoma progression. *Cancer Res* 2014; 74: 2499-2509.
301. Hall CN, Garthwaite J. What is the real physiological NO concentration in vivo? *Nitric Oxide* 2009; 21: 92-103.
302. Maffei A, Prestori F, Shibuki K et al. NO enhances presynaptic currents during cerebellar mossy fiber-granule cell LTP. *J Neurophysiol* 2003; 90: 2478-2483.
303. Lorincz ML, Kekesi KA, Juhasz G et al. Temporal framing of thalamic relay-mode firing by phasic inhibition during the alpha rhythm. *Neuron* 2009; 63: 683-696.
304. Wang M, Kaufman RJ. The impact of the endoplasmic reticulum protein-folding environment on cancer development. *Nat Rev Cancer* 2014; 14: 581-597.
305. Altaany Z, Moccia F, Munaron L et al. Hydrogen sulfide and endothelial dysfunction: relationship with nitric oxide. *Curr Med Chem* 2014; 21: 3646-3661.
306. Lecrux C, Hamel E. Neuronal networks and mediators of cortical neurovascular coupling responses in normal and altered brain states. *Philos Trans R Soc Lond B Biol Sci* 2016; 371.